HANDBOOK

AND

PROCEEDINGS

OF THE

TENNESSEE JUNIOR

ACADEMY OF SCIENCE

2011

Sponsored by the

Tennessee Academy of Science

Edited and Prepared by Jack Rhoton, Director
Tennessee Junior Academy of Science
P.O. Box 70301
East Tennessee State University
Johnson City, TN 37614
RhotonJ@etsu.edu

TENNESSEE JUNIOR ACADEMY

OF SCIENCE

ANNUAL MEETING

Belmont University

Nashville, Tennessee

Friday, April 15, 2011

Sponsored by the

TENNESSEE ACADEMYOF SCIENCE

TABLE OF CONTENTS

TENNESSEE ACADEMY OF SCIENCE OFFICERS: 2011

Jeff Boles……..…… President
Middle Tennessee State University, Murfreesboro

William H. Andrews…….…..…...President-Elect
University of Tennessee at Martin, Martin

Michael A. Gibson……...Immediate Past President
Middle Tennessee State University, Murfreesboro

Teresa Fulcher…….…….…..…….Secretary
Pellissippi State Technical Community College, Knoxville

C. Stephen Murphree…….…….…….…...Treasurer
Belmont University, Nashville

Steven J. Stedman……Editor, *Tennessee Academy of Science Journal*
Tennessee Technological University, Cookeville

TENNESSEE JUNIOR ACADEMY OF SCIENCE
Sponsored by the
TENNESSEE ACADEMY OF SCIENCE

Jack Rhoton…….…..Director Tennessee Junior Academy of Science
East Tennessee State University, Johnson City

READING COMMITTEE 2010-2011

Jack Rhoton……East Tennessee State University

William N. Pafford…….East Tennessee State University

Gary Henson...……East Tennessee State University

Timothy McDowell……East Tennessee State University

JUDGES

M. Gore Ervin……Middle Tennessee State University

Elbert Myles……..…….Tennessee State University

Preston J. MacDougall……...Middle Tennessee State University

Ningfeng Zhao……East Tennessee State University

LOCAL ARRANGEMENTS

Dr. Steven Murphree...……..Belmont University

INSTRUCTIONS FOR PARTICIPATION IN THE
TENNESSEE JUNIOR ACADEMY OF SCIENCE

Purpose. The Tennessee Junior Academy of Science (TJAS) is designed to further the cause of science education in Tennessee high schools by providing an annual program of scientific atmosphere and stimulation for capable students. It is comparable to scientific meetings of adult scientists. The Junior Academy supplements other efforts in the encouragement of able students of science by providing one venue of stimulation and expression

Rewards and Prizes. The student's primary rewards are the honor of being selected to appear on the program, experience in presenting his/her paper, opportunity to discuss this work with other students of similar interests, membership in the Tennessee Junior Academy of Science, and publication of his/her paper in the *Handbook and Proceedings of the Tennessee Junior Academy of Science.* However, the top two student writers will receive $500 each from the Tennessee Academy of Science, and other top writers will receive $200 for each paper published in the *Handbook.* In addition, the TAS will award $500 to each of the top two writers to participate in the Annual Meeting of the American Junior Academy of Science (AJAS). The AJAS meeting is held in a different city each year. All students who present papers to the TJAS are encouraged to enter their papers in other competitive programs, such as the Westinghouse Science Talent Search and the International Science and Engineering Fair. Students are also encouraged to solicit scholarships from individuals, companies, or institutions.

Preparation of the Report. The report should be an accurate presentation of a science or mathematics project completed by the student. It should be comprehensive, yet avoid excessive verbosity. Maximum length should be 1500 words. The report and the project it describes must be original with the student, not just a review of another article. It should be obvious that the experimentation and/or observations have been scientifically made. The paper should reflect credit on the writer and the school represented.

Visual aids such as slides, mock-ups, and charts may be used in presentation of the report. **PLEASE NOTE THE FOLLOWING: ILLUSTRATIONS WITHIN THE REPORT MUST BE RESTRICTED TO TABLES AND/OR SIMPLE LINE DRAWINGS. These must be done in BLACK ON 8 ½ X 11 WHITE PAPER. COLORED FIGURES CANNOT BE PRINTED IN THE HANDBOOK. Total width of the illustration itself cannot be more than 7". Illustrations submitted with the paper MUST be originals, NOT COPIES, and MUST be BLACK AND WHITE.**

The report must be **DOUBLE-SPACED** on 8 ½" by 11" paper. Give careful attention to spelling and grammar. **IT IS VERY IMPORTANT that YOU prepare a COVER SHEET** for the report, giving **ALL** the required information as specified, INCLUDING YOUR HOME TELEPHONE NUMBER **AND E-MAIL ADDRESS.** IF YOUR PAPER SHOULD BE SELECTED FOR PUBLICATION, IT MAY BE NECESSARY FOR OUR EDITORS TO CONTACT YOU. FAILURE TO PROVIDE CONTACT INFORMATION COULD PREVENT YOUR PAPER FROM BEING PUBLISHED. The cover sheet included with this material may be duplicated as needed. Prepare an abstract to accompany your paper (not more than 100

words). **NO PAPER WILL BE CONSIDERED UNLESS IT IS ACCOMPANIED BY AN ABSTRACT.**

Scientific or Technical Report Writing. A very important phase of the research of a scientist is the effective reporting of the research project attempted and completed. The technical report is different from other kinds of informative writing in that it has a single, predetermined purpose: to investigate an assigned subject for particular reasons. Technical reporting is done in the passive voice. Use of personal pronouns should be avoided except in rare instances. The telling portion of the research job is often underrated. Thus, communication is a very necessary part of research work. Any breakdown in communication means that the report has failed. The following functional analysis of the parts of the report is suggested to aid in organizing and presenting the results of scientific and experimental efforts.

I. Introduction
   A. Purpose of the investigation (why the work was done)
   B. How the problem expands/clarifies knowledge in the general field
   C. Review of related literature

II. Experimental procedure (how the work was done)
   A. Brief discussion of experimental apparatus involved
   B. Description of the procedure used in making the pertinent observations and obtaining data

III. Data (what the results were)
   A. Presentation of specific numerical data in tabulated or graphic form
   B. Observations made and recorded
   C. Any and all pertinent observations made that bear on the answer to the problem being investigated

IV. Conclusions (final contributions to knowledge)
   A. General contributions the investigations have made to the answer to the problem
   B. Further investigation suggested or indicated by the work

V. References –should be the **WORKS CITED ONLY** (the literature sources that are ACTUALLY **CITED** in the paper)
   A. Items arranged alphabetically by author's surname
      1. Author (surname, with initials only)
      2. Date, in parentheses
      3. Title, capitalize first work only
      4. Source: (periodical) (NO ABBREIVATIONS)
         (book) city, state of publication, publisher.

Each item in the Works Cited **MUST ALSO BE CITED WITHIN THE TEXT** of the student paper, using the parenthetical format of the APA Style Manual. Plagiarism is a serious offense, and is **not** limited to direct quotations. Any word, thought, statement, or instruction written by

another author and used in the student paper must be appropriately cited in the student paper presented to the Junior Academy.

Submission of the Report. Each report must bear an OFFICIAL COVER SHEET, which may be obtained in advance from:

Director of the Tennessee Junior Academy of Science
Dr. Jack Rhoton
Box 70301, East Tennessee State University
Johnson City, TN 37614
E-mail: Rhotonj@etsu.edu

The ORIGINAL COPY of the report should arrive on or before **March 1, 2012**. The parts of each report should be stapled or clipped, not bound. Heavy covers increase the cost of postage. The student should keep a copy of the report; the original cannot be returned. (We **MUST** have the **ORIGINAL** of all papers –and illustrations- for publication.)

Selection of the Report. Each report submitted must be endorsed by a local science or mathematics teacher. The teacher should approve the report as the first member of a selection committee. IT SHOULD BE APPROVED ONLY IF IT IS OF HIGH QUALITY AND REPRESENTS THE STUDENT'S OWN WORK IN RESEARCH AND PREPARATION. The science or math faculty submitting two or more papers in a given category will be asked to serve as judges for those papers and rate them in the order of 1, 2, 3, 4, etc., according to merit before submission to the Tennessee Junior Academy of Science for final judging. The report will then be read by a committee of two or more additional scientists in the field appropriate to the report. Reports will be selected on the basis of research design (30 points), creative ability (20 points), analysis of results (20 points), grammar and spelling (20 points), and general interest (10 points).

TENNESSEE JUNIOR ACADEMY OF SCIENCE CALENDAR FOR 2012

March 1	Final Date for Receiving Reports
March 20	Completion of Report Evaluation
March 30	Mailing of Invitations
April 20	Annual Meeting – Nashville

RESEARCH GRANTS FOR SCIENCE PROJECTS BY HIGH SCHOOL STUDENTS

The Tennessee Academy of Science has available a limited number of small research grants ($100-$300 per student) to assist high school students involved in developing scientific projects for the TJAS program. These grants are intended to be need-based. That is, we want to support good proposals from motivated students of adequate ability, where lack of some outside financial support might result in a poor project or possibly no project at all. These grants should not be regarded as competitive merit awards for outstanding proposals or outstanding students, and should not be given to students whose families, or whose project mentors, can readily provide

the resources needed. For instance, a project being conducted under the mentorship of a university professor would not, in general, be a good choice for a TAS grant, no matter how able the student and how good the proposed project. It is intended that the TAS research grants program create opportunities for adequately motivated students with access to limited resources to conduct significant, competitive projects. The Tennessee Academy of Science will depend on the sponsoring science or math teachers to provide input into the decision-making process as it concerns the need of applying students and worthiness of their proposed projects.

The application form for the TAS research grant included in these materials may be duplicated as needed. Please note the deadline for receiving grant applications is ***NOVEMBER 15, 2011***. However, the earlier grant applications are received, the sooner grant application funds can be distributed. If you desire further information concerning the TAS research grants program, please write to Dr. Jack Rhoton, Division of Science Education, Box 70684, East Tennessee State University, Johnson City, TN 37614 or E-mail: Rhotonj@ETSU.edu.

TENNESEE JUNIOR ACADEMY OF SCIENCE
SPRING MEETING – 2012

The Sixty-Third Annual Meeting of the Tennessee Junior Academy of Science will be held in **Nashville, on Friday, April 20, 2012**

All Tennessee high schools are invited to participate in the TJAS program leading up to the spring meeting. The program provides state-wide and national recognition for high school students' investigative or research-type science projects

TENNESSEE JUNIOR ACADEMY OF SCIENCE REGULATIONS

The following regulations have been developed to govern the Tennessee Junior Academy meeting by the Standing Committee on Junior Academies of the Academy Conference. Papers must be of a research problem type, with evidence of creative thought. Papers presented should be suitable for publication (typewritten, double-spaced, one side of paper only, name and address on each sheet) and between 1000 and 1500 words in length. Oral presentation will be limited to 10 minutes. Projectors and other audiovisual equipment will be available. Questions on paper presentation will be limited to 3 minutes. All papers should be postmarked **NO LATER THAN MARCH 1, 2012**, and sent to Dr. Jack Rhoton, PO Box 70684, East Tennessee State University, Johnson City, TN 37614. Certificates will be presented to all participants. Sponsoring schools or clubs should have insurance coverage to protect school participants. The Tennessee Junior Academy of Science can assume no responsibility in this matter.

WHAT YOU CAN DO NOW

If there is no science club at your high school, why not start one? A science club will provide many opportunities to work on problems that will be fun and relaxing. The ready, mutual exchange of ideas can provide a challenging experience in proposing, designing, and completing research into the unknown. Begin now to work on a scientific project to present at the next annual meeting of your local, state, and national Junior Science Clubs. For further information on the Junior Academy program, contact:

Tennessee Junior Academy of Science
Dr. Jack Rhoton, Director
PO Box 70301
East Tennessee State University
Johnson City, TN 37614
Phone: 423-439-7589
E-mail: Rhotonj@etsu.edu
Fax: 423-439-7530

PURPOSE OF THE ACADEMIES OF SCIENCE

The purpose of the various state and municipal Junior Academies is to promote science as a career at the secondary school level. The basic working unit is the science club or area in each school where the extracurricular science projects and activities are supervised by science teachers/sponsors. The American Junior Academy serves a state or city organization much the same as do the professional societies, and it functions in a similar manner; e.g., holding annual meetings for presenting research papers. The parent sponsor of a Junior Academy of Science is the State Academy of Science. The primary activity of the American Junior Academy of Science is the Annual Meeting held with the Annual Meeting of the American Association for the Advancement of Science and the Association of Academies of Science. Top young scientists in each state or city academy are encouraged to present papers and exchange research ideas at the national level. Tours and social hours are also arranged.

DIRECTORS OF THE TENNESSEE JUNIOR ACADEMY OF SCIENCE

1942-2012

The Tennessee Academy of Science has been the sponsor of the Tennessee Junior Academy of Science since its initial organizational meeting on the Vanderbilt University campus in 1942.

The Directors of the Junior Academy of Science since 1942 are as follows:

Dr. Frances Bottom – 1942-1955……..... George Peabody College
Nashville

Dr. Woodrow Wyatt – 1955-1958……...The University of Tennessee
Knoxville

Dr. Myron S. McCay – 1958-1963……..The University of Tennessee
Knoxville

Dr. Robert Wilson – 1963-1965……..The University of Tennessee
Chattanooga

Dr. John H. Bailey – 1965-1976…….East Tennessee State University
Johnson City

Dr. William N. Pafford – 1976-1992……..East Tennessee State University
Johnson City

Dr. Jack Rhoton – 1992-present…….….East Tennessee State University
Johnson City

TENNESSEE JUNIOR ACADEMY OF SCIENCE
Sponsored by the
TENNESSEE ACADEMY OF SCIENCE
Annual Meeting

Belmont University
Nashville, Tennessee
Friday, April 15, 2011

PROGRAM

9:00 –9:30 a.m.	Registration
9:30 – 9:40 a.m.	Welcome
9:40 –11:30 a.m.	Paper Presentations
11:35 a.m.	Special Presentations
12:00 –1:00 p.m.	Lunch
1:30 –4:00 p.m.	Paper Presentations
4:00 p.m.	Adjournment

TENNESSEE JUNIOR ACADEMY OF SCIENCE

Papers to be Presented at Annual Meeting
Title of Paper, Student's Name, School, City

YES, THERE ARE ATOMS. A COMPARISON OF THREE INDEPENDENT METHODS OF DETERMINING AVOGADRO'S NUMBER — **Physics**

Stephen Theyken
Webb School of Knoxville, Knoxville

REACTION-DRIVEN MIXING DURING ACID/BASE NEUTRALIZATION — **Chemistry**

Gavin B. Nixon
Greenbrier High School, Greenbrier

POTENTIAL SITE FOR THE TRANSLOCATION AND PROPAGATION OF THE SMOKY MADTOM, *Noturus baileyl* — **Zoology**

Katie Holmes & Andrea Tipton
Cleveland High School, Cleveland

THE EFFECTS OF GENDER ON THE OPERANT CONDITIONING OF MICE — **Zoology**

Jin Kim, Josh Schultz & Clayton Elrod
Siegel High School, Murfreesboro

EVALUATION OF CLIMATE TRENDS AND SALAMANDER POPULATION DENSITIES: A THREE YEAR STUDY — **Biology**

Wade Hubbs
Camden Central High School, Camden

CRYSTALLIZATION WITH VIBRATIONS II — **Physics**

Della Coleman
Northwest High School, Clarksville

CHARACTERIZATION OF IMMUNE RESPONSE RESULTING FROM ACUTE GENETIC OR PHARMACOLOGICAL INHIBITION OF NOTCH SIGNALING — **Medicine & Health**

Joseph Griggs
Pope John Paul II High School, Hendersonville

THE EFFECTS OF SURFACE AREA, DISTANCE, AND VOLTAGE ON THE PRODUCTION OF HYDROGEN BY MEANS OF SHORT-PULSE HYDROLYSIS — **Physics**

Ahbid Zein-Sabatto, Vikas Kumar, Shuvajit Das & Ravikanth Konjeti
School for Science and Math at Vanderbilt, Nashville

EFFECTS OF AIRPLANE DEICER ON *O.placidus* **IN TENNESSEE WATERWAYS** — **Chemistry**

Ryan Driscoll & Anne Holmes
School for Science and Math at Vanderbilt, Nashville

THE TOXICITY OF DIFFERENT CONCENTRATIONS OF ROUNDUP ON *Echiniscus* — **Environmental Science**

Elizabeth Glass
Pope John Paul II High School, Hendersonville

THE EFFECTS OF SURFACE AREA ON ELECTRICAL PRODUCTION IN A MICROBIAL FUEL CELL — **Environmental Science**

Gavin Dorrity
Northwest High School, Clarksville

THE EFFECTS OF OXYTOCIN ON *Nasonia vitripennis* AND *Nasonia girault*i ON LONGEVITY, NUMBER OF OFFSPRING, DIAPAUSE AND RECEPTOR GENE EXPRESSION **Bio-Chemistry**

HyunJeong Jin, Jordan Winters, Ronnie Cela-Bedoya & Kanyanta Mwenya
School for Science and Math at Vanderbilt, Nashville

RECOLONIZATION OF ALGAL ASSEMBLAGES AFTER FLOODING IN NASHVILLE CREEKS **Ecology**

Emily Alsentzer, Holden Bitner & Laura Moribe
School for Science and Math at Vanderbilt, Nashville

THE EFFECTS OF pH on ENZYME CATALYSIS **Chemistry**

Imani Chatman & Caroline Daws
Siegel High School, Murfreesboro

THE INFLUENCE OF RESITANCE AND SOAP CONCENTRATIONS ON THE INHIBITION OF GROWTH IN *E. coli* **Microbiology**

Vanessa Fuentes
Smyrna High School, Smyrna

THE EFFECT OF AMPICILLIN AND TEMPERATURE ON *E. coli* GROWTH RATES **Microbiology**

Sidhartha Sinha & Daniel Hutchison
Smyrna High School, Smyrna

THE EFFECT OF pH ON NIR-DYES: APPLICATIONS FOR PROTEOLYTIC BEACON OPTICAL PROBES **Chemistry**

Brian Allen, Samantha Soebbing, Ian McFadden, Lynn Matrisian & Oliver McIntyre
Siegel High School, Murfreesboro

TUMOR AND STROMAL ELEMENTS ARE REQUIRED FOR MACROPHAGE POLARIZATION FOLLOWING INDUCED LUNG TUMOR METASTASIS **Medicine & Health**

Kevin Clavin
Pope John Paul II High School, Hendersonville

MEASURING RATE OF PASAGE OF ASPIRIN AND BUFFERIN® THROUGH A SEMI-PERMIABLE MEMBRANE **Medicine**

Ashley E. Corson
Greenbrier High School, Greenbrier

Tgfbr2* and *Tgfbr3 si*RNA KNOCKDOWN REDUCES ENDOCARDIAL CELL TRANSFORMATION IN CHICK EMBRYOS IN *VITRO **Developmental Biology**

Anh Pham, Jamille Robinson & Joey Barnett
Hume-Fogg Academic High School, Nashville

THE EFFECT OF FERTILIZER POLLUTION ON ALGAL PROFILES IN RICHLAND AND HENRY CREEKS **Ecology**

Catherine Caffey, Lauren Lu & Shanna Rucker
School for Science and Math at Vanderbilt, Nashville

EFFECTS OF THE FIRING PROCESS FOR EASTERN DARK- FIRED TOBACCO ON AIR, WATER, AND SOIL QUALITY **Environmental Science**

Daniel Lawhon
Greenbrier High School, Greenbrier

cAMP SIGNALING CASCDE REGULATES THE Na-K-2Cl COTRANSPORTER **Molecular Biology**

Jenny S. Gray
Hume-Fogg Academic High School, Nashville

Students Who Submitted Papers to the Tennessee Junior Academy of Science

Allen, Brian; Siegel High School, Murfreesboro
Alsentzer, Emily; School for Science and Math at Vanderbilt, Nashville
Bailey, Alisha; Northwest High School, Clarksville
Barlow, Courtnee; Northwest High School, Clarksville
Barnett, Joey; Hume-Fogg Academic High School, Nashville
Becker, Ashley; Northwest High School, Clarksville
Biswas, Jyotishka; School for Science and Math at Vanderbilt, Nashville
Bitner, Holden; School for Science and Math at Vanderbilt, Nashville
Bourne, Conner; Northwest High School, Clarksville
Caffey, Catherine; School for Science and Math at Vanderbilt, Nashville
Calhoun, David; Greenbrier High School, Greenbrier
Caviness, Lisa, Northwest High School, Clarksville
Cela-Bedoya, Ronnie; School for Science and Math at Vanderbilt, Nashville
Chatman, Imani; Siegel High School, Murfreesboro
Cherry, Aaron; Northwest High School, Clarksville
Clavin, Kevin; Pope John Paul II High School, Hendersonville
Clayton, Allie; Siegel High School, Murfreesboro
Coleman, Della; Northwest High School, Clarksville
Comeaux, Darryel'; Northwest High School, Clarksville
Corson, Ashley; Greenbrier High School, Greenbrier
Craft, Andrew; Northwest High School, Clarksville
Cruz, Caleb; Northwest High School, Clarksville
Das, Shuvajit; School for Science and Math at Vanderbilt, Nashville
Davenport, Ryan; Blackman High School, Murfreesboro
Daws, Caroline; Siegel High School, Murfreesboro
Dorrity, Gavin; Northwest High School, Clarksville
Dorsey, Hailey; Northwest High School, Clarksville
Driscoll, Ryan; School for Science and Math at Vanderbilt, Nashville
Elrod, Clayton; Siegel High School, Murfreesboro
Erickson, Daniel; Northwest High School, Clarksville
Fatima, Tahreem; School for Science and Math at Vanderbilt, Nashville
Faul, Heather; Northwest High School, Clarksville
Felthauser, Katherine; Northwest High School, Clarksville
Ferranti, Justin; Northwest High School, Clarksville
Forest, Kaitlyn; Northwest High School, Clarksville
Froeba, Christopher; Northwest High School, Clarksville
Fuentes, Vanessa; Smyrna High School, Smyrna
Garner, Newton; Northwest High School, Clarksville
Geiger, Rachael; Pope John Paul II High School, Hendersonville
Gentry, Keith; Northwest High School, Clarksville
Giron, Laura; School for Science and Math at Vanderbilt, Nashville
Glass, Elizabeth; Pope John Paul II High School, Hendersonville
Glover, Kiera; Northwest High School, Clarksville

Gray, Jenny; Hume-Fogg Academic High School, Nashville
Greenarch, Destiny; Camden Central High School, Camden
Griggs, Joseph; Pope John Paul II High School, Hendersonville
Gross, John; Northwest High School, Clarksville
Gu, Jiahe; School for Science and Math at Vanderbilt, Nashville
Guilliams, Ronja; Northwest High School, Clarksville
Hawkins, Ambriell; Northwest High School, Clarksville
Heyward, Autumn; Northwest High School, Clarksville
Holliman, Colt; Greenbrier High School, Greenbrier
Holmes, Katie; Cleveland High School, Cleveland
Holmes, Anne; School for Science and Math at Vanderbilt, Nashville
Howard, Scott; Northwest High School, Clarksville
Huang, Lee; Siegel High School, Murfreesboro
Hubbs, Wade; Camden Central High School, Camden
Hughs, Alison; Northwest High School, Clarksville
Hutchinson, Danielle; Northwest High School, Clarksville
Hutchison, Daniel; Smyrna High School, Smyrna
Jackson, Jessica; Northwest High School, Clarksville
Jenkins, Allison; Pope John Paul II High School, Hendersonville
Jin, HyunJeong; School for Science and Math at Vanderbilt, Nashville
Kelly, Jasmine; School for Science and Math at Vanderbilt, Nashville
Kilpatrick, Chloe; Pope John Paul II High School, Hendersonville
Kim, Jin; Siegel High School, Murfreesboro
Kimbell, Greer; Blackman High School, Murfreesboro
Konjeti, Ravikanth; School for Science and Math at Vanderbilt, Nashville
Krishnamani, Yashna; Siegal High School, Murfreesboro
Kumar, Vikas; School for Science and Math at Vanderbilt, Nashville
Lavelle, Ian; Northwest High School, Clarksville
Lawhon, Daniel; Greenbrier High School, Greenbrier
Lu, Lauren; School for Science and Math at Vanderbilt, Nashville
Lucas, Grace; Pope John Paul II High School, Hendersonville
Matrisian, Lynn; Siegel High School, Murfreesboro
McFadden, Ian; Siegel High School, Murfreesboro
McIntyre, J. Oliver; Siegel High School, Murfreesboro
McRen, Emily; Pope John Paul II High School, Hendersonville
Melcher, Brendan; Pope John Paul II High School, Hendersonville
Mimms, Rebecca; Northwest High School, Clarksville
Montgomery, Ashley; Pope John Paul II High School, Hendersonville
Moribe, Laura; School for Science and Math at Vanderbilt, Nashville
Mwenya, Kanyanta; School for Science and Math at Vanderbilt, Nashville
Nielson, Niels; Northwest High School, Clarksville
Nixon, Gavin; Greenbrier High School, Greenbrier
Patel, Raina; Pope John Paul II High School, Hendersonville
Pavk, Sarah; Pope John Paul II High School, Hendersonville
Pham, Anh; Hume-Fogg Academic High School, Nashville
Phillips, Eric; Northwest High School, Clarksville

Price, Dylan; Northwest High School, Clarksville
Qu, David; Siegal High School, Murfreesboro
Ramos, Jacqueline; Pope John Paul II High School, Hendersonville
Reyes, Anthony; Northwest High School, Clarksville
Robinson, Jamille; Hume-Fogg Academic High School, Nashville
Ross, Julia; Pope John Paul II High School, Hendersonville
Rottman-Yang, Jaron; School for Science and Math at Vanderbilt, Nashville
Rucker, Shanna; School for Science and Math at Vanderbilt, Nashville
Sanderson, Schuyler; School for Science and Math at Vanderbilt, Nashville
Schultz, Josh; Siegel High School, Murfreesboro
Sellick, Katelyn; Northwest High School, Clarksville
Sellmer, Robert; Northwest High School, Clarksville
Sides, Kayla; Blackman High School, Murfreesboro
Sinha, Sidhartha; Smyrna High School, Smyrna
Sipos, Ilinca; Pope John Paul II High School, Hendersonville
Smith, Graham; Blackman High School, Murfreesboro
Soebbing, Samantha; Siegel High School, Murfreesboro
Spears, Shayna; Northwest High School, Clarksville
Stevens, Tonya; Northwest High School, Clarksville
Taylor, Juliana; Pope John Paul II High School, Hendersonville
Tepen, Erica; Northwest High School, Clarksville
Theyken, Stephen; Webb School of Knoxville, Knoxville
Thomas, Caithleann; Northwest High School, Clarksville
Tipton, Andrea; Cleveland High School, Cleveland
Trenkle, Max; Siegel High School, Murfreesboro
Vielma, Samantha; Northwest High School, Clarksville
Williams, Christopher; Northwest High School, Clarksville
Wilson, Breanna; Northwest High School, Clarksville
Wilson, Martavia; Northwest High School, Clarksville
Winters, Jordan; School for Science and Math at Vanderbilt, Nashville
Young, Cherie'; Northwest High School, Clarksville
Zein-Sabatto, Ahbid; School for Science and Math at Vanderbilt, Nashville

PAPERS OF EXCELLENCE

Effect of pH on NIR-Dyes: Applications for Proteolytic Beacon Optical Probes

Brian W. Allen
Siegel High School, Murfreesboro

Abstract

Near-Infrared (NIR) dyes are components of Proteolytic Beacons (PBs) used for *in vivo* optical imaging of tumor-associated proteinases. AF700 and AF750 compose a sensor-reference Förster resonance energy transfer (FRET) pair that can be used in PBs with dyes attached to peptide termini. Selective cleavage of the peptide by proteases, *e.g.*, matrix metalloproteinases (MMPs), often misregulated in cancer cells, separates the FRET pair, causing emission of light by the sensor dye. Optical imaging of fluorescence after proteolytic cleavage delineates the location of cancer *in vivo*. Prior experiments indicated pH sensitivity of both AF700 and AF750. To explore this phenomenon, each dye was solubilized in buffers ranging from pH 2-13 and measured UV-Vis and fluorescence spectra over ten days. We discovered that AF700 and AF750 were stable between pH 5-10 and 4-11, respectively. Reversibility of pH-induced spectral changes was investigated by switching the pH of dye-buffer solutions to pH 7. It was found that absorbance could be restored (>85%) for AF700 at pH 4-10 and AF750 at pH 3-11. Fluorescence of one-day samples confirmed reversibility at pH 2-12 with partial restoration at pH 13 for AF750. The researcher concluded that these dyes can be used as an optical imaging FRET pair at pH 5-10. In addition, the dyes can be manipulated during PB preparation from pH 3-12 if the pH is restored to neutral. This knowledge improves the understanding of AF700 and AF750 dyes used in PBs so that imaging probes can be used appropriately, depending on experimental conditions. In future studies, applications of dye-labeled peptides for *in vivo* imaging will be explored.

Introduction

Near-Infrared Proteolytic Beacons (NIR-PBs) are probes used for optical imaging of tumor-associated proteinases. This form of imaging is advantageous because animal tissue has minimal absorption of light in the NIR window (650 – 900 nm), and PBs have a miniscule risk of damaging cells (Lyons 2005 and Scherer 2008 – A). As compared to many other forms of *in*

vivo optical imaging, NIR-PBs allow for more effective imaging deeper into multi-layered tissues (Choy, G. Choyke, P., Libutti, S.K., (2003). The red and near-infrared spectrum reduces auto-fluorescence, making NIR-PBs ideal for *in vivo* imaging (Levin 2005).

A standard proteolytic beacon is composed of a peptide attached to a scaffold, called a dendron. On each side of this peptide is a NIR dye. Together, these two dyes, a sensor and a reference, form a Förster Resonance Energy Transfer (FRET) pair. In a FRET pair, the emission spectrum of the sensor dye is nearly tantamount to the excitation spectrum of the reference dye. The sensor transfers its energy to the reference dye when the sensor is excited at its characteristic wavelength and the dye pairs are in close proximity to each other. In an intact proteolytic beacon, the FRET pair is close together, allowing FRET, causing the emission of the sensor dye to be quenched. However, selective cleavage of the peptide by proteases separates the FRET pair. The energy transfer between the sensor and reference is halted, allowing emission of light by the sensor dye.

Peptides selectively cleaved by Matrix Metalloproteinases (MMPs) can be utilized in PBs to image cancer cells. MMPs are proteinases in the Extracellular Matrix (ECM) that degrade many components of the ECM. MMPs are over expressed in most cancer cells, causing severe degradation of the Extracellular Matrix (Scherer 2008 – A). This activity contributes to metastasis of tumors. MMPs are ideal targets for optical imaging by proteolytic beacons because of their misregulation in cancer cells. Optical imaging of fluorescence after proteolytic cleavage by MMPs delineates the location of cancer *in vivo*. Specifically, the proteolytic activity of MMP7 has been exploited in previously-designed PBs used in the Matrisian Laboratory to successfully image cancerous tissues (Scherer 2008 – B and McIntyre 2004).

Alexa Fluor®-700 and Alexa Fluor®-750 (AF700 and AF750, respectively) comprise a sensor-reference NIR FRET pair that can be utilized in proteolytic beacons. However, prior unpublished experiments performed by the Matrisian Laboratory in the Vanderbilt Ingram Cancer Center at Vanderbilt University indicated pH sensitivity of both AF700 and AF750. It is hypothesized that AF700 loses effectiveness in solutions of low pH, and AF750 loses effectiveness in solutions of high pH. During PB synthesis, the dyes are often submerged in solutions of extreme pH for purification purposes. An effective pH range for AF700 and AF750 must be determined for optimal cancer imaging results. Another important question is reversibility of dyes. If the FRET pair is exposed to environments of extreme pH that degrade

efficacy of dye function, can the solution be neutralized to return the effectiveness of the dyes? The researcher determined, for this project, an effective pH range for the AF700 and AF750 FRET pair and investigated reversibility of the dyes.

Methods and Materials

pH Sensitivity and Stability

Prior experiments suggested that the AF700 dye loses its effectiveness in acidic solutions, and the AF750 dye loses its effectiveness in basic solutions. Their absorbance spectra in buffers of varying pH were measured to experimentally determine the effect of pH on NIR-dyes. An effective AF700 dye absorbs light at around 700 nm and an AF750 dye at 750 nm. Absorbance was measured using a UV-Vis spectrophotometer. To prepare the samples, the AF700 dye was solubilized in 20 mM solutions of pH 2-10 and the AF750 dye in pH 2-13. Different chemicals, shown in **Table 1,** with various buffering pH and capacity were used to achieve the needed buffer solutions. A biologically-relevant buffer, phosphate-buffered saline (1xPBS) solution was used as a control buffer for the experiment. Dyes were stored in darkened tubes at room temperature to protect the samples from light, which can cause degradation of AF700 and AF750 dyes. Over the course of ten days, the absorbance was measured using UV-Vis spectroscopy.

pH	Buffer
2	Phosphate
3	Glycine
4	Acetate
5	Acetate
6	4-Morpholineethanesulfonic acid (MES)
7	Phosphate
8	Tris(hydroxymethyl)aminomethane (Tris)
9	Borate

Table 1: The chemicals used in each buffer solution of pH 2-13.

10	Glycine
11	Borate
12	Phosphate
13	Glycine

The absorbance and the fluorescence of the dyes were also measured. The fluorescence spectrum is composed of two contiguous bell-shaped curves: the excitation and emission spectra. The excitation spectrum peaks at the wavelength where light is absorbed by the solubilized dye. The zenith of the emission curve corresponds to the wavelength where the absorbed light is spontaneously emitted. The AF700 and AF750 dyes should excite at the same wavelength where the absorbance was previously determined, and emission should occur at a slightly longer wavelength, corresponding to the lower-energy emitted light. The samples used for absorbance studies were diluted as necessary for use in fluorescence studies.

Reversibility

Analysis of absorbance and fluorescence spectra was used to determine the effective pH where the dyes absorbed and emitted light per the manufacturer's description. The reversibility of AF700 and AF750 in buffers of pH outside the effective range (where degradation of dye can occur) was tested. Dye-containing solutions from days five and nine (AF700) and days four and ten (AF750) were diluted by a ratio of 2:3 with 200 mM pH 7 phosphate buffer to reverse the pH of the samples back to neutral. These new dilutions were utilized to measure absorbance by UV-Vis spectroscopy. Additional samples from day one were diluted 1:11 for measurement of fluorescence spectra.

Results

pH Sensitivity and Stability

AF700 - Absorbance

Over the course of nine days, the AF700 dye was tested for pH sensitivity and stability using UV-Vis spectroscopy. Absorbance was measured on days one, five, and nine. **Figures 1 - 3** display the results of the experiment. On the first day of testing, our hypothesis was confirmed

when the AF700 dye lost optical density (O.D.) at 691 nm in acidic solutions of pH 2-4, but retained its maximal absorbance at 691 nm in neutral and basic buffers. The AF700 dye can only serve as a functional FRET pair with AF750 if its maximum absorbance is at approximately 691 nm, with a concomitant emission at about 710 nm. However, in the solutions of low acidity, the AF700 dye absorbance peak shifted to 546 nm. This shift in absorbance would not result in a working FRET pair because it would prevent energy transfer between the two dyes. Data from day one are shown in **Figure 2** and more clearly demonstrate the range of effectiveness for the dye. For a functional FRET pair, the curve representing absorbance of AF700 at 691 nm versus pH should be maximized with minimal absorbance at a wavelength of 546 nm. Therefore, on day one, AF700 is optimal at pH 6-10. To determine stability of the dye over time, absorbance data were collected over nine days, as shown in **Figure 3**. According to the graph, AF700 maintains its stability at pH 6-10 for at least nine days and potentially longer.

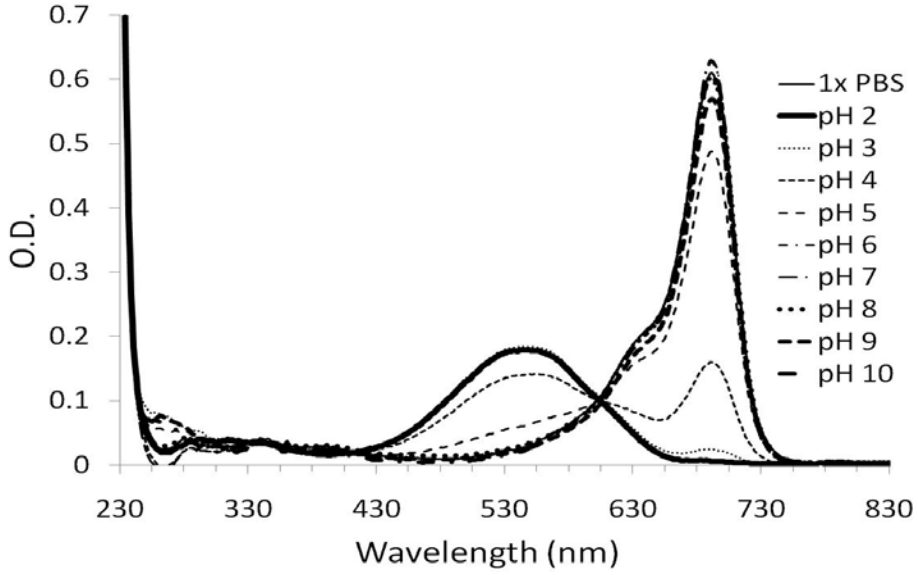

Figure 1: Absorbance of AF700 dye, dissolved in buffers of varying pH, on day one; maximum absorbance should occur at approximately 691 nm.

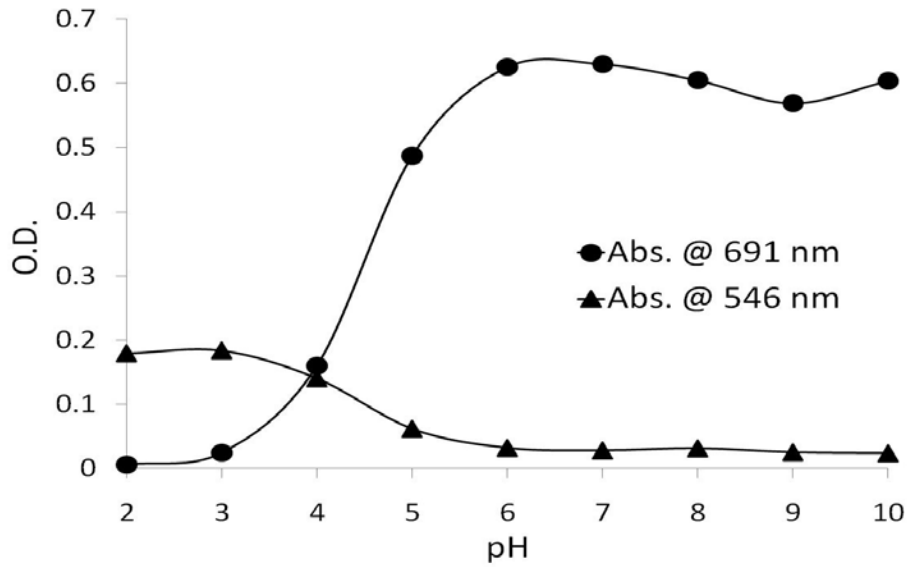

Figure 2: O.D. of AF700 at the two wavelengths (691 nm and 546 nm) where peaks occurred in **Figure 1**.

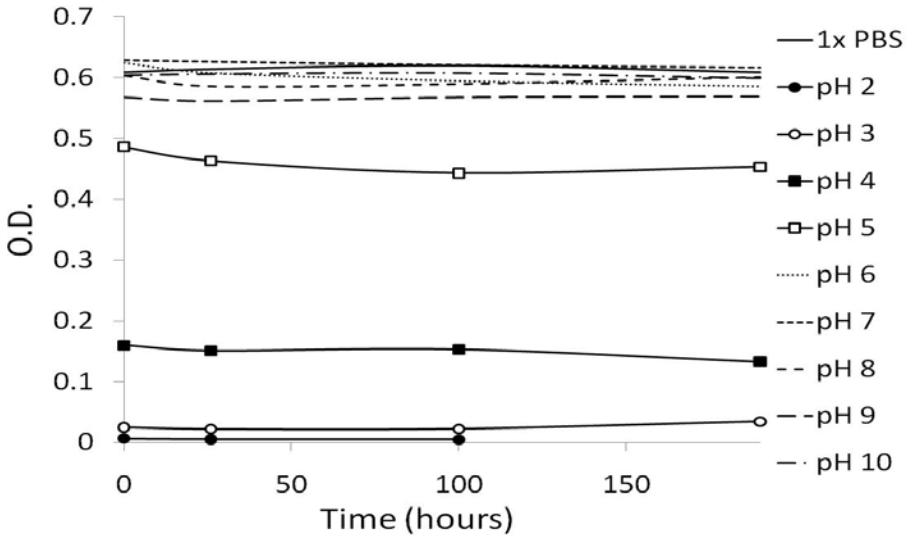

Figure 3: O.D. of each pH buffer solution containing AF700 dye, at 691 nm over the course of nine days.

AF750 - Absorbance

The absorbance data of the AF750 dye were collected over a time period of ten days. **Figures 4 – 6** summarize the findings of the experiment. The three graphs delineate the same information as those in **Figures 1 – 3**, but in this case for AF750 instead of AF700. **Figure 4** confirms that AF750 is degraded in basic solutions, but the efficacy of the dye is only lost at an extremely high pH of 13. **Figure 5** reveals that the effective range of AF750 on day one is between pH 2-12. However, a trade-off becomes blatantly apparent in **Figure 6**. While the pH range of use on day

one is large, the AF750 loses a substantial amount of effectiveness over a short period of time. In fact, the dye appears to be stable for ten days only at pH 8-11.

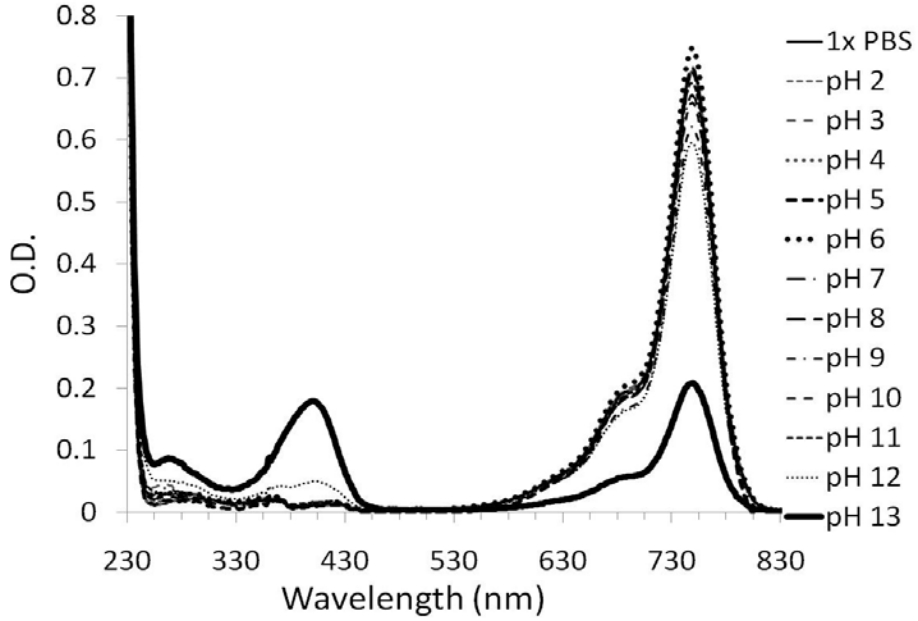

Figure 4: Absorbance of AF750, dissolved in buffers of varying pH, on day one; maximum absorbance should occur at approximately 749 nm.

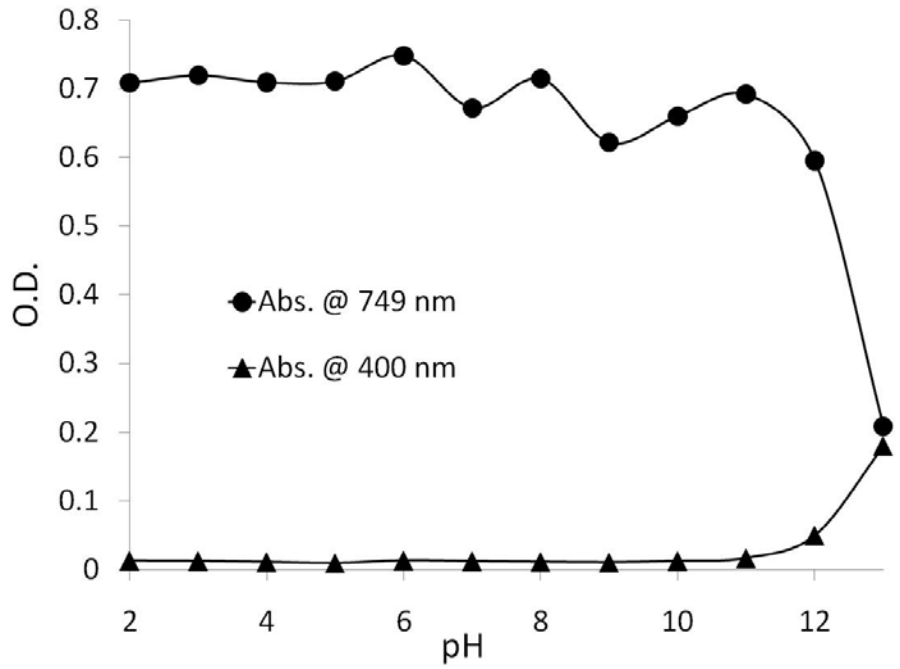

Figure 5: O.D. of AF750 at the two wavelengths (749 nm and 400 nm) where peaks occurred in **Figure 4**.

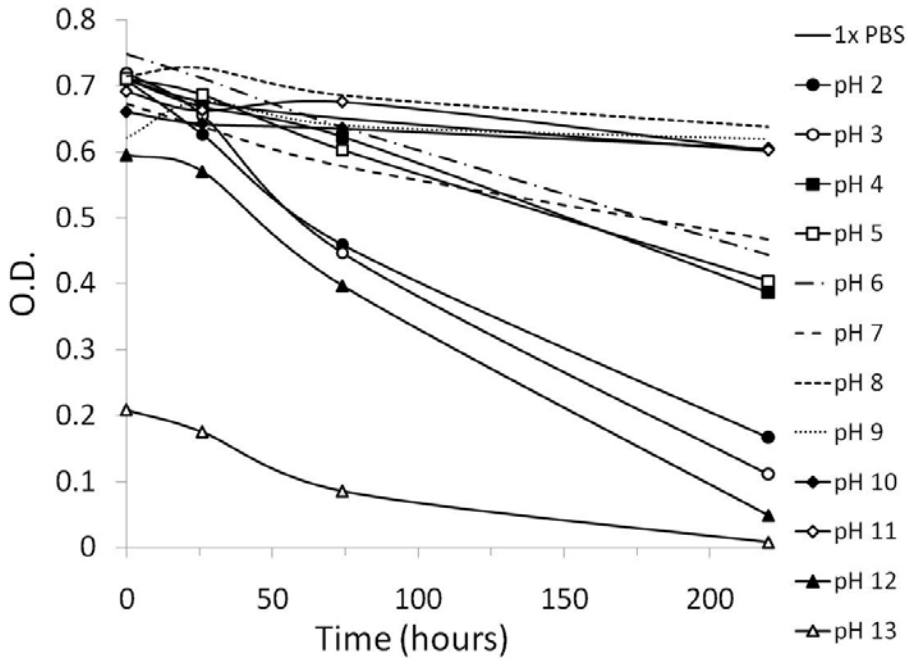

Figure 6: Optical density at 749 nm in each pH buffer containing AF750 dye, over the course of ten days.

AF700 and AF750 – Fluorescence

Fluorescence of each dye was measured on the second and the last days of the experiment. **Figures 7 – 10** show fluorescence spectra of each dye on day two in the pH buffers of interest, and data for both dyes confirmed findings from the previous absorbance experiments. Because AF700 lost effectiveness at pH 2-4, according to the absorbance data, the fluorescence of pH 2 and pH 4 samples was measured and plotted in **Figure 7 and 8**, respectively. The fluorescence spectra of AF750 were measured also at pH 12 and pH 13, where the absorbance appeared to deteriorate.

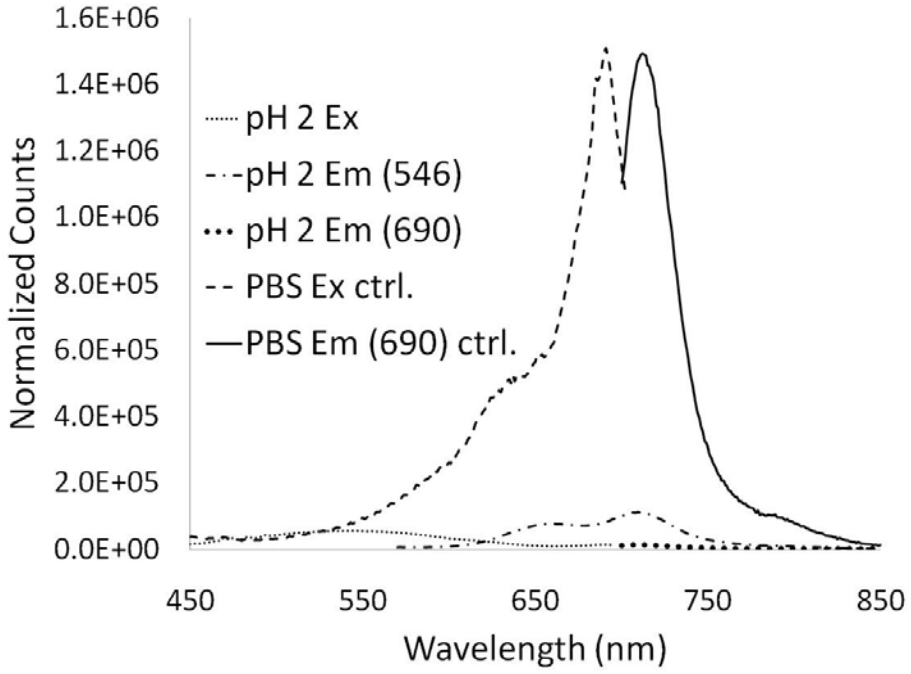

Figure 7: Fluorescence of AF700 in pH 2 buffer on day 2. Numbers in parentheses signify the wavelength in nm at which the dye was excited. In the legends, Ex is the abbreviation for excitation and Em refers to the emission spectrum.

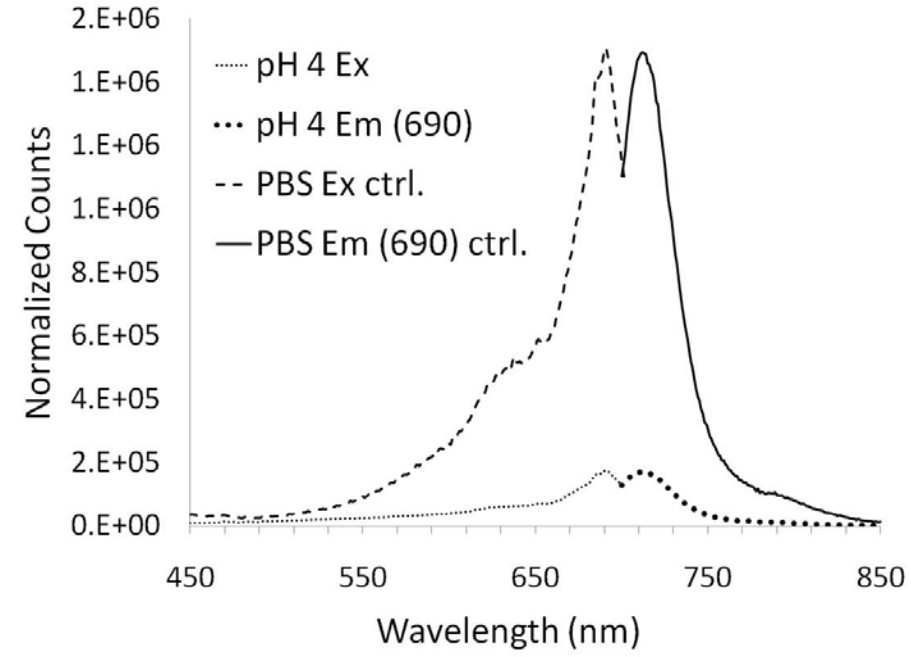

Figure 8: Fluorescence of AF700 in pH 4 buffer on day 2.

These data are plotted in **Figure 9 and 10** respectively. The fluorescence results supported in the

UV-Vis experiments for both dyes. A significant degree of AF700 degradation occurred at pH 2 and 4, such that the peaks of the fluorescence curves were substantially smaller than that of the PBS control sample. Furthermore, the AF750 dye in pH 13 buffer showed minimal emission when excited at 749 nm. In contrast, the fluorescence spectra of the AF750 dye in the pH 12 solution seemed nearly tantamount to the control's fluorescence. These findings confirm the validity of the absorbance spectrum for pH 12, which was also similar to the absorbance curve of the PBS solution.

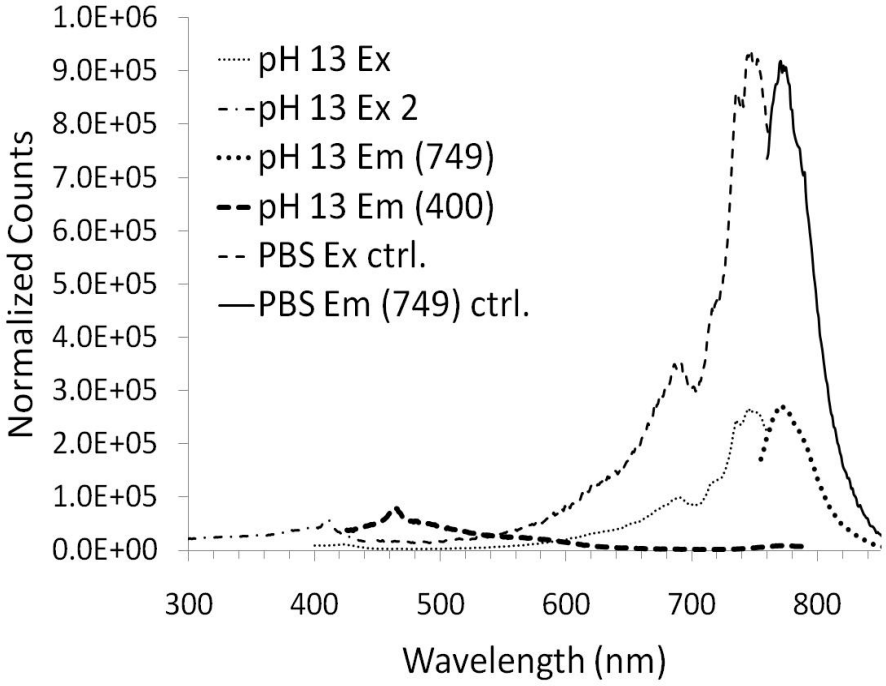

Figure 9: Figure Fluorescence of the AF750 dye in pH 12 buffer on day 2.

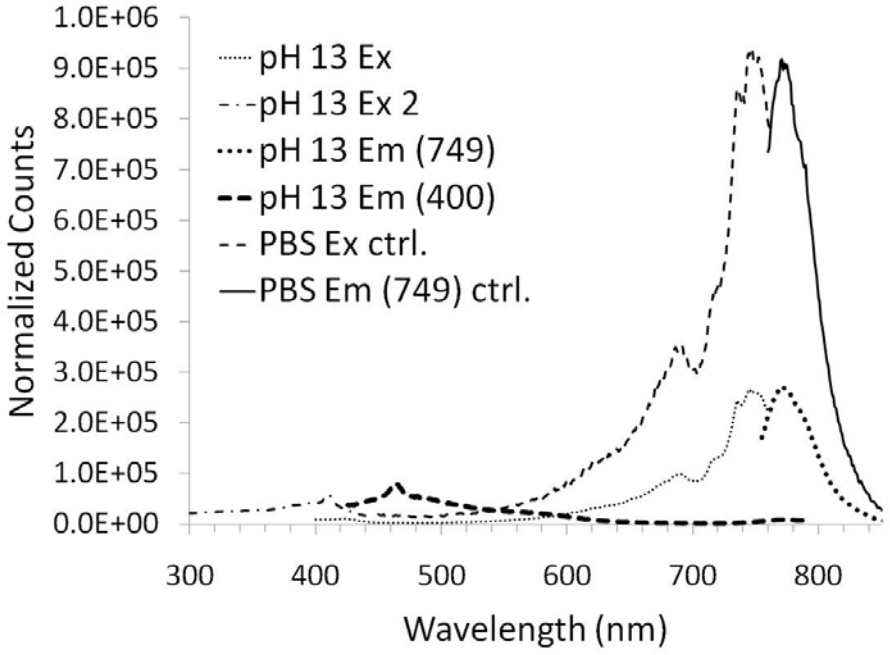

Figure 10: Fluorescence of the AF750 dye in pH 13 buffer on day 2.

Reversibility of Dyes

AF700

After determining the effect of pH on the NIR-dyes, AF700 and AF750, the possibility of reversibility was explored. If the dyes get degraded in solutions of extreme pH, can the solutions be returned to pH 7 and regain functionality as a FRET pair that can be used in cancer imaging? The results of the reversibility experiment for AF700 are presented in **Figures 11 – 13**. **Figure 11** shows the results of the absorbance measurements of day five and nine samples originally at pH 2 and 4 by showing the change in O.D. at 691 nm relative to absorbance the control sample. The absorbance spectra of the day-five AF700 samples, originally solubilized in pH 2 and pH 4 solutions and subsequently neutralized to pH 7, appeared to be reversed to a curve similar to that of the pH 7 control. However, by day nine, only the sample at pH 4 was reversible. In addition to absorbance, we tested the reversibility by fluorescence. **Figures 12 and 13** demonstrate that the fluorescence of AF700 on day one in pH 2 and pH 4 buffers is reversible (determined by peak shape, not amplitude).

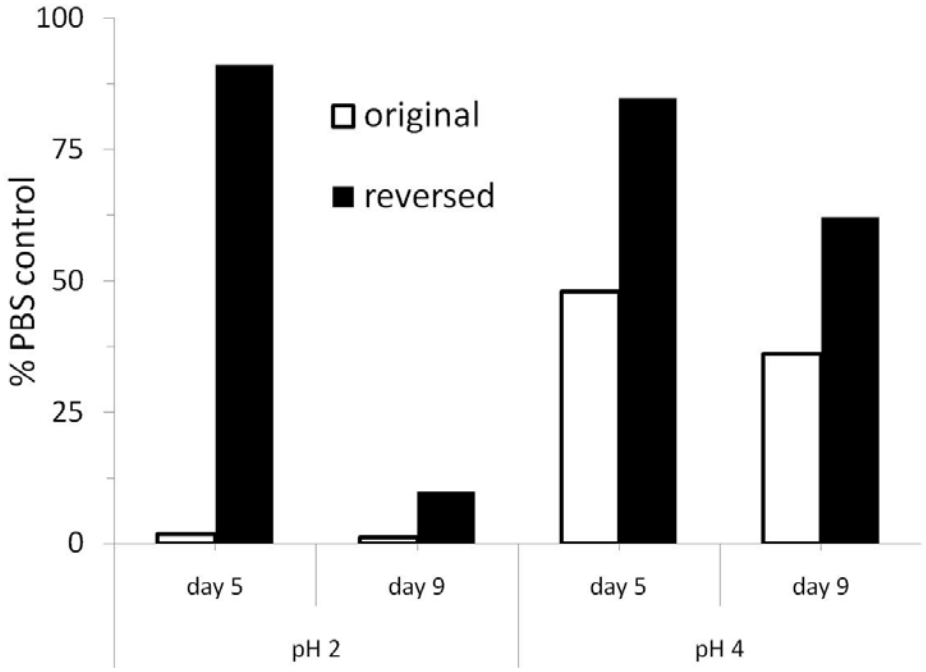

Figure 11: Comparison of absorbance of AF700 at 691 nm *vs.* pH 7 control. White bars represent absorbance before reversibility. Black bars represent AF700 dye that was neutralized to pH 7.

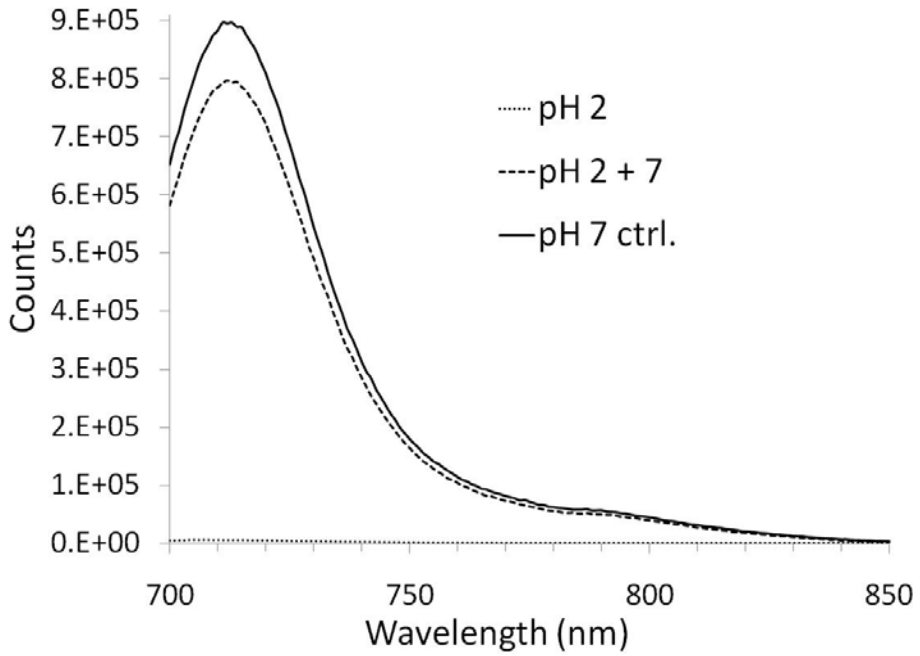

Figure 12: Reversibility of fluorescence of AF700 for day one samples with pH 7 as a control.

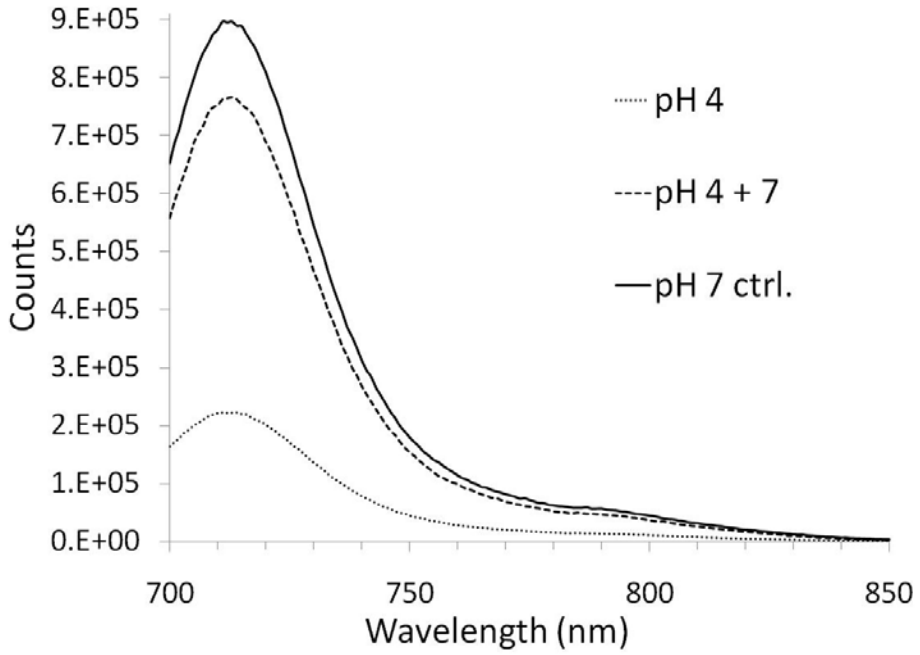

Figure 13: Reversibility of fluorescence of AF700 for day one samples with pH 7 as a control.

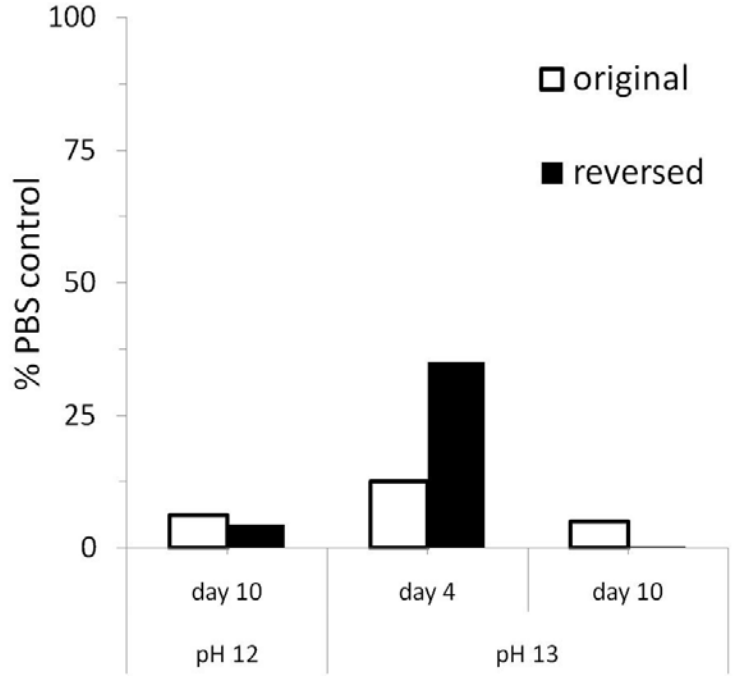

Figure 14: Comparison of absorbance of AF750 at 749 nm *vs.* pH 7 control. White bars represent absorbance before reversibility. Black bars represent AF750 dye that was neutralized to pH 7.

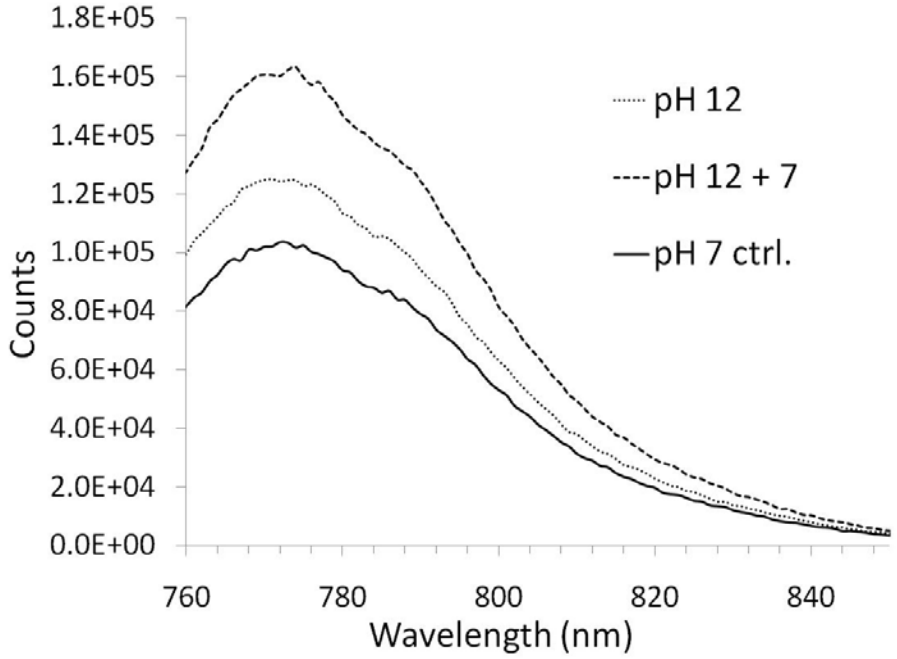

Figure 15: Reversibility of fluorescence of AF750 for day one samples with pH 7 as a control.

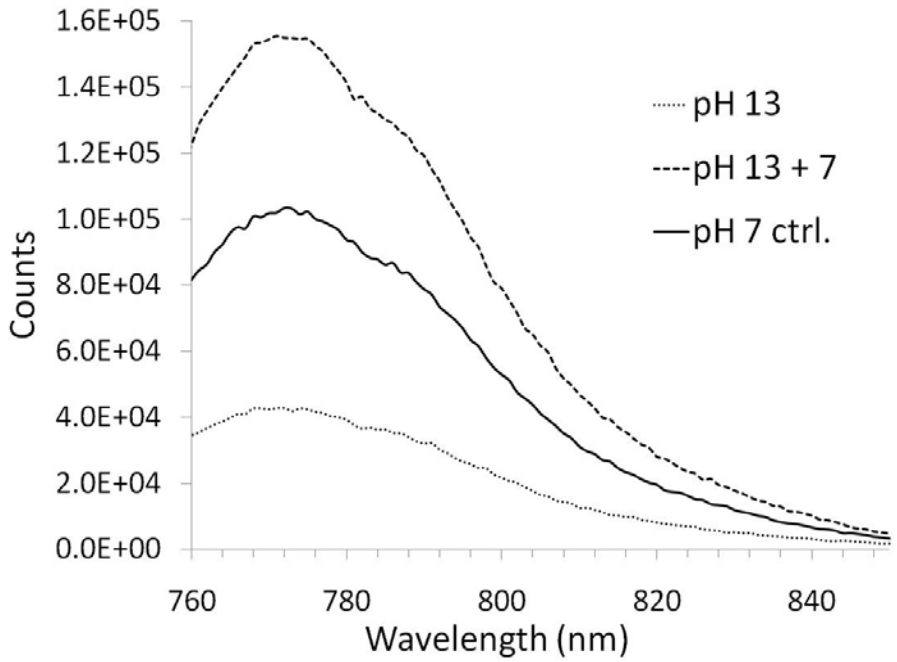

Figure 16: Reversibility of fluorescence of AF750 for day one samples with pH 7 as a control.

AF750

The reversibility of AF750 was tested in the buffers where deterioration of the dye occurred. **Figure 14** shows that the deterioration of the dye at pH 13 is not significantly reversible on day four, and neither pH 12 nor pH 13 is reversible by day ten. According to **Figure 15 and 16**, however, the fluorescence of both solutions appears reversible on day one.

Discussion/Conclusion

Proteolytic beacons (PBs) are used for *in vivo* optical imaging of tumor-associated proteinases. Cancer researchers in the Matrisian laboratory use PBs as an effective method of imaging cancer in mice, which are the most prevalent test subjects used in cancer studies. Furthermore, mice are useful in PB experiments because NIR light can better penetrate their bodies because they are small. Many types of dyes can be used as PBs, but near-infrared (NIR) dyes are becoming increasingly more prominent for *in vivo* optical imaging (OIM) (Scherer 2008 – B). OIM using NIR dyes is superior to imaging with visible dyes because the energy of light in the NIR window allows for minimal interference by tissue, thereby maximizing the quality of the image.

AF700 and AF750 are NIR dyes that form a FRET pair, and this phenomenon can be exploited by attaching them to protease substrates to make PBs, which can be used for cancer imaging. The purpose of this research is to improve the image quality of NIR-PBs by obtaining a comprehensive understanding of the effect of pH on AF700 and AF750. During the preparation and synthesis of PBs, purification steps are often necessary that require extreme pHs. Also, the pH of the fluid in laboratory animal tissues can vary from 7.2 to 7.4 in healthy tissues, and as low as 6.6 to 7.0 in tumors (Gillies 2004). Therefore, with knowledge of how acidic or basic environments can affect NIR dyes, PBs can be utilized to image tumors more effectively *in vivo*.

The practical pH range and stability of each dye was determined in this research. On day one, the AF700 dye can be exposed to environments between pH 6-10 and can maintain stability for at least nine days. The AF750 dye can be utilized in solutions of pH 2-12 on the first day, but only solutions of pH 8-11 remain stable for at least ten days. While the AF700 dye has a smaller pH range of effectiveness on day one, it is significantly more stable over time than the AF750 dye.

AF700 and AF750 were tested separately in these experiments. However, the dyes are used together as a FRET pair for cancer imaging. From the pH range of each dye, the effective pH range of the FRET pair can be determined. **Figure 17** shows part of the graphs of **Figures 2 and 5**.

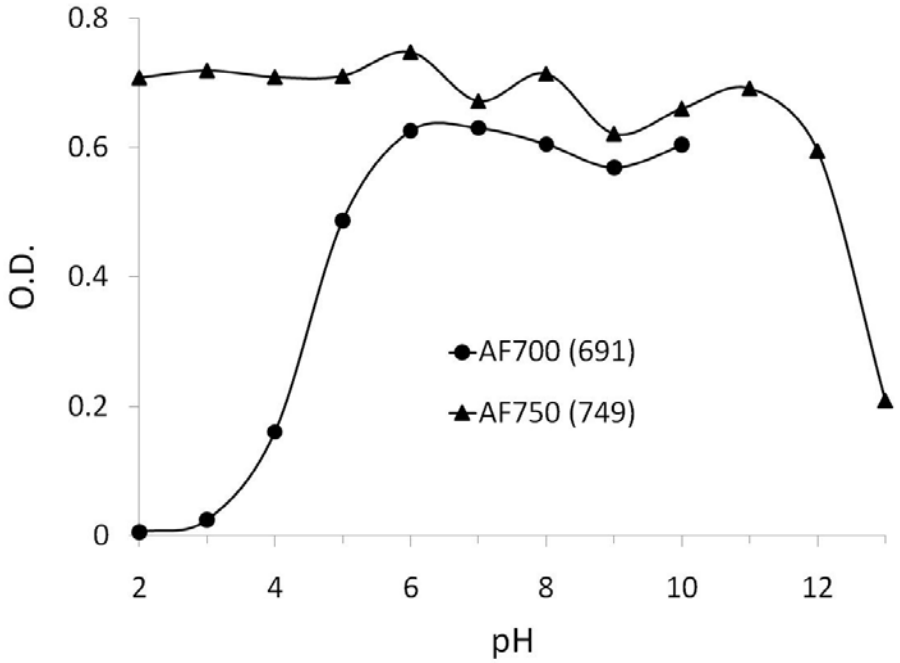

Figure 17: Absorbance of AF700 and AF750 on day one at wavelengths where absorbance should occur. These wavelengths in nm are specified in parentheses. The dashed black box shows where both dyes can maintain proper functionality.

The dashed box indicates the pH range where both dyes are effective on day one. Based on these data, it was determined that the AF700 and AF750 FRET pair works effectively between pH 6-10 on day one. After ten days, the range drops to pH 8-10 due to the instability of AF750.

The reversibility of degraded dye was also tested. The results indicated that the pH of both dyes can be manipulated between pH 3-12 during PB purification processes as long as the pH is restored to neutral on day one to recover effectiveness. Also, AF700 can be reversed more easily than AF750 due to its greater stability.

Additional experiments can be conducted to improve the quality of cancer imaging by NIR-PBs. Recall that a proteolytic beacon is composed of a scaffold called a Dendron, which is attached to a peptide with a dye on each end. Enzymes are extremely selective for their peptidic substrates. Therefore, depending on which enzyme is of interest, we need to determine the proper peptide to use. Experiments in our lab have begun to test the selectivity of various MMPs on certain peptides to be used in proteolytic beacons.

Literature Cited

Choy, G., Choyke, P., Libutti, S. K. (2003) Current Advances in Molecular Imaging: Noninvasive In Vivo Bioluminescent and Fluorescent Optical Imaging in Cancer Research. *Molecular Imaging*. 2: 303-312.

Gillies, R.J., Raghundand, N., Garcia-Martin, M.L.,Gatenby, R.A. (2004) pH Imaging. *IEEE Engineering in Medicine and Biology Magazine*. 23: 57-64.

Levin, C. S. (2005) Primer on molecular imaging technology. *European Journal of Nuclear Medicine and Molecular Imaging*. 32: 325-345.

Lyons, S. K. (2005) Advances in imaging mouse tumour models in vivo. *Journal of Pathology*. 205: 194–205.

McIntyre, J.O., Fingleton, B., Wells, K.S., Piston, D.W., Lynch, C.C., Gautam, S., Matrsian, L.M. (2004) Development of a Novel Fluorogenic Proteolytic Beacon for *In Vivo* Detection and Imaging of Tumour-Associated Matrix Metalloproteinase-7 Activity. *Biochemical Journal*. 377: 617-628.

Scherer, R. L., McIntyre J. O., Matrisian, L. M. (2008 - A) Imaging matrix metalloproteinases in cancer. *Cancer Metastasis Rev.* 27: 679-690.

Scherer, R. L., VanSaun, M. N., McIntyre, J. O., Matrisian, L. M. (2008 - B) Optical Imaging of Matrix Metalloproteinase-7 Activity In Vivo Using a Proteolytic Nanobeacon. *Molecular Imaging*. 7: 118-131.

List of Abbreviations

AF700	Alexa Fluor® 700 dye
AF750	Alexa Fluor® 750 dye
ECM	Extracellular Matrix
Em	Emission
Ex	Excitation
FRET	Förster Resonance Energy Transfer
MES	4-Morpholineethanesulfonic acid
MMP	Matrix Metalloproteinase
NIR	Near-infrared
O.D.	Optical Density
OIM	Optical Imaging
PB	Proteolytic Beacon
PBS	Phosphate-Buffered Saline
Tris	Tris(hydroxymethyl)aminomethane
UV-Vis	Ultraviolet-Visible

Acknowledgments

I would like to thank the members of the Matrisian Laboratory at Vanderbilt Ingram Cancer Center. I sincerely appreciate the opportunity to work under the guidance of Dr. Lynn Matrisian, the Endowed Chair of Cancer Biology at Vanderbilt, and my mentor, Dr. Oliver McIntyre. Every day during the summer, whenever I needed help, Dr. Samantha Soebbing was always there to explain things to me. She always treated me like a colleague and not a high school student. I am also indebted to other members of the Matrisian team who helped me, especially Ian McFadden, Kathy Carter, Michelle Martin, and Lynn Samuelson.

I performed this research as part of the Center for Science Outreach Research Internship Program. I appreciate Dr. Stephanie Farmer for shepherding the interns through the process of working in a major research medical school. Special thanks to my father, Dr. Michael D. Allen, for helping me secure summer internships.

Tumor and Stromal Elements are Required for Macrophage Polarization Following Induced Lung Tumor Metastasis

Kevin Clavin
Pope John Paul II High School, Hendersonville

Abstract

Macrophages are the broadly defined cell population among the immune cell types infiltrating tumors. Early immune response macrophages, have been found to contribute to tumor cell killing, yet macrophage presence in tumors has been associated with poor prognosis. Two distinct macrophage activation states (M1/M2) have been reported. M1 macrophages are positively associated with a better prognosis, due to their tumor killing abilities. M2 macrophages in contrast, support tumor growth by releasing high levels anti-inflammatory cytokines and angiogenic factors. The purpose of this study was to investigate whether direct interactions between macrophages and tumor cells result in their polarization (M1 or M2 phenotype). The Lewis Lung Carcinoma (LLC) model was used to study macrophage phenotyping in vivo . LLC cells were implemented by tail vein injection to wild-type mice. Animals were euthanized on Day 12 post injection, chest was exposed, Broncho-Alveolar Lavage (BAL) cells were collected and lungs were harvested for macrophage phenotype characterization by Flow cytometry and histology. Injection of LLC cells to mice caused an increased number of total BAL cells, specifically macrophages. Flow cytometry showed increased expression of both M1 and M2 macrophage markers. Immunohistochemistry staining of lung sections for the M2 marker Arginase 1 revealed both arginase positive and negative macrophages surrounding tumors.Macrophage polarization was investigated in vitro by direct co-culture with MLE12 lung epithelial and MC38 colon cancer cells. Incubation of bone-marrow derived macrophages (BMDM) with tumor cells resulted in increased expression of M1 markers CD80/CD86, but unchanged expression of the M2 markers, the Scavenger and Mannose receptors (CD204/CD206).

Introduction

Cancer claims millions of lives a year in the United States. Much research provides evidence that cancer is associated with inflammation within the tumor microenvironment. Inflammation is an occurrence in which immune cells are recruited to fight off a foreign threat, whether it be a bacteria, a wound, or in this case, a tumor. Inflammation, under normal conditions, is beneficial to the stability of the immune system; however, there are several factors that contribute to the pro-tumor activities as a result of inflammation. Several immune cell types define the tumor infiltrated area, but it has been determined that the population of these cells

within the tumor environment is broadly defined by the presence of white blood cells known as macrophages. Based on this fact, the presence of macrophages in tumors is linked to a poor prognosis in cancer patients (Colotta, F., Allavena, P., Garlanda, C., & Mantovani, A. (2009).

Macrophages serve a vital role in immune defense, but their function in tumor infiltration has been found to vary. These cells originate in the bone-marrow, and they are activated upon recruitment. Their main function in the immune system is to act as an APC (antigen-presenting cell). They engulf, through a process known as phagocytosis, foreign bodies and present to other immune cell types (such as T cells and B cells), communicating through the exchange of receptor proteins known as cytokines and chemokines (Fogg, D., Sibon, C., Jung, S., Aucouturier, P., Littman, D. & Geissmann, F. (2006). However, in tumor association, macrophages are known to play a dual role due to the wide range of phenotypes they express. The first phenotype, known as M1, relates to pro-infammatory macrophages that perform cytotoxic activities, suppressing tumor growth and metastasis. They are classically activated, or by a cytokine known as interferon-gamma (IFN-γ), or a bacterial cell wall component known as a lipopolysaccharide (LPS). Tumor necrosis factor-alpha (TNF) is a ctyokine that induces the anti-tumor activities of macrophages. These components are received by macrophages and activate pro-inflammatory cytokines such as Interleukin-1 and Interleukin-12 (IL-1, IL-12). Another key component of M1 macrophages is the production of inducible nitric oxygen synthase (iNOS), produced through activation by IFN-γ, produce nitric oxygen that give macrophages their cytotoxic characteristics (Redente, E.F., Orlicky, D.J., Bouchard, R. J., & Malkinson, A.M. , (2010).

There are also tumor-supporting macrophages possessing an M2 phenotype, also known as tumor-associated macrophages (TAMs). These macrophages are alternatively activated by two cytokine pathways known as the interleukin-4 and interleukin-13 (IL-4 and IL-13) (Gordon,

S. & Martinez, F. O., (2010). They result in the up regulation of anti-inflammatory cytokines such as the mannose and scavenger receptors (CD206 and CD204), IL-10, among several others (Redente, 2010). Another marker of M2 macrophages whose role is unknown in regards to tumor activities is a factor known as Migration Stimulating Factor (MSF) (Solinas, 2010). Through release of growth factors that promote angiogenesis, as well as the production of Arginase-1 (ARG-1), which suppresses the production of cytoxic NO, M2 macrophages inhibit TFN production, allowing metastasis to occur. Studies confirm that the majority of macrophages within a tumor are of the M2 phenotype (Colotta & et al., 2009).

The presence of M1 macrophages can correlate to the survival of cancer patients. A study involving humans with non-small lung cancer (NSLC) was performed to study whether M1 forms of macrophages are positively associated with survival time. 100 tissue samples were taken from patients with NSLC, 50 with a long term survival rate and 50 with a short survival rate. Following immunohistochemistry analysis (staining for the presence of M1/M2) of the samples, it was proven that patients given a long term of survival have proven to possess a higher density of M1 macrophages compared to patients with a short survival rate (Ma, J., Liu, L. , Che, G. , Yu, N., Dai, F., You, Z., (2010).

However, the number of M1/M2 polarized macrophages fluctuates throughout the period of time the tumor has been present. This was proven by a study on mice with lung tumors following urethane treatment (a method of inducing lung tumorigenesis). Part of the study included a long-term evaluation of macrophage polarization in different time intervals. Initially, there are both M1 and M2. As tumors that are not detected continue to exist in their normal form, more macrophages are polarized towards M2, and fewer M1 macrophages exist. This continues until tumor metastasis and angiogenesis have occurred. At that point, macrophages stop M2

polarization. (Redente & et al., 2007). Therefore, due to their ability to switch phenotype, recognizing the numbers of macrophages of a certain phenotype in the early stage is crucial to patient prognosis.

The location of macrophages in relation to the tumor is also an important way of recognizing their role in infiltration, known as microlocalization. The tumor microenvironment is comprised of several components. Macrophages located in the stroma, or surrounding blood vessels, are associated with a poor prognosis. This is due to the interactions of macrophages and stromal cells that contribute to the "angiogenic switch," promoting metastasis by carrying tumors into the bloodstream to other areas of the body. However, macrophages in the islets, away from blood vessels, are associated with a better prognosis in patients. This is most likely due to the fact that they are not going to possess angiogenic factors and are more likely to possess tumor suppressing qualities (Ma & et al., 2010). Location of macrophages in tumors is key to determining survival time of macrophages.

Still, an unanswered question within macrophage phenotype polarization is whether direct interaction of macrophages with tumors results in a M2 polarization. Understanding the interactions of macrophages only within a tumor environment can lead to therapeutic advances in cancer patients. If macrophages are polarized towards M2 in the presence of tumors, then several components can be targeted to inhibit the M2 phenotype from polarizing. Then, classically activated macrophages can suppress tumor growth.

Methods and Materials

To study the macrophage-tumor interaction, both *in vivo* and *in vitro* models were constructed. For *in vivo*, six wild type mice (C57BL/6) were used, three of which were injected with $200x10^3$ Lewis Lung Carcinoma (LLC) cells, a well established model for the development

of lung tumors, via the tail vein. The other three mice were used as controls. Twelve days post-injection, the animals were euthanized by a CO_2 asphyxiation chamber. First, the lungs were washed three times with 0.8 ml of PBS through the trachea. The fluid from the lungs, or broncho alveolar lavage (BAL) fluid, was collected for total and differential cell counting to characterize the airway inflammation. 500 µl of each sample was cytospun for 10 minutes at 500 rpm onto microscope slides. Each slide was stained via the Diff Quick method (www.ihcworld.com). In order to count, different slides were placed under a microscope, and cells were counted based on immune cell type (lymphocytes, neutrophils, or macrophages). The lungs, following removal, were kept overnight in Bouin's fixative and surface tumors were counted.

The lung tissue was processed and sectioned onto slides for histological analysis (Hemotoxlyin and eosin stain and Arginase staining). A standard H&E stain protocol was used to detect the presence of tumors (www.ihcworld.com). An arginase (M2 marker) stain to determine location of the M2 phenotype was conducted; the primary antibody for the stain was the Santa Cruz sc-20150 (Arginase 1) and the secondary was a biotinylated secondary antibody. The protocol was one specific to the Blackwell Laboratory at Vanderbilt University. Arginase postive macrophages appeared red underneath a microscope, while arginase negative macrophages (M1) appeared purple. For characterization of macrophages by Flow cytometry, single cell suspensions from lungs of naïve and LLC injected mice were stained using anti-CD68, CD11b, CD80, CD86, CD204, and CD206 antibodies. A standard Flow cytometry protocol was used (www.cellsignal.com).

For investigation of macrophage polarization *in vitro*, bone marrow-derived macrophages (BMDMs) ($300x10^3$ per well in 6 well plates) were activated with 100 ng of E. coli lipopolysaccharide wall (LPS) or co-cultered directly for 72 hours with $6x10^5$ cells per well of

MLE12 lung epithelial and MC38 colon cancer cell lines. All cell counts were conducted using a hemocytometer. Flow cytometry was performed once again in the exact same manner as in the *in vivo* in order to determine macrophage polarization following the culturing.

Data and Analysis

In Vivo

BAL Study

Figure 1

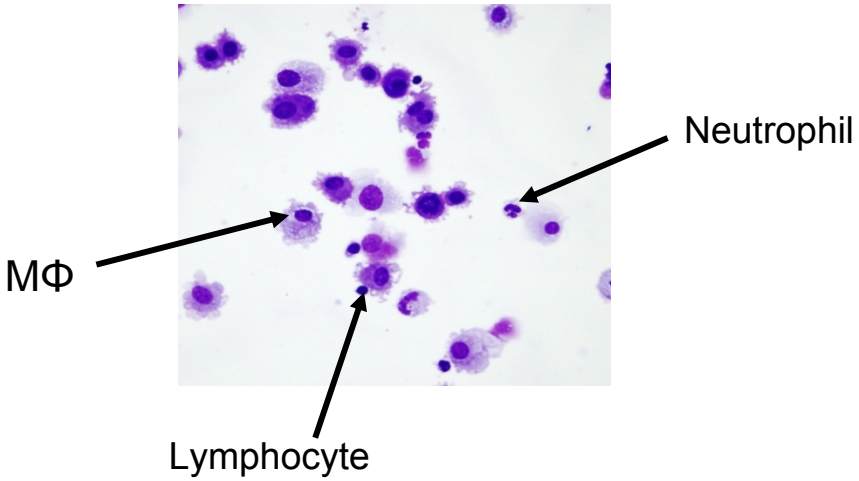

Figure 1 indicates an image taken on a microscope of a slide with a BAL sample. Each arrow indicates an immune cell type: Macrophages, Neutrophils, and Lymphocytes. Total numbers of these cells were taken from each sample and overall average was recorded.

Figure 2

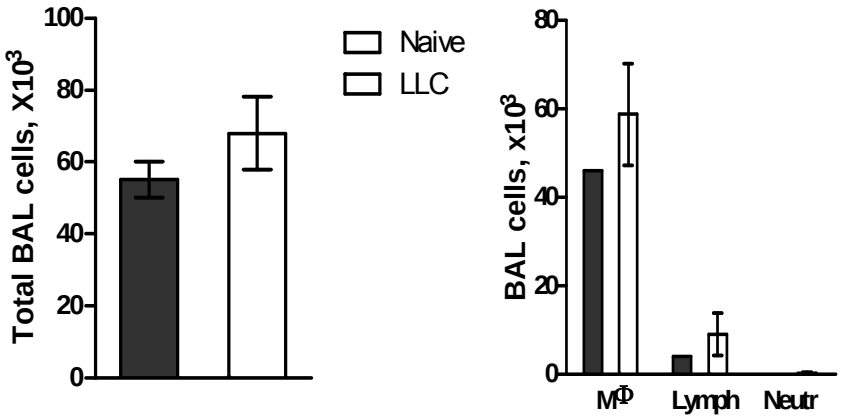

Figure 2 shows two graphs show the results from the BAL cell count. On the left, the graph shows an increase in total BAL cells following LLC injection, with around 60,000 cells

without LLC injection and 75,000 cells following LLC injection. The graph on the right characterizes the BAL cell types that made up the airway inflammation. Macrophages increased around 15,000, lymphocytes increased by about 5,000, and there were a small number of lymphocytes counted. As shown, LLC injection resulted in a primarily macrophage cell population infiltrating the area of airway inflammation. The error bars for this graph, as well as all graphs, indicate uncertainty in the cell counts.

Figure 3

H&E

Naïve LLC

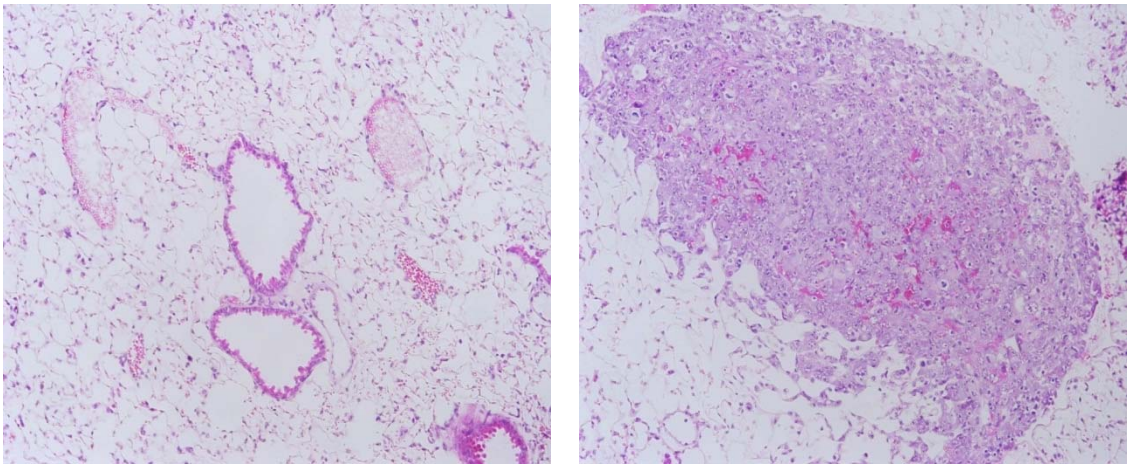

Lungs processed and embedded onto slides were used first for an H&E stain to detect tumor presence in the lungs, and the results of the stain are revealed in Figure 3. The first image on the left was taken of a naïve mouse (without LLC injection). No tumors were present in the lungs of the mouse. On the right, the image shows the lungs of a mouse injected with LLCs, showing the presence of a large tumor. Therefore, an interaction between macrophages and the tumor cell was going on.

Flow Cytometry

The lungs were also used for analysis by flow cytometry. Samples were marked for M1 (CD80 and CD86) and M2 (CD 204 and CD 206). Following preparation, the samples were run through the flow cytometer, which recognized the macrophage markers. The results are seen below.

Figure 4

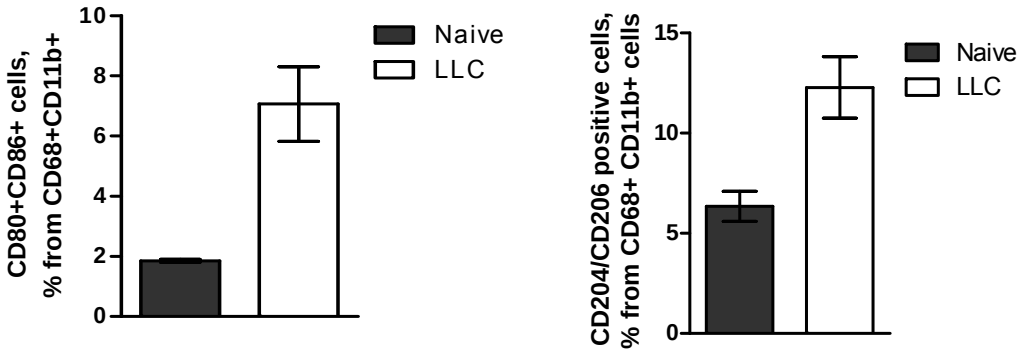

The two graphs show in *Figure 4* the percentage of M1 (left) and M2 (right) macrophages marked in the samples in both a normal mouse and one with tumors. M2 macrophages, as predicted, did increase in percentage following LLC injection (from about 7% to 13%). However, the graph on the left reveals a five percent increase in the M1 macrophages as well (2% to 5%).

Figure 5*: Arginase Staining*

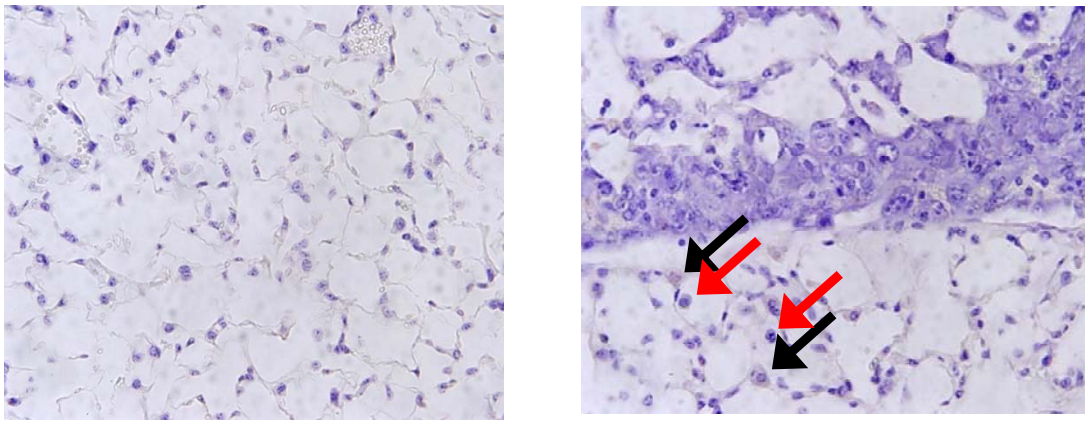

Figure 5 shows two samples embedded onto slides that were stained for Arginase (M2 marker) for determining location of polarized macrophages. The left image shows a naïve mouse, containing no tumors. However, on the right there is a tumor, therefore macrophages surround the tumor. It was predicted that tumor-macrophage interaction, causes an M2 polarization, meaning that only M2 macrophages would be within the microenvironment. M2 macrophages were located in the tumor microenvironment, indicated by black arrows (appearing slightly red). However, M1 macrophages, appearing deep purple in color (indicated by black arrows). This shows that M1 macrophages were around the tumor, thus disproving part of the hypothesis.

In Vitro

Tumor cells were cultured with bone-marrow derived macrophages for 72 hours to test whether direct macrophage-tumor interaction (without any other elements). Some wells were given 100 ng of LPS); M1/M2 polarization was determined by flow cytometry, using the same markers as the *in vivo* experiment.

Flow Cytometry

(***Figure 6***)

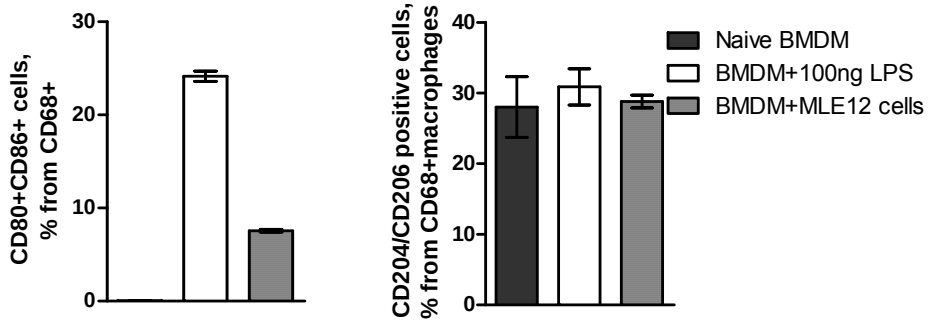

Figure 7

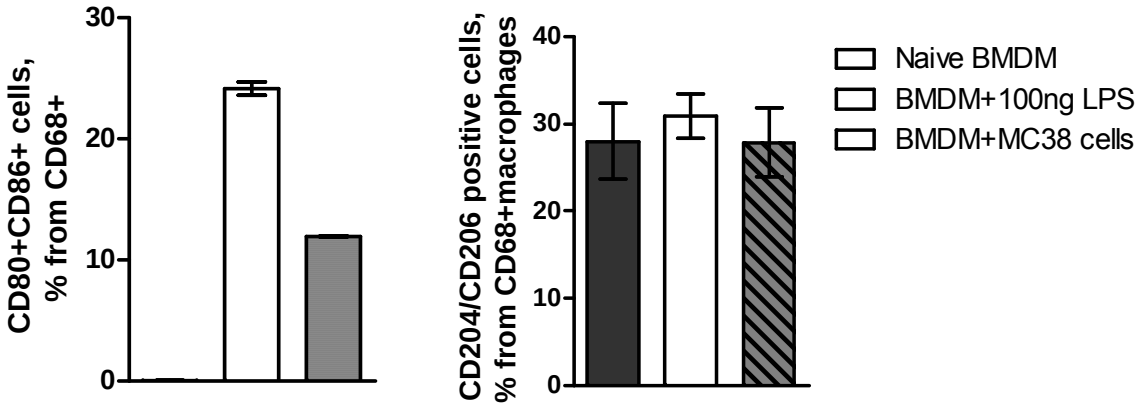

The results of flow cytometry are shown in *Figures 6 and 7*. *Figure 6* shows the results of the culturing macrophages and the first tumor cell line, MLE-12, while *Figure 7* shows results the macrophages cultured with the MC38 tumor cell line. Both studies yielded similar outcomes. On the left, M1 macrophages increased as a result of culturing (0-10%) and activation by LPS (0-25%). However, this study had no significant impact on M2 percentage, as the number of M2 macrophages stayed from its initial percentage of 25-30%. Therefore, M2 macrophage polarization is not a result of macrophage-tumor interaction.

Discussion

The data reveal multiple findings on M2 polarization, contrary to the previous prediction that M2 macrophages would polarize following direct interaction with the tumor cells. The *in vivo* model, shows that in the body, macrophage and tumor interaction caused an increase in both M1 tumor suppressive and M2 tumor supportive macrophages. Both types of macrophages were located near tumors, as shown in the Arginase stain. The data revealed in the *in vitro* model showed that macrophages tend to polarize towards an M1 phenotype when cultured directly with tumor cells, contrary to the hypothesis. Other factors are needed for M2 macrophage polarization when in contact with tumors.

These factors for M2 polarization are stromal elements, or outside the tumor, along with factors as released by tumors, as stated in the introduction. Most of these factors are released by surrounding immune cells that assist in the alternate activation of macrophages. It has been revealed that cytokines released by T-cells assist in acquiring the M2 phenotype. That is, when tumors are present, T-cells recruited by macrophages release certain factors that are received by macrophages, and these signals cause macrophages to obtain the pro-tumor characteristics, or the M2 phenotype (Montovani, 2002). Another study indicates the link between B-cells (lymphocytes that play a large role in the immune response) and M2 polarization. The figure below supports this.

Figure 8

Interaction Between Macrophages and B cells in Tumor Metastasis

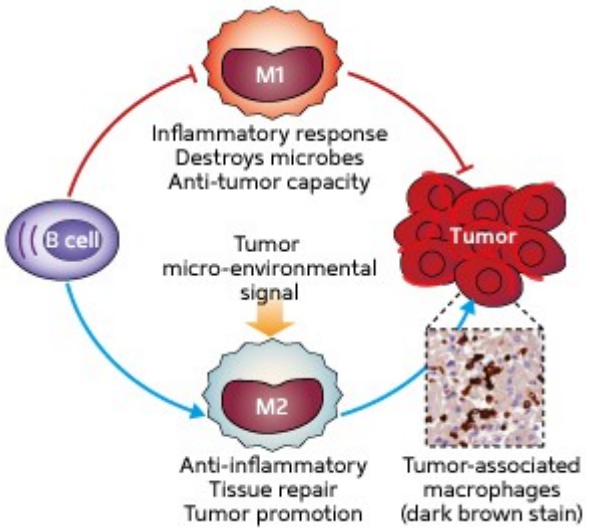

(Wong, 2010)

Figure 8, taken from a study on the correlation between B cells and macrophage polarization, suggests that while B-cells are recruited by M1 macrophages when tumors are recognized, B-cells release factors that cause the M2 polarization, and tumor growth continues.

Lymphocytes, as well as neutrophils, release factors for the support of tumors by the M2 phenotype (Wong, S.C, Puaux, A.L., Chittezhath, M., Shalova, I., Kajiji, T.S., Wang, X., 2010).

Figure 9

Stromal Elements of Immune Cells in Macrophage Polarization

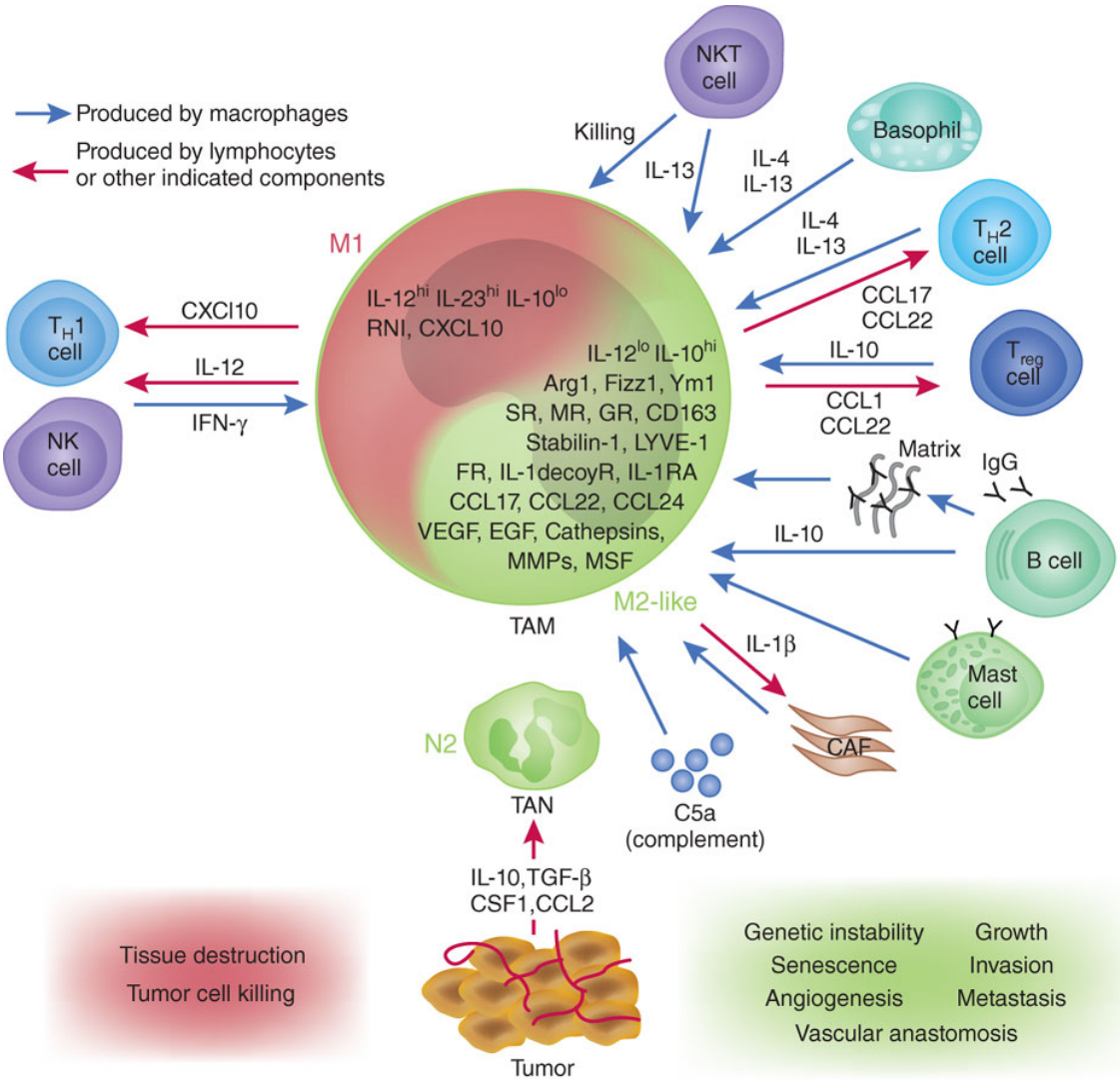

(Mantovani, 2010)

Figure 9 shows an image taken from another study expanding on the interactions of other immune cells and macrophages that promote M1 or M2 polarization. The image, there are several factors released by both macrophages and several immune cell types that lead to

polarization. Macrophages communicate with immune cells that cause the release of these factors. There are more interactions between immune cells and macrophages that lead to a polarization of the M2 phenotype, and metastasis is more likely to occur as a result (Mantovani, 2010).

Recognizing these factors will assist in clinical trials to stop the continued growth of tumors. Certain methods may result in induced activation of the M1 macrophage phenotype. For example, certain mechanisms can include the effects of the reactive oxygen and nitrogen of M1 macrophages, as well as effects of the recruitment of the cytotoxic T cells. Inducing these reactions around tumors might cause the polarization of M1 macrophages, which would prove therapeutic for cancer patients (Ohno, 2002). Another therapeutic method could be blocking the CREB-C/EBPβ protein pathway responsible for the production of Arginase, the characteristic of the M2 phenotype, which is also responsible for anti-inflammatory and pro-tumor activities of the M2 phenotype. Blocking the pathway could result in the up regulation of cytotoxic iNOS, a key characteristic of the M1 phenotype (Nerlov, 2009). The ability of blocking the M2-promoting factors shown in Figure 9 could prove to be clinically successful as well. The inability for immune cells to produce these factors could allow more M1 associated factors to be produced

One limitation in the study was the CD68 marker for identifying macrophages. The marker is used for many macrophage studies, but it has been a proven marker for dendritic cells, possibly indicating not all CD68 expressing cells were macrophages. An important modification would be to use multiple markers for macrophages (Ma & et al., 2010).

Summary

Injection of LLC cells to wild-type mice increased airway inflammation mostly due to recruitment of macrophages. Following analysis of lung macrophage phenotype on Day 12 post LLC injection, the data showed increased expression of both M1 and M2 macrophage markers. Direct co-culture of bone marrow-derived macrophages with tumor cells *in vivo* increased expression of M1 macrophage markers did not change expression of M2 markers. In conclusion, the data show that direct interaction of macrophages with cancer cells can induce M1 polarization; however, induction of macrophages with the M2 phenotype likely requires the presence of additional stromal components in tumors.

Literature Cited

Biswas, S. K., & Mantovani, A. (2010, September). Macrophage plasticity and interaction with lymphocyte subsets: cancer as a paradigm. *Nature Immunology*, 889-896. doi:1038/ni.1937

Colotta, F., Allavena, P., Sica, A., Garlanda, C., & Mantovani, A. (2009, May). Cancer-related inflammation, the seventh hallmark of cancer: links to genetic instability. *Carcinogenesis, 30*(7), 1073-1081. doi:10.1093/carcin/bgp127

Diff-Quick (Diff-Quik) Staining Protocol. (n.d.). Retrieved July 6, 2010, from IHC World website: http://www.ihcworld.com/_protocols/special_stains/diff_quick_ellis.htm

Flow Cytometry Protocol for Extracellular Staining Using Conjugated Secondary Antibodies. (n.d.). Retrieved June 23, 2010, from Cell Signal Technology website: http://www.cellsignal.com/support/protocols/4744_flow.html

Fogg, D., Sibon, C., C, M., Jung, S., Aucouturier, P., Littman, D., . . . Geissmann, F. (2006, January). A clonogenic bone marrow progenitor specific for macrophages and dendritic cells. *Science, 6*(331), 83-87.

Gordon, S., & Martinez, F. O. (2010, May). Alternative Activation of Macrophages: Mechanism and Functions. *Immunity, 32*(5), 593-604.

Hematoxylin and Eosin (H&E) Staining Protocol. (n.d.). Retrieved July 6, 2010, from IHC World website: http://www.ihcworld.com/_protocols/special_stains/h&e_ellis.htm

Kisley, L. R., Barrett, B. S., Bauer, A. K., Dwyer-Nield, L. D., Barthel, B., Meyer, A. M., . . . Malkinson, A. M. (2002, December). Genetic Ablation of Inducible Nitric Oxide Synthase Decreases Mouse Lung Tumorigenesis. *Cancer Research, 62*, 6850-6856.

Ma, J., Liu, L., Che, G., Yu, N., Dai, F., & You, Z. (2010, March 25). The M1 form of tumor-associated macrophages in non-small cell lung cancer is positively associated with survival time. *BMC Cancer, 10*(112). doi:10.1186/1471-2407-10-112

Redente, E. F., Higgins, D. M., Dwyer-Nield, L. D., Orme, I. M., Gonzalez-Juarrero, M., & Malkinson, A. M. (2010, July). Differential polarization of alveolar macrophages and bone marrow-derived monocytes following chemically and pathogen-induced chronic lung inflammation. *Journal of Leukocyte Biology, 88*, 1-10.

Redente, E. F., Orlicky, D. J., Bouchard, R. J., & Malkinson, A. M. (2007, February). Tumor Signaling to the Bone Marrow Changes the Phenotype of Monocytes and Pulmonary Macrophages during Urethane-Induced Primary Lung Tumorigenesis in A/J Mice. *The American Journal of Pathology, 170*(2), 693-708. doi:10.1186/1471-2407-10-112

Ruffell, D., Mourkioti, F., Gambardella, A., Kirstetter, P., Lopez, R. G., Rosenthal, N., & Nerlov, C. (2009, September 24). A CREB-C/EBPβ cascade induces M2 macrophage-specific gene expression and promotes muscle injury repair. *Immunology, 106*(41), 17475–17480. doi:10.1073/pnas.0908641106

Solinas, G., Mantovani, A., & Allavena, P. (2010, June). Tumor-Conditioned Macrophages Secrete Migration-Stimulating Factor: A New Marker for M2-Polarization, Influencing Tumor Cell Motility. *The Journal of Immunology, 185*, 642 -652 . doi:10.4049/ jimmunol.1000413

Wong, S.-C., Puaux, A.-L., Chittezhath, M., Shalova, I., Kajiji, T.S. Wang, X., Abastado, J.-P., Lam, K.P. & Biswas, S.K. Macrophage polarization to a unique phenotype driven by B cells. European Journal of Immunology 40, 2296–2307 (2010).

Acknowledgements

Thanks in Particular to the Blackwell Laboratory at Vanderbilt University, especially to Rinat Zaynagetdinov for his dedication to mentoring me, and Timothy Blackwell for providing the research opportunity. Also thanks to Jennifer Dye and the Scholars of Science Research for reviewing and revising this paper.

The Effects of Surface Area, Distance, and Voltage on the Production of Hydrogen by Means of Short-Pulse Hydrolysis

Ahbid Zein-Sabatto, Vikas Kumar, Shuvajit Das, Ravikanth Konjeti
School for Science and Math at Vanderbilt, Nashville

Abstract

Methods of producing clean, renewable energy are costly and inefficient due to the current energy crisis. Fortunately, harnessing naturally occurring lightning can provide a revolutionary energy source, due to its high energy content. One example of utilizing lightning is the production of hydrogen through hydrolysis. This study simulated lightning-induced hydrolysis, by means of a voltage spike. The method used a variable power supply that charged two capacitors, which then rapidly discharged into an electrolytic water bath. Multiple tests were run: changing plate surface area, plate distances, and voltages to create an optimization curve to find the hydrogen production peak. The hydrogen bubbles were then collected by water displacement. Voltage had the greatest effect on hydrogen production; of the variables measured, increased voltage yielded more hydrogen. Additionally, the smallest surface area produced the most hydrogen. An optimization curve was developed, relating voltage, surface area of electrodes, and distance between electrodes to the amount of hydrogen produced: $Hydrogen\ Produced = 1.184e^{-3} \bullet voltage + 0.387e^{-3} \bullet distance - 4.80e^{-3} \bullet surface\ area - 3.19e^{-3}$. This experiment forms a foundation for developing methods to utilize lightning's energy more efficiently in practical applications.

Introduction

The world's energy infrastructure is undermined by the unavailability of reliable energy sources. One of the main energy sources, fossil fuels, is nonrenewable; it is outdated, environmentally toxic, and also scarce. However, clean renewable energy sources are either inefficient or not monetarily feasible. Lightning, a naturally occurring energy spike, has great potential in the new search for clean and effective energy; but lightning has still not been harnessed effectively, making it a widely open energy commodity.

Is lightning's energy even worth harnessing? It was calculated, based on the data provided by the U.S. Dept. of Energy, that one lightning strike can provide the entire city of Nashville 835.1 hours of usable energy (U.S. Department of Energy, 2008); since lightning is produced from voltage differences between the clouds and ground, it can generate up to $1.0e^{8}$ volts and $1.0e^{4}$ amps of current (Haramija, 1997). However, directly harnessing the raw power of lightning is risky, inefficient, and impractical, due to the transformation needed to reduce the voltage to grid-safe levels. Instead, indirectly using the power to produce hydrogen through short

pulse hydrolysis may prove to be more practical. Previous studies provide evidence that short pulses of electricity are capable of creating measurable amounts of hydrogen by hydrolysis, as long as the voltage is greater than 1.6V (Shimizu, 2005).

Hydrogen is more energetic than fossil fuels and only produces water as a byproduct of combustion. Hydrogen is produced currently by DC electrolysis, and this process draws in massive amounts of electricity from coal power plants, making it an unproductive and inefficient technique. Thus, creating hydrogen from a high energy source, such as lightning, would be beneficial. Production of hydrogen in this manner would greatly contribute to the emerging hydrogen industry. Possible uses of hydrogen include hydrogenation of food, fuel cell technology, and lighter than air flight.

In this experiment, lightning was simulated using capacitors and voltage; surface area and distance between electrodes during short-pulsed water electrolysis were examined in an attempt to find a feasible method of hydrogen production. An optimization curve was created to improve the efficiency of lightning induced hydrogen production. It was hypothesized that the optimization curve would be logarithmic, that the smallest surface area would produce the most hydrogen, the highest voltages would produce the most hydrogen, and that every plate size would have an ideal distance at which it would produce the most hydrogen.

Methods

Apparatus

A water bath with a specific gravity of 1.022 was obtained by mixing Instant Ocean® Sea Salt Mix (Kingman, AZ) with distilled water following directions accompanying the salt mix.

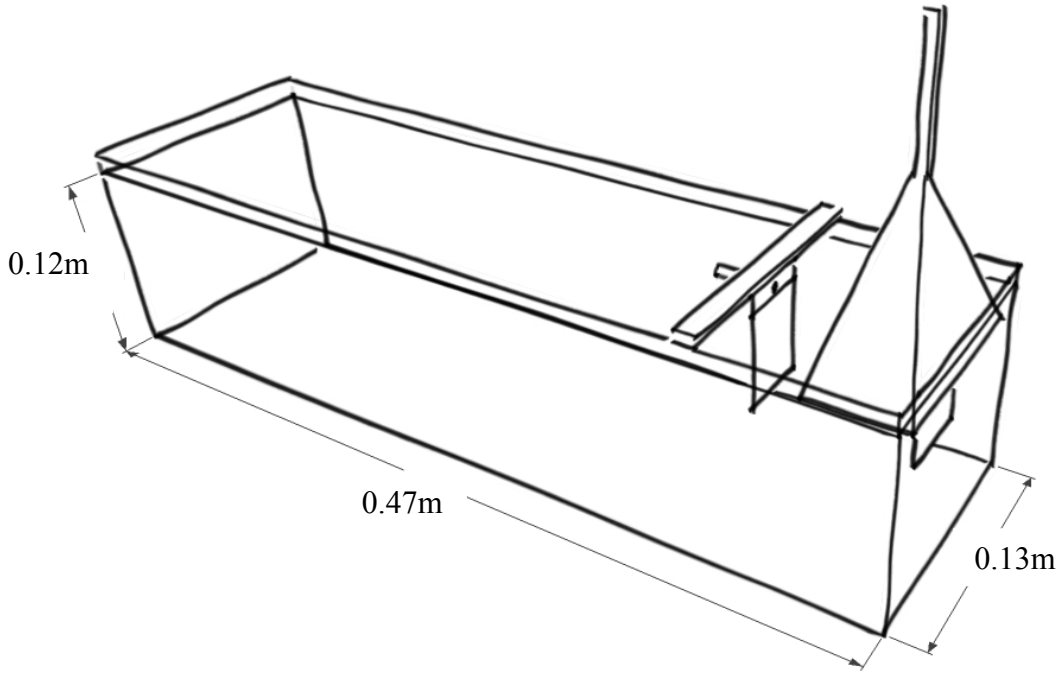

Figure 1. Water bath and hydrogen collection apparatus

The water bath shown in Figure 1 has the dimensions of 0.47m x 0.13m x 0.12m. The hydrogen collection appartus consisted of a rectangular pyrimid with the dimensions of 0.11m x 0.05m x 0.09m, with a 0.01m x 0.01m open passage on top, where a second rectangular piece with the dimensions of 0.07m x 0.015m x 0.01m was placed over the passage, with one end sealed to collect the rising hydrogen. Figure 2 displays an alternative view to the apparatus's setup.

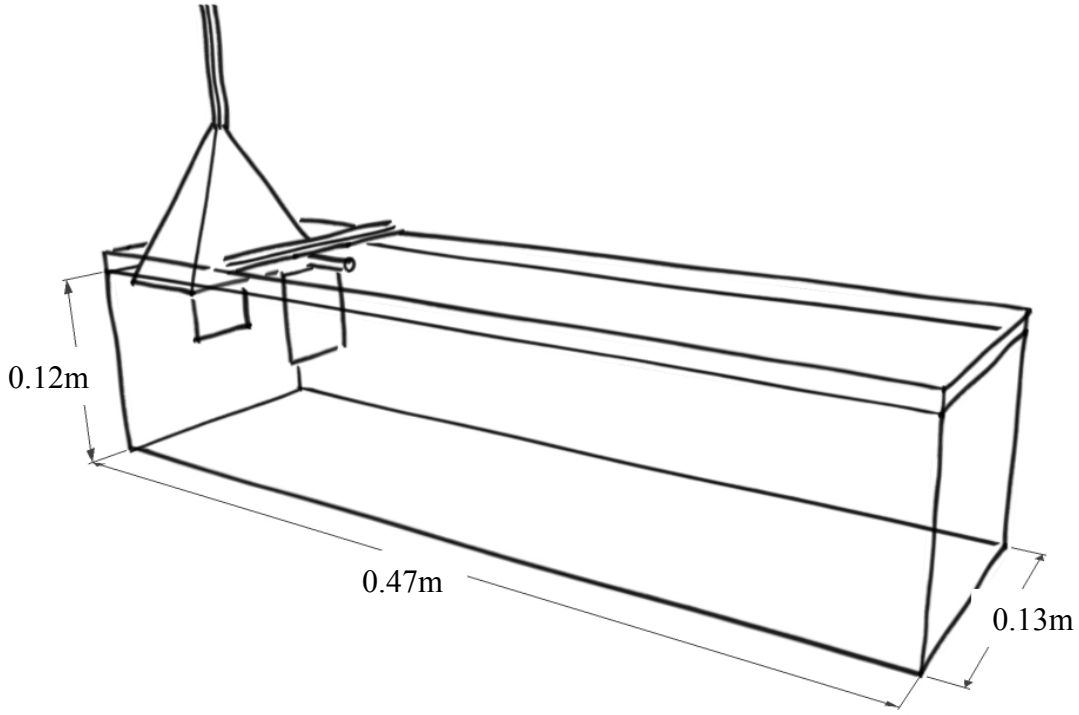

Figure 2. Water bath and hydrogen collection apparatus

Circuitry

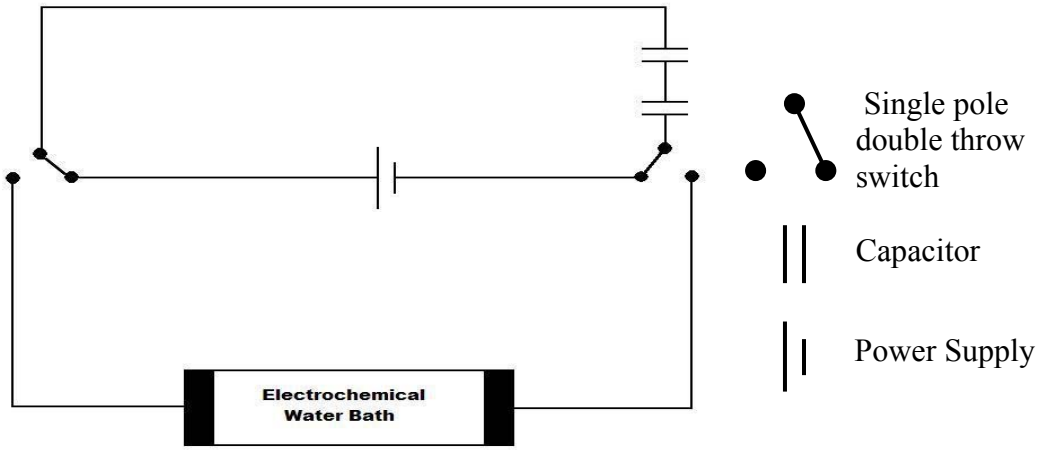

Figure 3. Circuit set up

Figure 3 illustrates the electrical circuit that was constructed for the experiment. First, the switches were used to connect the capacitors to the variable power source to charge the two 18-F

capacitors in a series circuit. The switches were then used to connect the capacitors to the water bath, allowing the capacitors to discharge into the water bath, creating a voltage spike mimicking a lighting strike.

Experimental Design

Optimum hydrogen production was determined by varying the applied voltage, plate surface area, and distance between plates were varied. Copper plates with surface areas of 2.54 x 5.08 x 0.0635 cm3 (1 x 2 x 0.025in^3), 2.54 x 7.62 x 0.0635 cm3 (1 x 3 x 0.025in^3), 5.08 x 5.08 x 0.0635 cm3 (2 x 2 x 0.025in^3), and 5.08 x 7.62 x 0.0635 cm^3 (2 x 3 x 0.025in^3) were submerged in the bath and attached to a hydrogen collecting apparatus as seen in Figures 1 and 2 in pairs. The plates will be referred to as 1x2, 1x3, 2x2, and 2x3, respectively. The plates were then tested for 15v, 30v, 50.8v, 75v, and 90v at 4cm, 7cm, 9cm, 11cm, and 13cm each.

Table 1. Number of discharges per voltage

Voltage (v)	Number of discharges
15	20 (30 for 2x3)
30	10
50.8	10
75	5
90	5

Quantifiable amounts of hydrogen were measured after multiple discharges, as seen in Table 1. The plates were scraped every 5 discharges to keep the plates clean, and the hydrogen was collected by means of water displacement after the capacitors were discharged and the hydrogen rose into the collection chamber forming a bubble at the tip. Hydrogen that collected at the sides of the chamber was scraped to the top before analysis. The hydrogen accumulated at the top of the collection chamber was then photographed for analysis and examined by the program GIMP. The volume of the final hydrogen bubbles was attained by using a ratio of pixel to centimeter measurements. Total hydrogen production per discharge was calculated after multiplying the width and length (0.624 cm x 0.657 m) by the resulting height, and dividing that by number of discharges.

Results

The experiment showed differing relationships between voltage, surface area, distance and hydrogen production. These relationships were used to create an optimization model. Incorporating the 3 variables, this equation could be used to hypothesize the amount of hydrogen production.

Figure 4 represents hydrogen produced per pulse in cm^3 versus voltage. The R^2 value for the linear regression is 0.941, a strong correlation. Hydrogen production clearly rises as voltage is increased.

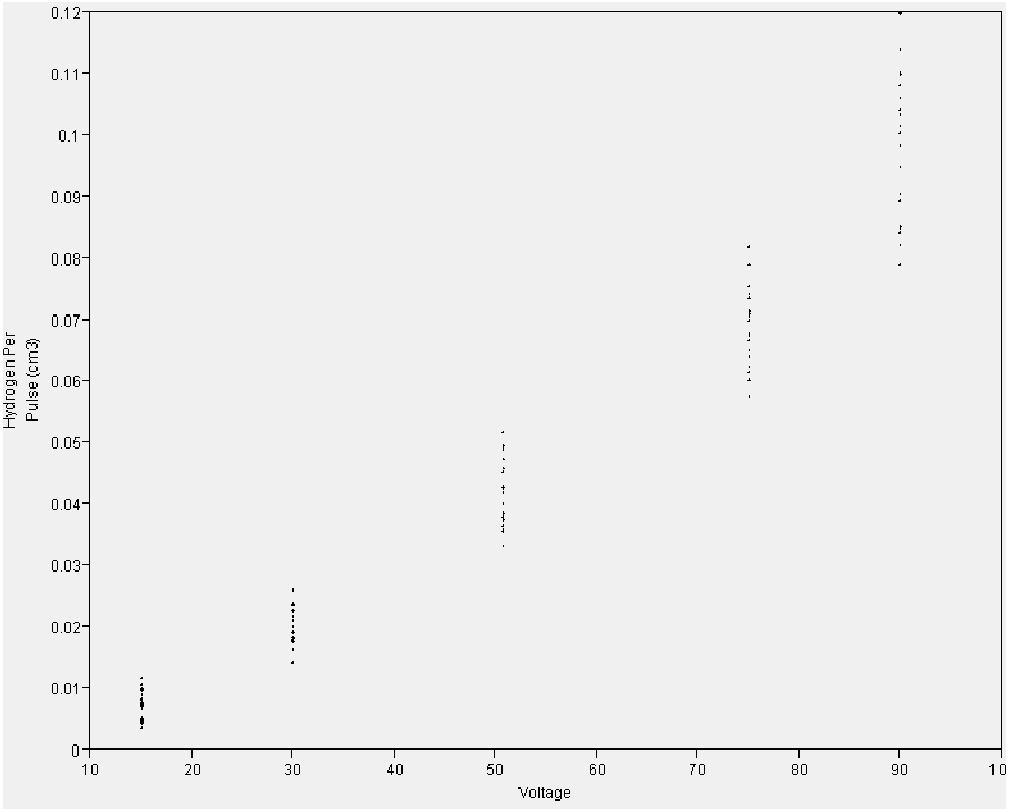

Figure 4. Hydrogen Produced per Pulse (cm^3) vs. Voltage

Figure 5 represents the relationships between volume of hydrogen per pulse in cm^3 and surface area. The R^2 values for each linear regression are as follows: 15v = 0.441; 30v = 0.262, 50.8v = 0.690, 75v = 0.0001, 90v = 0.892. Larger surface areas, evidently, caused drops in hydrogen production, and this pattern becomes more visible as voltage is increased. The 2x3 plate was excluded from the analysis because it had high variation, especially at low voltages. This variance skewed the results greatly, which caused a misrepresentation of the actual effect of surface area.

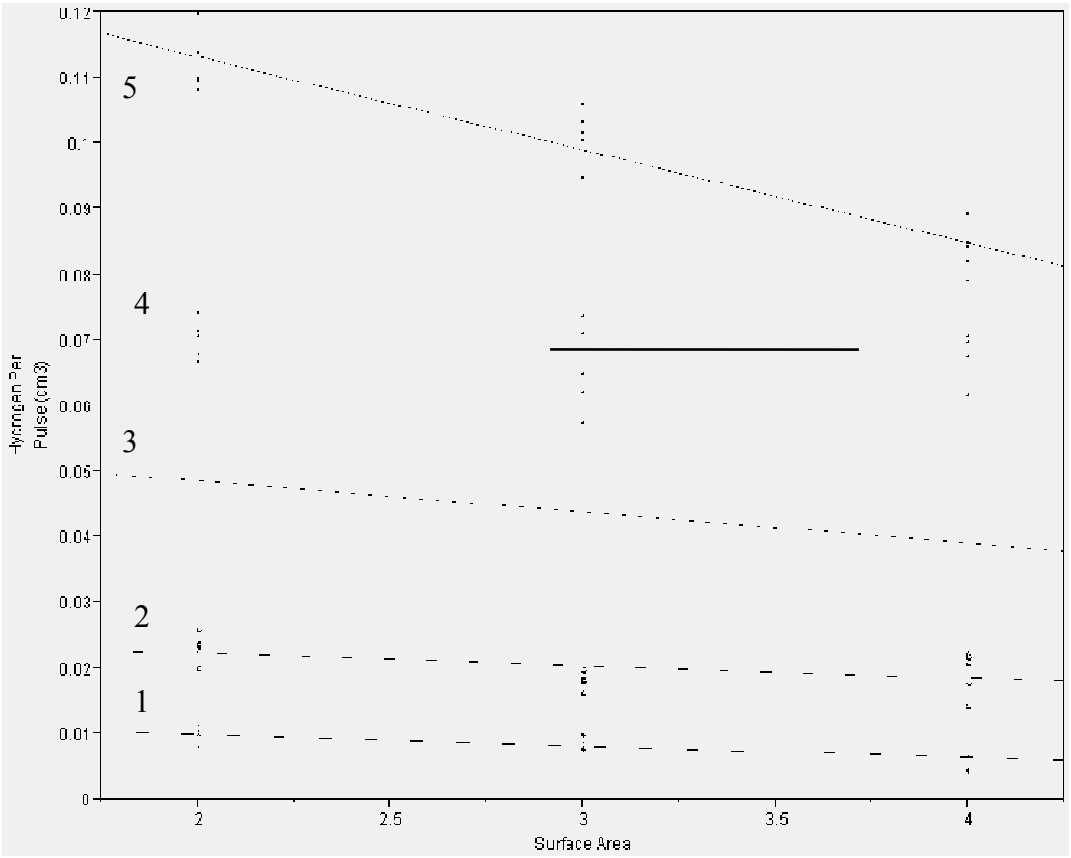

1. 15 volts
2. 30 volts
3. 50.8 volts
4. 75 volts
5. 90 volts

Figure 5. Hydrogen Produced per Pulse (cm^3) vs. Surface Area of Electrodes

The representation of hydrogen produced per pulse in cm^3 vs. distance is shown in Fig. 6. The R^2 value for each regression is given: 15v = 0.00907, 30v = 0.000898, 50.8v = 0.0184, 75v = 0.600, 90v = 0.00863. As expressed by these values, modifications to distance did not have significant trends.

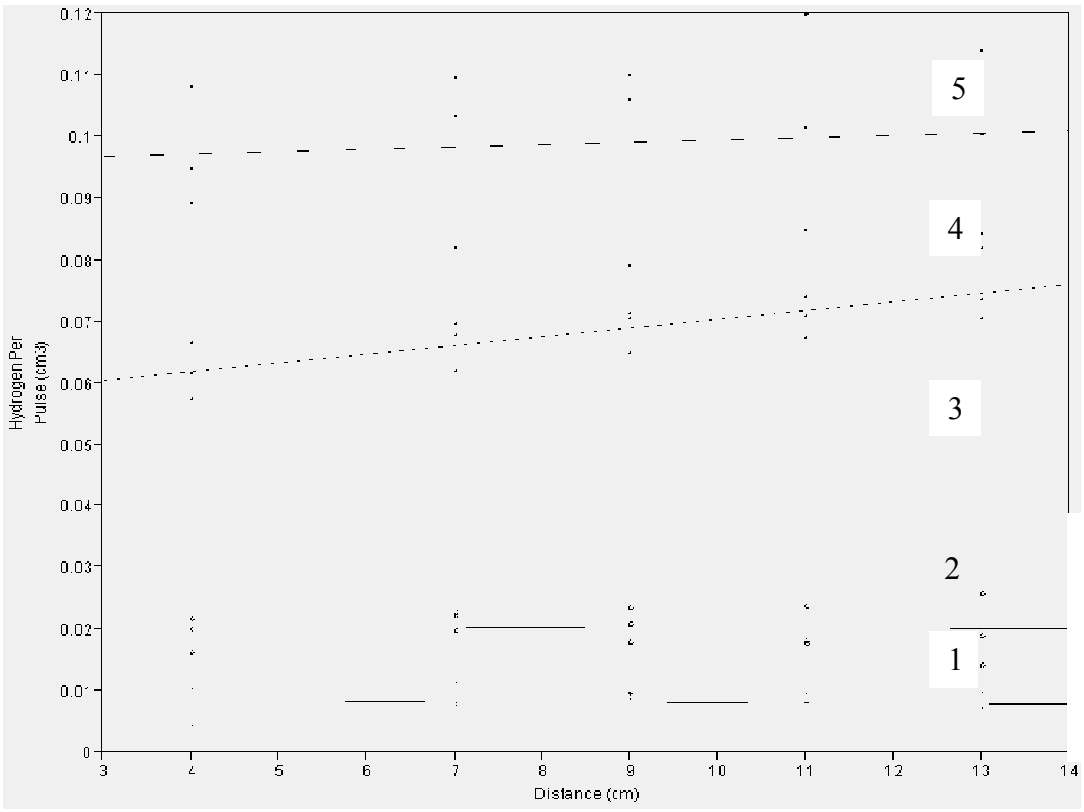

1. 15 volts
2. 30 volts
3. 50.8 volts
4. 75 volts
5. 90 volts

Figure 6. Hydrogen Produced per Pulse (cm^3) vs. Distance between Electrodes

Figures 7, 8, and 9 are 3D representations of hydrogen produced by each surface area, (excluding the 2x3 plate), relative to the distance and voltage applied. The 1x2 produced the most hydrogen at its peak and the 2x2 produced the least hydrogen. Hydrogen production peaked at different distances between the plate sizes. The 2x3 plate had high variation and was thus excluded from this analysis.

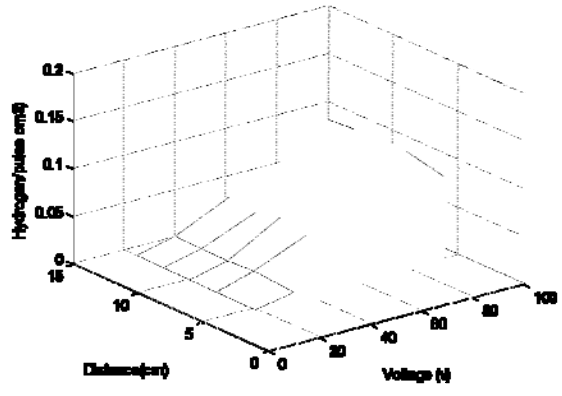

Figure 7. Hydrogen Production per Pulse for 1x3 Plate (peaks at 0.1061 cm^3)

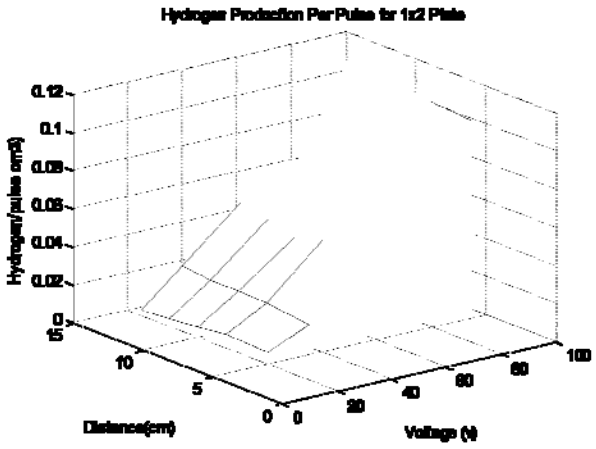

Figure 8. Hydrogen Production per Pulse for 1x2 Plate (peaks at 0.1197 cm^3)

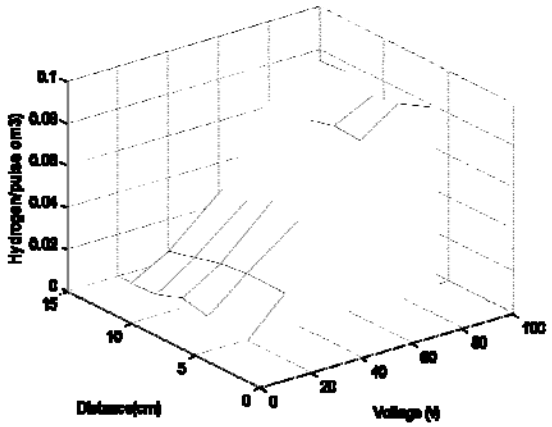

Figure 9. Hydrogen Production per Pulse for 2x2 (peaks at 0.0892 cm^3)

This graph represents the optimization regression that was calculated by the creation of a model by incorporating all variables into a function of actual hydrogen produced, to theoretical hydrogen, produced as dictated by the equation. The R^2 value was 0.95 and the p value was 0.00001. The optimization curve again excluded the 2x3 plate due to high variance (Fig. 10). The data were assigned a linear line of best fit.

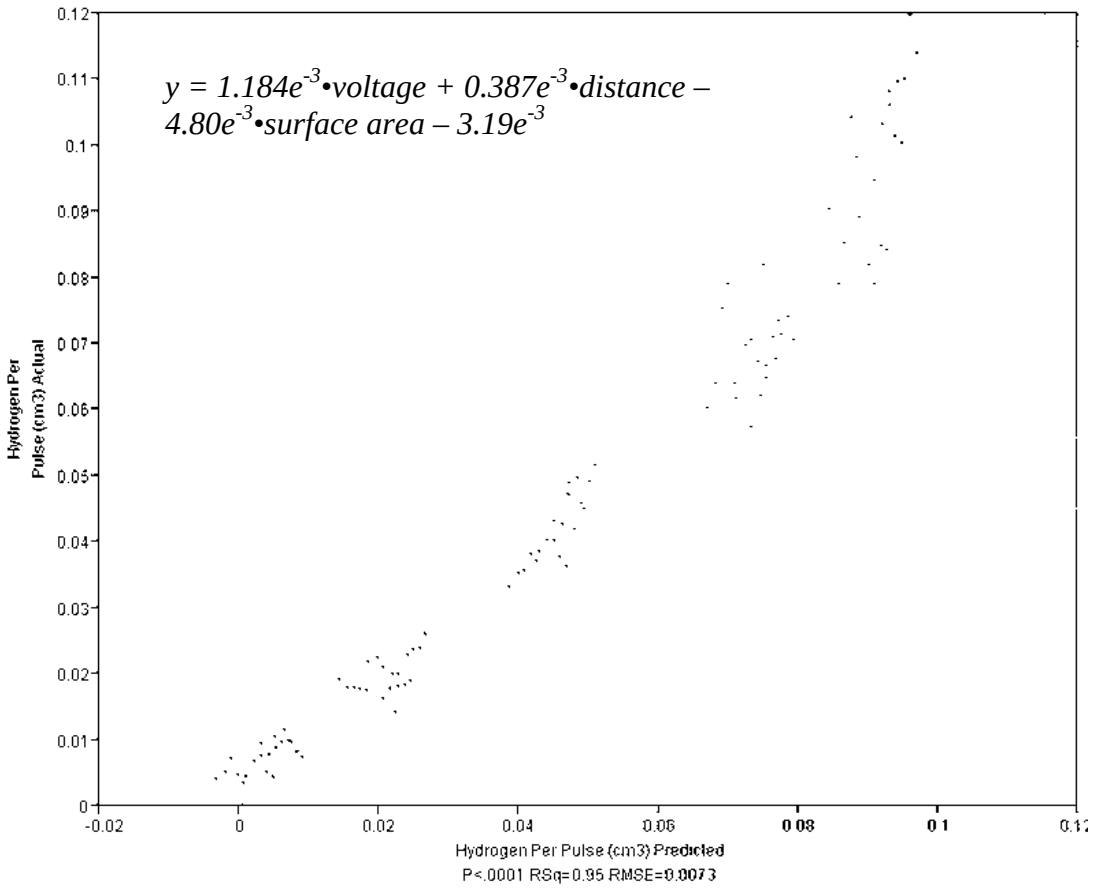

Figure 10. Optimization Curve without the 2x3 Plate

Conclusion

This experiment found the optimum surface area and distance between electrodes per given voltage in order to calculate hydrogen produced by short-pulsed hydrolysis. There is a strong positive trend indicating that as voltage is increased, the hydrogen production increases (Figures 4, 7, 8, and 9). A lesser trend shows that decrease in surface area results in greater hydrogen production (Figures 5, 7, 8, and 9) because a decreased surface area leads to longer exposure to the electric shock (Zein-Sabatto et al., 2010). The distance between electrodes also had barely any correlation (Figures 6, 7, 8 and 9). The 2x3 plate had high variation: a 13.897% coefficient of variation, as well as no conclusive trends. If the 2x3 were included in the optimization curve, then the coefficient of the surface area would change 188.387%; therefore it was excluded. Though a linear optimization curve was formulated, the data seemed to hint towards a rather exponential correlation. This is because the model deviates from a linear pattern, but most tests need to be done to confirm this. For example, as voltage increased five-fold,

average hydrogen production increased nine-fold. Therefore, future experiments need to be conducted to examine the effects of higher voltages, additional distances, as well as various other surface areas on hydrogen production, to allow for a better understanding of how these variables factor into total hydrogen production. Nevertheless, the hypothesis formulated was partially true concerning the effects of surface area and voltage on hydrogen production; however, not enough data were present to defend a logarithmic approach to the optimization curve and the effect distance had on hydrogen production. This research provides a fundamental step towards the practice of a method that would be highly beneficial in the generation and production of clean, renewable energy.

Literature Cited

Haramija, B. "Electric Current through a Lightning Bolt." *The Physics Factbook.* 1997. The Physics Factbook. 18 Nov. 2010 <hypertetbook.com/facts/1997/BrookeHaramija.shtml>

Shimizu N, S Hotta, T Sekiya, O Oda. "A novel method of hydrogen generation by water electrolysis using an ultra-short-pulse power supply." *Journal of Applied Electrochemistry*. **2005** (36):419–423.

Taylor, Y. "Consumption, Price, and Expenditure Estimates." *U.S. Energy Information Association.* 2010. U.S. Department of Energy. 18 Nov. 2010 <http://www.eia.doe.gov/states/_seds.html>

U.S. Department of Energy. "Tennessee Energy Consumption". *Energy Efficiency and Renewable Energy.* 2008. US Department of Energy. 9 Dec. 2010 <http://apps1.eere.energy.gov/states/electricity.cfm/state=TN#total>

Zein-Sabatto A, V Kumar, S Das. "Effects of Surface Area and Distance on Single Pulse Hydrolysis." School for Science and Math at Vanderbilt University Joint Symposium Poster Presentation; July 2010

cAMP Signaling Cascade Regulates Na-K-2Cl Cotransporter

Jenny S. Gray
Hume-Fogg Academic Magnet High School, Nashville

Abstract

SPAK (*S*te20p-related-*P*roline-*A*lanine-rich-*K*inase) and OSR1 (oxidative-stress-response-1) phosphorylate and activate the Na-K-2Cl cotransporter, NKCC1. It was necessary to determine whether the two kinases are part of the same signaling cascades. The activation level of SPAK and OSR1 were examined in HEK293 (human embryonic kidney) cells and exposed to drugs known to affect NKCC1 activity. Because NKCC1 activity is modulated by the cAMP-dependent signaling cascade, the level of cAMP in HEK293 cells was manipulated. Forskolin and 2'5' dideoxyadenosine, activator and inhibitor respectively of the adenylate cyclase enzyme as well as IBMX, an inhibitor of the phosphodiesterase, were applied to cell cultures for treatment. Also, isoproterenol, an activator of β-adrenergic receptors, leading to the activation of adenylate cyclase and IL1-β, an inhibitor of adenylate cyclases, were used to treat HEK293 cells. The activation state of SPAK and OSR1 is assessed using Western blot analysis and a phospho-specific antibody. The data show that SPAK and OSR1 phosphorylation in HEK293 cells is decreased by elevating cAMP, as demonstrated by forskolin, IBMX, and isoproterenol, but increased by a reduction of cAMP, as shown by 2'5' dideoxyadenosine and IL1-β. In conclusion, SPAK and OSR1 is regulated by the cAMP-dependent signaling cascade.

Introduction

There are many processes within organisms which require specific ions. If the body does not have sufficient concentrations of these ions certain functions within the body will not be able to be carried out. A variety of cells contain Na-K-2Cl (NKCC), a cotransporter which uses the gradient of sodium (Na^+) and potassium (K^+) ions across the cell membrane to regulate chloride (Cl^-). The cotransporter is found in the brain, kidneys, and in many other organs throughout the body. NKCC1 has been linked to epileptogenesis (Kahle, 2008), the control of blood pressure, and to pain perception (Delpire and Austin, 2010). NKCC1 is believed to transport ions in a specific sequence: Na^+ first, followed in order by Cl^-, K^+, and Cl^- (Lytle, 1998) (See Figure 1). According to the Lytle model, NKCC1 follows a strict "first ion on, first ion off" model. Following this model, the Na^+ is first to be 'picked up' from the outside of the cell, and then first to be 'dropped off' inside the cell. Furthermore, the cotransporter cannot, by the Lytle model, pick up the next ion without the previous ion within the

Figure 1 Lytle Model of NKCC1 Cotrransporter

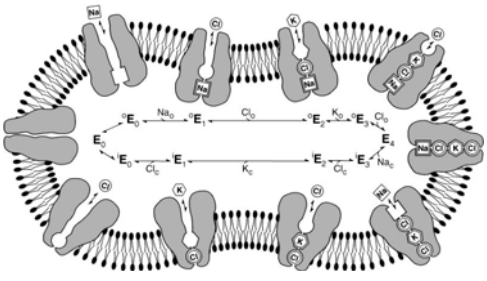

sequence having been placed within the cotransporter. This model was considered correct until further investigation by the Delpire laboratory demonstrated that the ion fluxes did not always follow the strict rules of the Lytle model (Personal Communication with Eric Delpire, Ph.D.). The kinetics predicted by the Lytle model did not match the data obtained after the flux of the ions was measured (Delpire and Gagnon, 2011). The importance of understanding the kinetics behind the NKCC1's function is to better predict the reaction of a drug treatment on the cotransporter for future pharmaceutical work.

Figure 2: NKCC1 Activation

The regulation of NKCC1 is still not completely understood. It is known that NKCC1 function is dependent on the salinity of the external environment. There are likely a number of intermediate steps (still unknown) that participate in the activation and inhibition of the cotransporter (See Figure 2). Two steps that have already been identified consist of a cascade of kinases that lead to NKCC1 activation by phosphorylation (for review, see Delpire and Gagnon, 2008). The kinases are WNK1-WNK4 as well as two PKC (Protein Kinase C) isotopes, which phosphorylate two closely related kinases that directly interact with the cotransporter (Figure 2). These interacting kinases are SPAK (*S*te20p-related *P*roline *A*lanine-rich *K*inase) and OSR1 (Oxidative Stress Response-1). Both SPAK and OSR1 and the NKCC1 cotransporter are co-expressed in many cell types (Delpire and Gagnon, 2008).

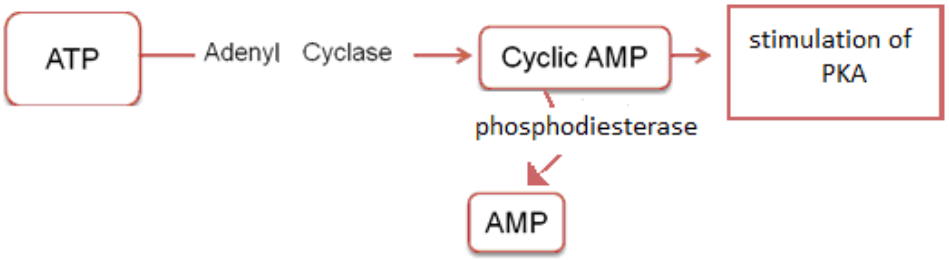

Figure 3: cAMP Signaling Cascade

Protein Kinase A (PKA) has also been shown to affect the function of NKCC1 in a variety of cells. Whether the PKA effect is mediated by SPAK and OSR1 is unknown. In order

to test the effect of PKA on SPAK and OSR1 activation, the researchers proposed to manipulate PKA activity through cyclic-AMP and a pharmacological approach. The cyclic-AMP signaling cascade is the process by which ATP (Adenosine-5'-triphosphate), a major source of energy for the cell, is modified into a cyclic nucleotide. The transformation of ATP to cyclic-AMP (cAMP, cyclic Adenosine Monophosphate) is aided by the catalyst, adenylyl cyclase, whereas the degradation of cAMP into AMP (Adenosine Monophosphophosphate) is mediated by the catalyst, phosphodiesterase. Cyclic AMP exerts many effects in cells, one of which is to stimulate protein kinase A (PKA). It was hypothesized that drugs which are known to modulate cAMP levels would lead to the modulation of SPAK and OSR1 phosphorylation.

Methods

Maintenance of Cell Cultures: As a cell model, the Delpire laboratory uses human embryonic kidney cells in culture. HEK293 cells were developed as an established cell line in the 1970s and they have been widely used as an experimental model. The cells are cultured in 10-cm dishes containing 10 ml DMEM-F12 supplemented with 10% Fetal Bovine Serum, and 1.8% Penicillin/Streptomycin. The dishes are kept for 2-3 days in a 37 degrees Celsius incubator with 5% Carbon Dioxide.

Drug Treatment Protocols: The cells were incubated for for treatment 10-60 min in the presence of compounds, then washed with PBS (phosphate buffered saline), then lysed in a buffer containing Triton-X100 (a detergent). The buffer lyses the cells and solubilized the proteins. After a 30-min incubation on ice, the lysate was centrifuged for 10 min at 10,000 rpm and the supernatant was collected. Proteins then were quantitated using the Bradford assay and an equal amount of protein was loaded per lane on a 9% polyacrylamide gel.

Protein Analysis: During electrophoresis, the proteins migrate in the Western blot gel depending upon their size. The proteins were then transferred from the acrylamide gel to a membrane, which is incubated with antibodies. Activation of SPAK and OSR1 was determined by using a phosphoSPAK/OSR1 specific antibody. The antibody is directed against a specific threonine residue in the catalytic domain of SPAK/OSR1, and was raised in sheep. SPAK residue threonine 243 is conserved in OSR1, along with surrounding residues. Therefore, the antibody cannot distinguish between SPAK and OSR1. However, the two kinases have different sizes and therefore they migrate differently in a gel. The phosphorylation of the SPAK and OSR1

kinases was monitored by applying a primary antibody to tag the proteins and then a secondary antibody which recognizes the primary antibody. This secondary antibody is then recognized by a phosphor- luminescent antibody which can be detected on autoradiography film when applied to the western blot membranes holding the proteins. The concentration of the kinases was then determined by the densitometry of the signal in various lanes (each lane represents a different treatment).

Results

To test whether cAMP was involved in the activation of SPAK and OSR1, the HEK293 cells were treated with the adenylcyclase activator forskolin (10-50 uM). Instead, it was observed that there was significant decrease in signal (Figure 4, left), suggesting that an increase in cAMP leads to inactivation of SPAK and OSR1. An additional experiment was performed to assess the time course of the forskolin effect (Figure 4, right). It can be seen that forskolin induces reduction in SPAK and OSR1 phosphorylation already after 10 min treatment. The effect of forskolin was verified by using IBMX (10 uM), an inhibitor of the phosphodiesterase, the enzyme that degrades cAMP into AMP. As with forskolin treatment, it was found that IBMX induces an increase in cAMP. Inhibition of the phosphodiestarase also resulted in decreased SPAK and OSR1 phosphorylation (Figure 5).

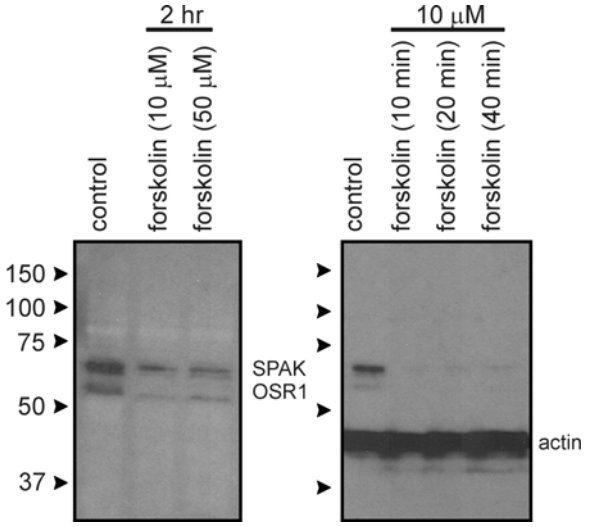

Fig. 4: Left: Western blot analysis of HEK293 cells treated with 10 μM and 50μM forskolin. Top band represents SPAK, the bottom band OSR1. Right: Time course after treatment with 10μM forskolin. The membrane was also subjected to an anti-actin antibody to verify equal loading.

Because an increase in cyclic-AMP levels resulted in a decreased SPAK and OSR1 phosphorylation, next, researchers wanted to determine whether a decrease of cAMP levels would have the opposite effect. To decrease the level of cAMP, 2'5' dideoxy adenosine was used, an inhibitor of the adenylate cyclase enzyme. As anticipated, we observed an increase in

SPAK and OSR1 phosphorylation signal (Figure 5), confirming the relationship between cAMP levels and SPAK and OSR1 activity.

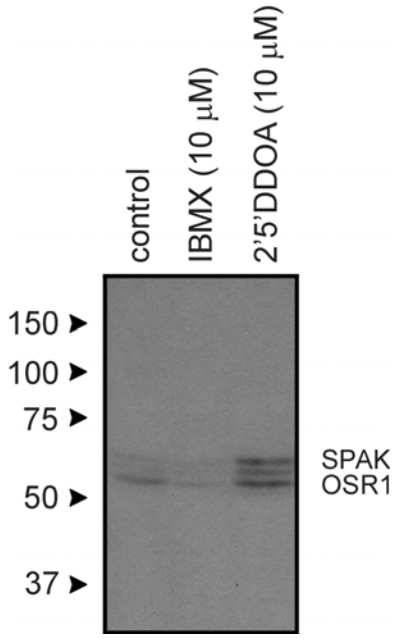

Fig. 5: Western blot analysis of HEK293 cells treated with 10 μM IBMX or 10μM 2'5' dideoxyadenosine.

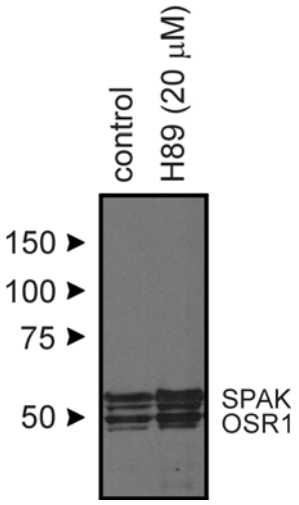

Fig. 5: Western blot analysis of HEK293 cells treated with 20 μM H-89, a PKA inhibitor.

Since PKA is the major target of cAMP, H89 (dihydrochloride salt) was used, an inhibitor of PKA, to assess the direct role of the kinase on SPAK and OSR1 phosphorylation. H89 increased the levels of SPAK/OSR1 phosphorylation (Figure 6), indicating that PKA activity leads to SPAK/OSR1 inhibition. Note that in the course of this experiment, the effect of isoproterenol was tested, an agent that stimulates adrenergic receptors, leading to an increase in cAMP levels. The effects of isoproterenol were similar to those of forskolin

In conclusion, SPAK and OSR1 phosphorylation (activation) is affected by the cAMP-dependent signaling cascade. This is a novel observation. It is not yet known whether PKA acts directly on SPAK and OSR1, or the kinase affects upstream kinases known to directly phosphorylate SPAK and OSR1. These intermediate kinases are WNK 1 to 4 (**W**ith **N**o **K** = Lysine 1 to 4) and PKC□ and PKC□.

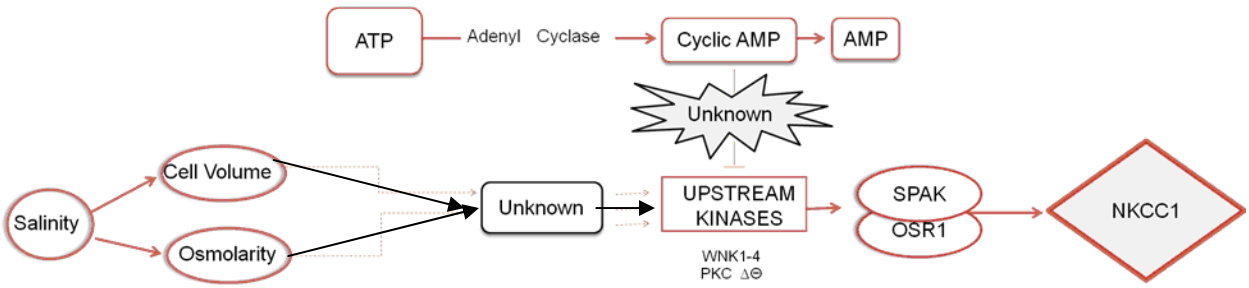

Figure 7. NKCC1 Activation and AMP Signaling Cascade

A better understanding of the phosphorylation of the NKCC1 may be attained by future experiments that could include, but not be limited to, measuring the amount of AMP and cAMP produced during the time courses with the various drugs known to activate and deactivate the NKCC1. Furthermore, experiments designed to identify the precise target of PKA could be designed. These experiments would at least demonstrate whether PKA is a direct modulator of SPAK and OSR1 function through direct interaction and phosphorylation. With antibodies able to detect the phosphorylation of the kinases upstream SPAK and OSR1, it should be possible to determine whether affecting cAMP levels also affect the state of phosphorylation of these intermediate kinases.

Literature Cited

Delpire, E. and Austin, T.M. (2010). Kinase regulation of Na^+-K^+-$2Cl^-$ cotransport in Primary afferent neurons. *J Physiol* 588: 3365-3373.

Delpire, E. and Gagnon K.B. (2008). SPAK and OSR1: STE20 kinases involved in the regulation of ion homoeostasis and volume control in mammalian cells. *Biochem J* 409: 321-331.

Delpire, E. and Gagnon, KB. (2011). Kinetics of hyperosmotically-stimulated Na-K-2Cl cotransporter in Xenopus laevis oocytes. *FASEB J* 25: 6157.12.

Dzhala, V., Talos, D.M, Sdrulla, D.A., Brumback AC, Mathews GC, Benke TA, Delpire E, Jensen FE, and Staley KJ. (2005). NKCC1 transporter facilitates seizures in the developing brain. *Nat Med* 11: 1205-1213.

Jiang, G., Akar, F., Cobbs, S., Lomashvilli, K., Lakkis, R., Gordon, F.J., Sutliff, R., and O'Neill, W. (2004). Blood pressure regulates the activity and function of the Na-K-2Cl

cotransporter in vascular smooth muscle. *Am J Physiol Heart Circ Physiol* 286: H1552-H1557.

Kahle, K., and Staley, K.. (2008). The bumetanide-sensitive Na-K-2Cl cotransporter NKCC1 as a potential target of a novel mechanism-based treatment strategy for neonatal seizures. *Neurosurg Focus* 25: E22.

Kaplan, M.R., Mount, D.B., Delpire, E., Gamba, G. and Hebert, S.C**.** (1996) Molecular mechanisms of NaCl cotransport. *Annu Rev Physiol* 58: 649-668.

Lytle, C., McManus, T.J., and Haas,M.(1998). A model of Na-K-2Cl cotransport based on ordered ion binding and glide symmetry. *Am J Physiol* 274: C299-C309.

Recolonization of Algal Assemblages after Flooding in Nashville Creeks

Emily M. Alsentzer, Holden D. Bitner, Laura K. Moribe
School for Science and Math at Vanderbilt, Nashville

Abstract

The redistribution of sediment and the accumulation of chemicals from the surrounding lands cause floods that can alter the biotic populations of streams. Periphyton, which is often the basis of food chains, is especially affected by flooding. Its colonization is dependent on nutrient densities, which can change significantly with floods. This study identified the algal populations of Henry and Richland Creeks, and quantified less than three weeks prior and two months following the Nashville flood of 2010. Periphyton was sampled by swabbing algae-covered rocks and assessed using algal field guides and light microscopy. Algal assemblages prior to the flood were found to be drastically different from those sampled afterwards. The prevalence of *Cocconeis* increased significantly, which correlates with its ability to adhere tightly to its substrata. However, overall species diversity also increased significantly after the flooding, which suggests that flash flooding lends to a type of succession which increases overall species diversity, yet allows taxa most adapted to disturbances to recolonize more rapidly.

Introduction

Flooding provides important sources of natural disturbance in streams. Floodwaters cause changes in the hydrology of streams and the shape of riparian buffers, which in turn alters the biotic population (Vitousek, R.M., Mooney, H.A., Lubchenco, J., & Melillo, J.M., 1997). Such changes lead to biological succession, in which invasive species commonly benefit over less tolerant native species (Unknown[1], 1999). High flows due to flooding can transport sediment through streams, killing or relocating benthic invertebrates and their habitats (Unknown[1], 1999). Flood disturbance patterns are thought to be determining factors of benthic algae colonization in streams (Stevenson, R., Bothwell, M.L., & Lowe, R.L., 1996). Not only does flooding act as a mechanism for biomass loss, but the frequency and intensity of floods can affect stream geomorphology, nutrient concentrations, water clarity, substratum size, and baseflow velocities, which are all critical variables in algae colonization (Stevenson, 1996). Nevertheless, recovery of individual species of benthic algae after disturbances occurs relatively quickly as a result of its high reproductive rates, short life cycles, mobility, and its ability to colonize on substrates (Stevenson, 1996). This combined with their ability to persist before and after disturbances suggests that benthic algae are useful tools for studying the succession of a biotic population after flooding.

This study focuses on the effects of the May 2010 Cumberland River Basin flood on Richland and Henry Creeks in Nashville, Tennessee. Beginning on May 1, the Cumberland Basin experienced 36 hours of rainfall, resulting in approximately 17 inches of rain in some areas (Unknown[2], 2010). Richland Creek surged past the 20-foot flood stage mark, flooding the surrounding residential and commercial areas (Fig.1) (Unknown[2], 2010). These floodwaters breached a crack in the limestone underlayment of the creek bed downstream (Swartz, 2010). Rock and soil from the creek bed were washed into a nearby pit belonging to Reostone Quarry, causing the water to demolish a section of Richland Creek's west bank (Swartz, 2010). As a result, Richland Creek bed was exposed to a number of pollutants, and its riparian buffer makeup was altered. Similar, but less drastic flooding occurred in Henry Creek, which is located in Beaman Park in Northwest Nashville.

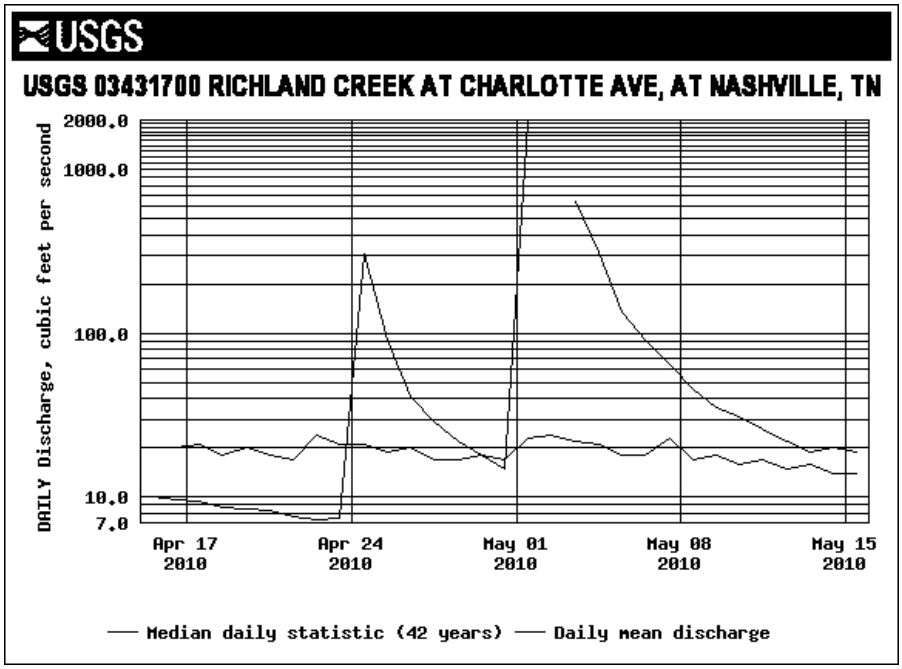

Fig. 1: This hydrograph shows the daily discharge of water in Richland Creek before and after the Nashville flood. The gap in the data following May 1 is most likely a result of instrument error due to extreme flooding (Unknown[3], 2010).

This study analyzes the change in the composition of algal assemblages prior to and following the Cumberland River Basin flooding, in order to study the recolonization of periphyton and species diversity after disturbances in the ecosystem. Recolonization after natural disasters has the potential to allow for proliferation by algal species, similar to floral succession in a forest environment. Taxa capable of rapid recolonization and of close adherence to substrata are likely to show the greatest net gain in percent composition post flooding, as they will

colonize the substrata more rapidly, overtaking other species. However, the overall species diversity of the stream could still increase due to the decrease in total algal biomass as the result of the flood. This provides more space for colonization allowing for the growth of a variety of taxa.

Methods

Water Quality Sampling

Water quality data were gathered at Richland Creek four days prior and two months following the Nashville Flood of May 2, 2010, while at Henry Creek data were gathered three weeks prior and two months following the flood. Four water quality samples at each creek were taken, at 25-meter intervals on alternating banks, approximately 0.5 meters from the bank (Fig. 1). Temperature, pH, and nitrate, phosphate, and dissolved oxygen concentration data were gathered at each sample site. These data ensured that there was a change in nutrient concentrations post flood, which in turn confirms that the difference in algal assemblage composition correlates to a change in creek health.

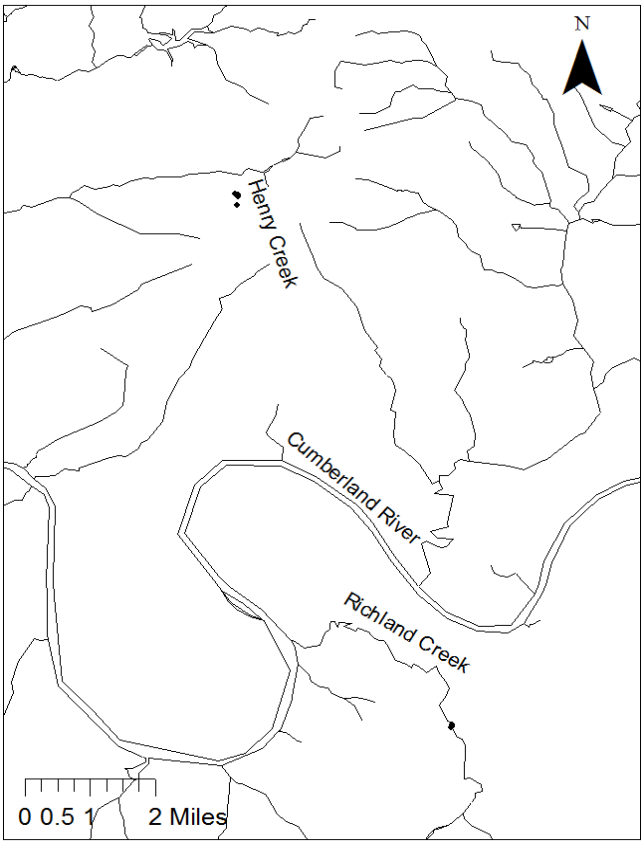

Figure 2: Richland Creek, which is located in West Nashville, neighbors McCabe Golf Course near Charlotte Road. Henry Creek, located in northwest Davidson County, is found in Beaman Park.

Algae Sampling

Periphyton samples were collected from both Henry and Richland Creeks at the time of water quality sampling. Vials were filled with creek water and discarded two times at each of the water quality sampling sites (Zheng, 2006). Four to five periphyton-covered rocks were inserted into the vial, on the third time, and the vial was capped underwater. The samples were immediately covered with aluminum foil to prevent exposure to light, and were stored in a cooler.

Algae Identification

Periphyton samples were transported back to the laboratory and stored at 2 °C for approximately 10 days for samples taken prior to the flood and approximately 3 days following the flood. Using gridded slides, light microscopy, and algal field guides, all sampled algae were identified and quantified. Finally, pre- and post- flood algal assemblage data were compared, to determine the change in assemblage composition and species diversity.

Results

Post-flood analysis yielded significant changes in the population of three periphyton genera (Fig. 3). Performing a Student t-test on each algal taxon, the change in the population of *Cocconeis*, *Nitzschia*, and *Cyclotella* was determined to be a result of the flood and not chance alone. *Cocconeis* demonstrated the most obvious increase in prevalence, increasing from 0.5% to 19.2% in Henry Creek and from unobserved to 16.4% in Richland Creek (Table 1). *Nitzschia* also increased significantly from 0.5% to 8.6% in Henry Creek, and 3.0% to 9.5% in Richland Creek

Genus	Average change	Standard Deviation	p-value
Navicula	-23.3%	21.04%	0.2694
Cymbella	-1.8%	12.07%	0.4399
Surirella	3.8%	2.46%	0.1286
Gomphonema	1.0%	1.58%	0.3704
Amphora ovalis	1.2%	2.56%	0.3945
Surirella	-3.0%	2.13%	0.1021
Nitzschia	7.3%	4.36%	0.0342
Diatoma	0.2%	1.66%	0.4721
Cyclotella	-2.4%	1.39%	0.0366
Microspora	6.0%	7.76%	0.2583
Fragilaria	0.1%	0.52%	0.4690
Cocconeis	17.6%	10.21%	0.0213
Staroneis	-2.0%	1.41%	0.1490
Gonatozygon	0.4%	0.26%	0.0697
Closterium	4.6%	4.37%	0.2376

Table 1: For each of the observed periphyton taxa in Henry and Richland Creek, t-tests were run to determine the significance of the change in algal assemblage composition.

(Table 1). The only significant decrease in prevalence post flooding was that of Cyclotella, which decreased from 2.5% to 0.3% in Henry Creek and from 3.0% to 0.3% in Richland Creek (Table 1). Using Simpson's Diversity Index, it was determined that diversity increased in both creeks following the flood; however, the greatest increase in diversity occurred in Richland Creek (Table 2). The abundance of periphyton taxa decreased from 17 to 15 genera in Henry Creek post flooding, but increased from 11 to 18 genera in Richland Creek.

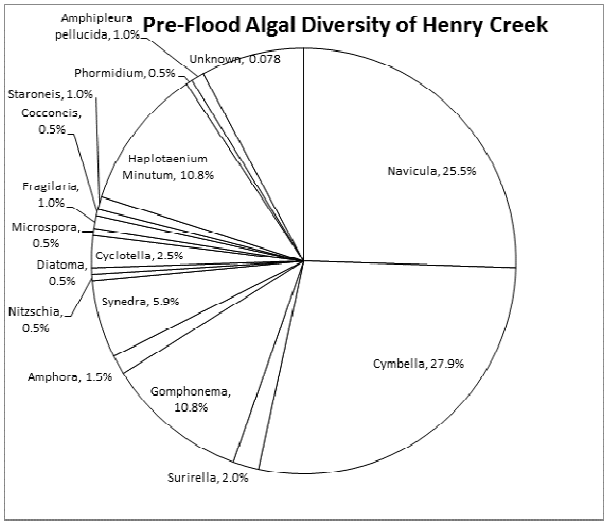

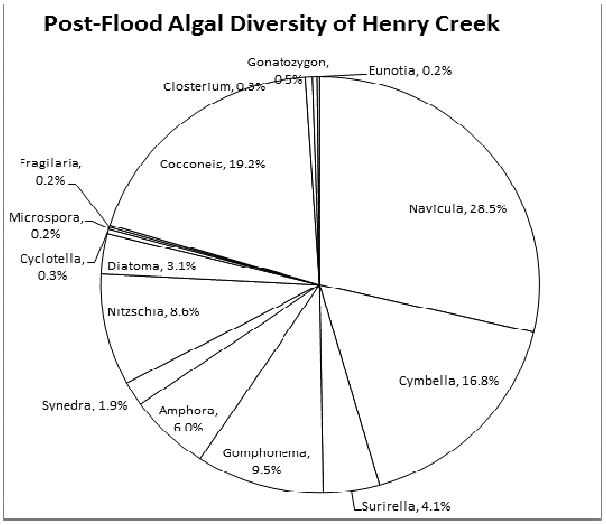

a b

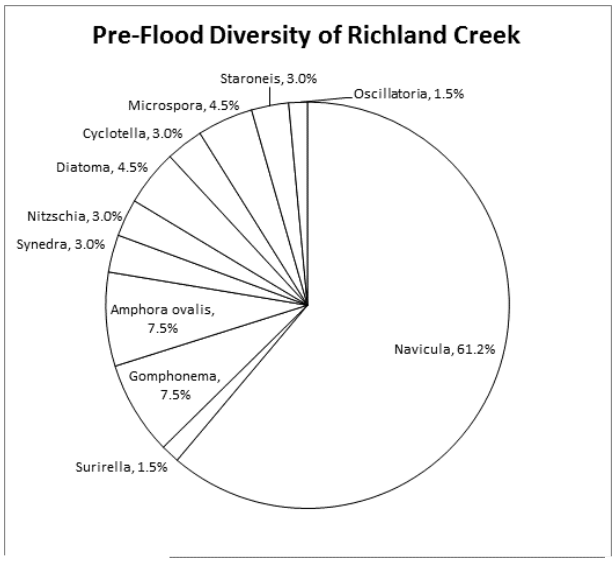

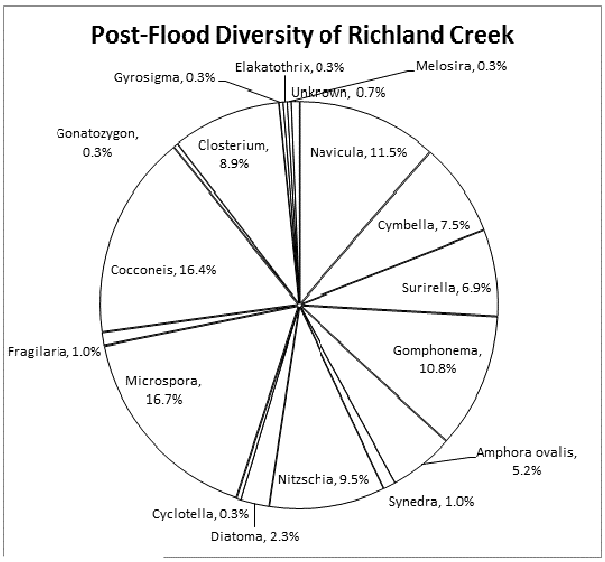

c d

Figure 3 a-d: Algal assemblage data were gathered and compared pre and post flood for both Henry and Richland Creeks.

Simpson's Index of Diversity		
	Pre-Flood	Post-Flood
Henry Creek	0.827752782	0.831662438
Richland Creek	0.615558571	0.892342537

Table 2: The Simpson's Index of Diversity was used to quantify the biodiversity of a given environment. It takes into account the richness, or the number of species per sample, as well as the evenness, or the relative abundance of the different periphyton taxa.

Conclusion

The observed change in algal population in Richland and Henry Creek supports the hypothesis that the diversity after the flood was significantly greater than the diversity prior to the Nashville Flood of 2010. The total number of different species in both Richland and Henry Creek did not increase significantly; however, the colonization was more evenly distributed post flooding. The hypothesis that benthic algae, which adhere tightly to substrata, are more likely to increase in composition was confirmed. *Cocconeis*, which is known for its adherence to its substratum, showed a significant increase in percent composition following the flood.

While the data show significant trends in the redistribution of these algal assemblages, it should be note that algae quantification is not an objective process because human judgment is involved. Due to multiple people quantifying algae, there is likely to be variation among algal counts. Furthermore, gridded slides were only used in post flood identification a week lapsed between the sampling and identification of algae. This time span could have led to a change in the algal composition of the sample as a result of its exposure to external factors. It is also possible that the algae covered slides were not representative of the algal population of the entire stream, as swabbing of the rocks could have been biased. Per chance, certain rocks could exhibit a greater prevalence of particular algal species than is characteristic of the algal population of the stream.

Previous studies have shown that periphyton abundance and diversity decreases with a disturbance in their substrata (Matthaei and Townsend, 2000; Death, 2002). This contradicts the findings that species diversity increased post flash flooding. However, our data were taken only one time following the flood during a period in which there could have been decreased invertebrate grazing. This decrease in predation could have led to an increased opportunity for

periphyton to thrive. Nevertheless, this study coincides with former findings that *Cocconeis* dominates in areas with medium to high flood disturbance frequency (Stevenson, 1996). The findings of this study further show that *Cocconeis* tends to dominate in areas of infrequent flooding after one substantial flood, not just in areas of frequent flooding.

It is evident that flooding can greatly influence algal assemblage composition. These findings help to clarify the effect of flash flooding on relative algal abundances. Future studies could illuminate the long-term effects of flash flooding through the monitoring of algal population over a longer period of time. This could give further insight into the succession of algae and the time at which the population stabilizes. In addition, different characteristics of periphyton such as biovolume, nutrient status indices, and pigment ratios, could be studied to provide a greater understanding of flooding on periphyton morphology. These metrics provide good assessments of shifts in biomass, nutrient content of algal cells, and divisional composition of algal assemblages (Stevenson, 1996). In order to further study succession after flooding, the relative abundances of other organisms such as invertebrates can be observed in addition to periphyton assemblages. By studying the relationship between periphyton and invertebrates one can examine the role invertebrates play in periphyton recolonization and how such biotic factors may influence algal succession. It is important to utilize a wide variety of metrics as well as consider an assortment of external factors in order to better comprehend the mechanisms of algal recolonization after a flood.

Literature Cited

Death, R G. "Predicting Invertebrate Diversity from Disturbance Regimes in Forest Streams." *Oikos* 97 (2002): 18-30.

Matthaei, C D, and C R Townsend. "Long-term effects of local disturbance history on mobile stream invertebrates." *Oecologia* 125 (2000): 119-126.

Stevenson, R. Jan., M. L. Bothwell, and Rex L. Lowe. *Algal Ecology: Freshwater Benthic Ecosystems*. San Diego: Academic, 1996.

Swartz, Steve. "Richland Creek and Reostone Quarry." *Creek Voice*. Aug. 2010. <http://rcwa.nodiehl.com/media/creekvoice_SUM10WEB.pdf>.

Unknown[1]."Considering Ecological Processes in Environmental Impact Assessments." US Environmental Protection Agency. EPA Office of Federal Activities, July 1999. Web. 8

Dec. 2010. <http://www.epa.gov/compliance/resources/policies/nepa/ecological-processes-eia-pg.pdf>.

Unknown[2]. "May 2010 Flood Event Cumberland River Basin: 1-3 May 2010 Great Lakes and Ohio River Division." US Army Corps of Engineers. US Army Corps of Engineers, 21 July 2010. Web. 8 Dec. 2010. <http://www.lrn.usace.army.mil/LRN_pdf/AAR_May_2010_ Flood_ Cumberland_Draft_V7_21.pdf>.

Unknown[3]. "USGS 03431700 RICHLAND CREEK AT CHARLOTTE AVE, AT NASHVILLE, TN." *U.S. Geological Survey*. U.S. Department of the Interior, 9 Dec. 2010. Web. 9 Dec. 2010. <http://waterdata.usgs.gov/tn/nwis/dv/?site_no=03431700&agency_cd=USGS&referred_module=sw>.

Vitousek, R. M., H. A. Mooney, Jay Lubchenco, and J. M. Melillo. "Human Domination of Earth's Ecosystems." *Science* 227 (1997): 494-99.

Zheng, Lei. "Chapter 5.0 Algae." United States Environmental Protection Agency. EPA, 11 Dec. 2006. <http://www.epa.gov/eerd/rivers/non-wadeable_ch05.pdf>.

Influence of Resistance and Soap Concentrations on the Inhibition of Growth in *E. Coli*

Vanessa Fuentes
Smyrna High School , Smyrna

Abstract

The purpose of this research study was to determine the effect of disinfectant concentration on the growth of *E.coli*. Various concentrations of soap containing triclosan were used to treat the bacteria. Bacterial resistance to disinfectant was determined by measuring the inhibition zone caused by the disinfectant. Triclosan resistance was also studied in this lab by repeating trials. The hypotheses are (1) that as the soap concentration increases, the zone of inhibition will increase, and (2) that the zone of inhibition will decrease across all generations at all soap concentrations. The inhibition zones around each disc were measured and recorded after each trial. The most resistant bacteria were being selected for growth for each successive generation . The results suggest that as the disinfectant, or soap, concentration increases, the width of the inhibition zone also increases. The results suggest that the size of the inhibition zone decreases from generation to generation for all soap concentrations, indicating that triclosan resistance evolved. The overuse of antibacterial soaps containing triclosan can pose a problem because bacteria can develop resistance to triclosan.

Introduction

E.coli, short for *Escherichia coli*, was identified by German pediatrician Theodor Escherich in 1885. *Escherichia coli* was originally identified as *Bacterium coli commune*. *E.coli* was considered to be an omnipresent organism; this bacterium was later suspected to be the cause of an outbreak of neonatal diarrhea fifty years after its initial discovery (White, 2006). The *E.coli* bacterium is rod-shaped and measures 2-3 microns in length, and one micron wide. The bacterium is covered in small pili and has flagella that aid in mobility. *Escherichia coli* inhabits the intestinal tract of humans and some warm-blooded animals. There are many pathogenic *E.coli* strains that can cause a variety of diseases in humans and animals, such as pneumonia and urinary tract infection (Lawrence and Ochman 1998). *Escherichia coli* is well-adapted to its characteristic habitats, and can grow in media with glucose as the only organic constituent (Todar, 2008).

Scientists use serotyping in order to compare *E. coli* strains. Serotyping is based on the O (somatic lipopolysaccharide), F (fimbrial), K (capsular), and H (flagellar) antigens. More than 700 serotypes of *E.coli* have been identified. Pathogenic types of *E.coli* are classified by pathogenesis, serotypes, and specific virulence mechanisms such as toxins and adhesins. At least

seven distinct classes of pathogenic *E.Coli* are recognized: enterotoxigenic, enteropathogenic, enterohemorrhagic, enteroinvasive, diffuse-adhering, necrotoxigenic, and enteroaggregative (White, 2006).

Triclosan is a broad-spectrum antimicrobial and antibacterial agent; studies have shown that triclosan resistance exists among several bacterial species (Wignall, G.R., Goneau, L. W., Chew, B.H., Denstedt, J.D., & Cadieux, P.A. 2008). This problem has not been well studied, and several experiments are being conducted to further understand the relationship between triclosan and bacterial susceptibility to antibiotic. One experiment examined the possible relationship between triclosan and bacterial susceptibility to antibiotics among staphylococci and several species of gram-negative bacteria, such as *E. coli*. The bacteria were isolated from the hands of individuals in a community setting. The statistics did not support an association between triclosan MICs and the susceptibility to antibiotics; there was an increasing trend in the association; the odds ratios for all species were compared at baseline versus at the end of the year. The scientists concluded that a relationship may emerge after longer-term or higher-dose exposure of bacteria to triclosan in the community setting (Aiello, A.E., Marshall, B., Levy, S.B., Della-Latta, P. & Larson e., 2004). This conclusion is important because the overuse of antibacterial soaps containing triclosan is common in the community.

The purpose of this research was to determine the effect of disinfectant concentration on the growth of *E.coli*. Various concentrations of soap were used to treat the bacteria. Bacterial resistance to disinfectant was determined by measuring the inhibition zone caused by the disinfectant. Dial antibacterial soap was used, and the active ingredient in the soap was triclosan. Triclosan has been used in soaps, toothpastes, deodorants, and mouth washes since 1972. Triclosan has been shown to be effective in reducing and controlling bacterial contamination. At bactericidal concentrations, triclosan appears to act upon multiple nonspecific targets, causing disruption of bacterial cell wall functions, while at sublethal concentrations, triclosan affects specific targets (Heath, R.J., Holland, D.R., Zhang, E.M., Snow, M.E. & Rock, C.O., 1999).

The hypotheses were that as the soap concentration increases, the zone of inhibition will increase, and that the zone of inhibition will decrease across all generations at all soap concentrations because studies have shown triclosan resistance exists among several bacterial species.

Experimental Procedure

Dial antibacterial soap was used. Various concentrations of soap were made by diluting the soap; the soap concentrations used were 5%, 1%, 0.5%. The soap was introduced to the bacterial cultures using a small paper disc with a diameter of 6 mm. A micropipetter was used to make the solutions. The control group consisted of one untreated disc. The purpose of the control group was to determine whether the untreated paper disc affected the bacteria and caused inhibition.

A flame from a Bunsen burner was used to sterilize the equipment, along with seventy percent isopropyl alcohol. Tryptic soy agar and petri dishes measuring 100 x15 mm were used and stored in the refrigerator at 4ºC. A bacterial culture of *E.coli* in tryptic soy broth was obtained, and an innoculating loop was sterilized. The loop was first dipped into the bacterial culture and then streaked across the agar. Sterile tweezers were used to grab a 6mm diameter, blank paper disc from Carolina Biological Supply Company and dip it into the corresponding soap concentration; the disc was then lightly dabbed on a paper towel and placed in the center of the agar plate streaked with *E. coli.* The agar plate was incubated at 37º C for one day. This process was repeated for each soap concentration. The same procedure was used to set up control plates.

The inhibition zones around each disc were measured and recorded after one day. The inhibition zone is the clear region around the paper disc in which no bacteria grew. Once the inhibition zones were measured, a sterilized inoculating loop was used to pick up bacteria adjacent to the inhibition zone. The loop was then spread around a new agar plate. Sterilized tweezers were used to place a new disc with the appropriate soap concentration in the center of the plate. This process was repeated for every soap concentration. The plates were placed in the incubator for one day at 37º C. This process was repeated twice more, measuring and recording the inhibition zone after each trial.

Data

The results suggest that as the disinfectant, or soap, concentration increases, the width of the inhibition zone also increases. The results also suggest that the size of the inhibition zone decreases from the generation to generation for all soap concentrations (see Table 1 and Figure 1).

Table 1 – Influence of resistance and soap concentration on the size of the zone of inhibition

Generation	Soap Concentration				
		0% (Control)	.5%	1%	5%
	1 generation	0.4 cm	0.7 cm	1.1 cm	1.7 cm
	2 generation	0.0 cm	0.6 cm	0.8 cm	1.1 cm
	3 generation	0.0 cm	0.4 cm	0.6 cm	1.0 cm
	4 generation	0.0 cm	0.1 cm	0.1 cm	0.2 cm

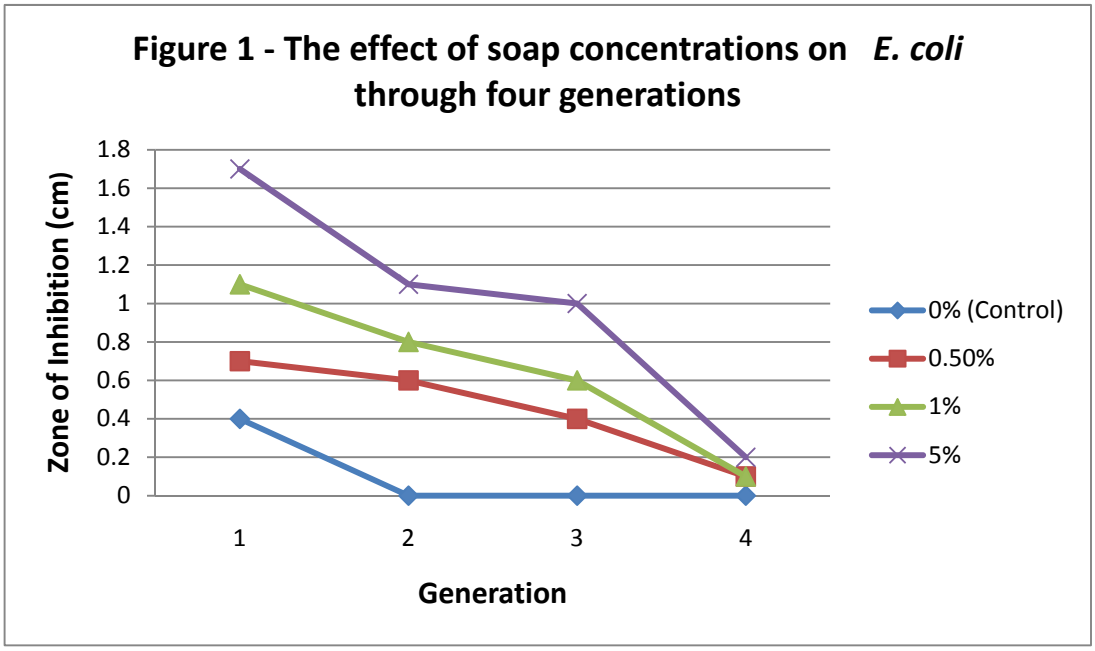

Conclusions

The results support the hypothesis. As the soap concentration increased, the zone of inhibition increases, thereby better inhibition bacterial growth. Usually the zone of inhibition decreased from generation to generation, due to the evolution of resistance to triclosan within bacterial populations. The zone of inhibition increased as the soap concentration increased because of the active ingredient in soap. The active ingredient in soap is triclosan, and triclosan is used to reduce and control bacterial contamination. Triclosan is an antibacterial agent, and therefore a higher soap concentration has a higher concentration of triclosan, thus leading to a larger zone of inhibition. Triclosan targets bacteria by inhibition fatty acid synthesis, binding to bacterial enoyl-acyl carrier protein reductase enzyme; this enzyme is encoded by the gene FabI. The binding of triclosan to this enzyme increases the enzyme's affinity for NAD+. A ternary complex of ENR-NAD+-triclosan forms and is unable to participate in fatty acid synthesis. In order to reproduce and build cell membranes, fatty acids are necessary; therefore, inhibiting bacterial growth (Heath et al. 1999). Because of FabI mutations, some bacterial species can develop low-level resistance to triclosan at its lower bacteriostatic concentrations. This results in a decrease of triclosan's effect on ENR-NAD+ binding in E. coli. If bacteria overexpress the FabI gene, the bacteria can also gain low-level resistance to triclosan (McMurry, L.M. , Oethinger, E. & Levy, S.B., 1998). This explains why the zone of inhibition decreases with each generation. Using the loop to take bacteria closest to each disc, the most resistant bacteria were being selected. Therefore, the next generation had a smaller zone of inhibition because the bacteria were more resistant to triclosan. This problem caused an overall shift in resistance via directional selection.

Resistance to triclosan and other disinfectants is a threat to the reduction and control of bacterial contamination. Antibiotic-resistant bacterial strains are emerging, and the overuse of triclosan can cause resistance to develop in bacteria. The results support this evidence because usually; the zone of inhibition decreased from generation to generation, indicating a higher resistance to triclosan. The E.coli develops tolerance to the triclosan from generation to generation , the active ingredient in the soap disinfectant. This mechanism may be linked to aminoglycoside susceptibility. Experiments suggest that changes in outer membrane, or loss or plasmids, may cause this development of tolerance (Cottell et al. 2009). A major concern is the

possibility that triclosan resistance may contribute to reduced susceptibility to important antimicrobials, due to either cross-resistance or co-resistance mechanisms; studies have been limited but for future research, it is important to investigate if the widespread use of triclosan may represent a potential public health risk in regard to development of concomitant resistance to clinically important antimicrobials (Yazdankhah, S.P., Scheie, A.A., Hoiby, E.A., Lunestad, B.T., Heir, E. Fotland, T., Naterstad, K. & Kruse, H. 2006).

Triclosan resistance is also important in modern medicine, and many experiments are being conducted to investigate the effect of triclosan on antibiotic resistance. They concluded that the synergistic effects of triclosan and several antibiotics are consistent with a triclosan-dependent metabolic strain and/or membrane disruptive effect. This experiment is important in modern medicine because of the combined use of antimicrobial compounds in clinics (Wignall et al. 2008) A possible mechanism by which bacteria can acquire resistance to triclosan is a mutation of the FabI gene; these mutant *E.Coli* strains can survive in triclosan treated soaps. Bacteria can also develop resistance to Triclosan by pumping out the antibacterials by an efflux mechanism. Bacteria developing resistance to triclosan is a potential public health risk (Levy, 2001).

Triclosan resistance is also important in modern medicine. Triclosan can affect infections such as the *Staphylococcus aureus* (MRSA) infection. Another concern is that the inappropriate or unnecessary use of antibiotics occurs when treating the *Staphylococcus aureus* infection. Avoiding the inappropriate use of antibiotics will also reduce the likelihood of the emergence and spread of strains with reduced susceptibility to glycopeptides (Coia et al., 2006). Previous experiments have shown that overexpression of FabI in Staphylococcus aureus results in reduced susceptibility to triclosan. The abundance of FabI and two other proteins were examined by Western immunoblotting for five of the triclosan-sensitive strains and seven of the strains for which triclosan MICs were elevated. The results suggest not only that a mutation in FabI is required for triclosan resistance but also that this altered FabI needs to be overexpressed at three- to fivefold higher levels than the level of expression in triclosan-sensitive strains (Fan et al. 2002). Many experiments are being conducted to investigate the effect of triclosan on antibiotic resistance. An experiment suggested that the synergistic effects of triclosan and several antibiotics are consistent with a triclosan-dependent metabolic strain and/or membrane disruptive effect; this experiment is important in modern medicine because of the combined use

of antimicrobial compounds in clinics (Wignall et al., 2008). Understanding the relationship between triclosan tolerance and antibacterial resistance is crucial to modern medicine.

Literature Cited

Aiello, A.E., Marshall, B., Levy, S.B., Della-Latta, P., and Larson, E. (2004). Relationship between triclosan and susceptibilities of bacteria isolated from hands in the community. Antimicrob Agents Chemother 48(8): 2973–2979.

Coia, J.E., Duckworth, G.J., Edwards, D.I., Farrington, M., Fry, C., Humphreys, H., Mallaghan, C., and Tucker, D.R. (2006). Guidelines for the control and prevention of meticillin-resistant *Staphylococcus aureus* (MRSA) in healthcare facilities. Journal of Hospital Infection 63(1): S1-S44.

Cottell, A., Denyer, S.P., Hanlon, G.W., Ochs, D.,and Maillard, J.Y. (2009). Triclosan-tolerant bacteria: changes in susceptibility to antibiotics. Journal of Hospital Infection 72(1): 71-76.

Fan, F., Yan, K., Wallis, N.G., Reed, S., Moore, T.D., Rittenhouse, S.F., DeWolf, W.E., Huang, J., McDevitt, D., Miller, W.H., Seefeld,M.A., Newlander, K.A., Jakas, D.R., Head, M.S., and Payne, D.J. (2002).Defining and combating the mechanisms of triclosan resistance in clinical isolates of *Staphylococcus aureus*. Antimicrob Agents Chemother 46(11): 3343–3347.

Heath, R.J., Rubin, J.R., Holland, D.R., Zhang, E.M., Snow, M.E., and Rock,C.O. (1999). Mechanism of triclosan inhibition of bacterial fatty acid synthesis. Journal of Biological Chemistry 274: 11110-11114.

Lawrence, J.G.,and Ochman, H. (1998). Molecular archaeology of the *Escherichia coli* genome. Proceedings of the National Academy of Sciences of the United States of America 95(16): 9413–9417.

Levy, S.B. (2001). Antibacterial household products: cause for concern. Emerging Infectious Diseases 7(3):512-515.

McMurry, L.M., Oethinger, E., and Levy, S.B. (1998). Triclosan targets lipid synthesis. *Nature* 394:531-532.

Todar, K. (2008). Pathogenic *E. coli.* In: Online Textbook of Bacteriology. <http://www.textbookofbacteriology.net/e.coli.html>

White, D.G. (2006). Antimicrobial resistance in pathogenic *Escherichia* coli from animals. In: antimicrobial resistance in bacteria of animal origin. Washington D.C.: ASM Press. 145-146.

Wignall, G.R., Goneau, L.W., Chew, B.H., Denstedt, J.D., and Cadieux, P.A. (2008). The effects of triclosan on uropathogen susceptibility to clinically relevant antibiotics. *Journal of Endourology* 22(10): 2349-2356.

Yazdankhah, S.P., Scheie, A.A., Høiby, E.A., Lunestad, B.T., Heir, E., Fotland, T., Naterstad, K., and Kruse, H. (2006). Triclosan and antimicrobial resistance in bacteria: An Overview. Microbial Drug Resistance 12(2): 83-90.

The Effects of Oxytocin on *Nasonia vitripennis* and *Nasonia giraulti* on Longevity, Number of Offspring, Diapause and Receptor Gene Expression

HyunJeong Jin, Jordan A. Winters, Ronnie Cela-Bedoya, Kanyanta L. Mwenya
School for Science and Math at Vanderbilt, Nashville

Abstract

Oxytocin is a mammalian hormone involved in positive sexual and social behaviors; in 2007, *Nasoniavitripennis* and *Nasoniagiraulti* were among the few insects found to carry an oxytocin-like receptor. The effect of oxytocin on longevity, copulation rate, and number of offspring, along with the gene expression of *Nasonia*'s oxytocin-like receptor, were examined. It was hypothesized that the three factors would show a significant increase, and the gene would be expressed. Two trials, each composed of three separate groups, which were exposed to a different concentration of oxytocin, were attempted accordingly. The copulation stages were observed; the offspring were counted, the longevity was recorded daily, and qPCR was used to measure the gene expression throughout different life stages. The copulation rate did not have a significant correlation; however, there was a positive effect on the longevity and number of offspring. The higher rates of oxytocin increased the rate of diapause, a hibernation phase for the wasps' egg. According to qPCR data, a higher expression of the oxytocin-like receptor gene was found in the earlier developmental stages of *Nasonia*. The results may indicate that insects such as *Nasonia* wasps can carry an oxytocin-like receptor and accept the oxytocin hormone.

Introduction

Oxytocin is a hormone found in all known species of mammals. Studies of oxytocin and its biological and physical effects on mammals show stimulation of uterine contractions during pregnancy in females (Zeeman, Khan-Dawood, Dawood, 1997). Human studies show that, the presence of oxytocin in the system appears to play a positive role in maternal and social relations between offspring and members of the opposite sex respectively (Panksepp, 2006). Oxytocin also shows signs of playing a role in various human organ functions (Lippert, T.H., Seeger, H., & Pfaff, A. 2003).

Oxytocin, being a mammalian-type hormone, the hormone and its corresponding receptors are typically not found in non-mammalian organisms; however, discoveries of specific species of insects, spanning a period of over 20 years, have been found to possess genetic coding for oxytocin/vasopressin-like receptors (Stafflinger et al, 2008). *Nasonia vitripennis* is a wasp whose gDNA sequence is known to possess a gene (XM_001600153) coding for an oxytocin-like receptor (Stafflinger, E., Hansen, K., Hauser, F., Scheneier, M., Gazzamali, G., Williamson, M., & Grimmelikhuijzen, C. 2008). The biological, physiological, and social effects of insects with oxytocin-like hormonal receptors induced with oxytocin have never been studied, and the

concept of using hormones from different phylogenetic groups for physiological and medicinal purposes is not a widely researched topic; however, from studying the effects of organisms using hormones from different phylogenetic groups, new windows in therapeutic uses and medical treatment can be opened and used to help treat modern human diseases.

This study assessed these effects by observing oxytocin's influence on the longevity, copulation rate and patterns, quantity of total offspring, and quantity of offspring in diapause, a hibernation-like state which larvae enter until conditions in the surrounding environment improve to assure survival. *Nasonia vitripennis* being the original model, another species of *Nasonia* was included in the study. Using a BLAST genetic comparison of the XM_001600153 gene sequence to the entire gDNA sequence (txid7426) of a similarly related species of *vitripennis* called *Nasonia giraulti*, indicated a match of the XM_001600153 sequence in *giraulti,* making it an ideal additional organism for the study.

Increases were hypothesized in all four variables, and noticeable differences were recognized in the wasps' copulation patterns. But it had to have been taken into consideration that between different species of organisms, the rate of inter-species mating can change drastically in value. This study crossed male *Nasonia vitripennis*wasps with female *Nasonia giraulti*, and the average rate of successful inter-species copulations between this cross is 36.2% (Bordenstein and Werren, 1998). Since these were indirect measures of the receptor function, the researchers directly measured the receptor gene. Quantitative PCR was run on RNA samples of *Nasonia vitripennis*, taken from its different life-stages (larva, white pupa, black and white pupa, black pupa, and adult), and levels of receptor expression were recorded with an expectation of high expression in the white and black pupae stages.

Methods

Separation

For all experiments, the wasps were divided into three replicates. Each group had 20 male *Nasonia vitripennis* and 20 female *Nasonia giraulti*. They were separated during the black pupa stage and refrigerated at 24°C to ensure that all of them would be in the same stage.

Concentrations

Wasps were fed sugar water; 1g of sugar was added to 10ml of H_2O in 3 recipients. Trial A, 0.02mg oxytocin/1mL of water was mixed in, then for trial B, 0.002mg oxytocin/1mL of

water was mixed in, and trial C did not have oxytocin. Next, for trial D, 0.02mg oxytocin/1ml of water was mixed in, for trial E, 0.002mg oxytocin/1ml of water was mixed in, and trial F did not have oxytocin.

Copulation

Two days after adult wasps were fed oxytocin, their copulation rituals were observed. A male and female were added to a single tube and observed for 10 minutes. Observed rituals included the male chasing the female, mounting the female, the male initiating an antennae sweep, the female standing still, the female opening abdomen and the male copulating. If copulation didn't occur after 10 minutes, the copulation was considered incomplete.

Adding the Host

After observing for copulation, a host, a blow fly pupa, was added to the tube, so the female would lay her eggs. A small amount of honey for nutrients was also added in the tube.

Counting Offspring

The adults were separated from the host during the black pupae stage. The hosts' shells were opened and frozen in a 4°C freezer. Thirty minutes later, they were removed and pupaewere separated by sex under a microscope. The number of eggs in diapause was also recorded.

Recording Longevity

Following copulation, the longevity of both the male and female adults was recorded. Each trial was recorded separately.

Extracting RNA

Live *N. vitripennis* samples were collected in triplicate and separated into four different life stages (old adult, young adult, black pupae and white pupae). The wasps were frozen with liquid nitrogen. The RNA was isolated, using the Bio Rad RNA aurum kit. Five homogenized adult insects and ten pupae were placed into RNase-free 1.5mL tubes with 700µL of lysis solution and centrifuged for 3 minutes. The supernatant was then transferred to a 700µL tube with 60% ethanol. The homogenized lysate was pipetted into the RNA binding column and washed with 700µL of low stringency wash solution. Next, 80 µl of diluted DNase I was added to the membrane stack and incubated for 30 minutes at room temperature. Then, 700µl of high stringency wash solution was run through the RNA binding column. Next, 700µl of low

stringency wash solution was added to the column and was subsequently completely removed. Finally, 20µl of the elution solution was added onto the membrane stack.

cDNA Reverse Transcription

Ten microliters of 2x RT master mix was added into the wells of a 96- well reaction plate. Next, 10µl of RNA sample was added into each well. Then, two cDNA samples were chosen and 12 reactions were set up for the three primer sets. Next, 6µl of Forward primer, 6µl of Reverse Primer and 135µl of Taq Polymerase Supermix were added to the master mix. Each tube received 24.5µl of the master mix and 2.5µl of the appropriate cDNA or water. The thermocycler was set with the following conditions: initial denaturation at 94°C for 2 minutes, denature at 94°C for 3 seconds, anneal at 72°C for 30 seconds, extend at 70°C for 30 seconds , final extension at 72°C for 2 minutes and infinity at 4°C.

Gel Electrophoresis

A 1% agarose gel was created. It was set to 120 volts for 40 minutes. Each well had 15µl of the appropriate sample. Finally, 10µl of O'GeneRuler™ 1kb Plus DNA ladder was added to the proper well.

qPCR Protocol

The master mix was created by adding 98µl of Nuclease Free water, 56µl of Forward primer 1, 56µl of Reverse primer 3 and 700µl of SYBER green. Then, 13µl of the master mix was added to each well. The plates were spun in the centrifuge for 600x g for one minute. Finally, qPCR was run following the BioRad qPCR protocol.

Results

Longevity

The survival rate of *Nasonia vitripennis* and *Nasonia giraulti* in groups A, B, C, D, E and F were recorded every day at an exact time for a time period of twenty one days. As seen in Figure 1, all the wasps in control groups died by day 17. However, wasps in groups with the concentration of 0.02mg/mL and 0.002mg/mL survived until day 21.

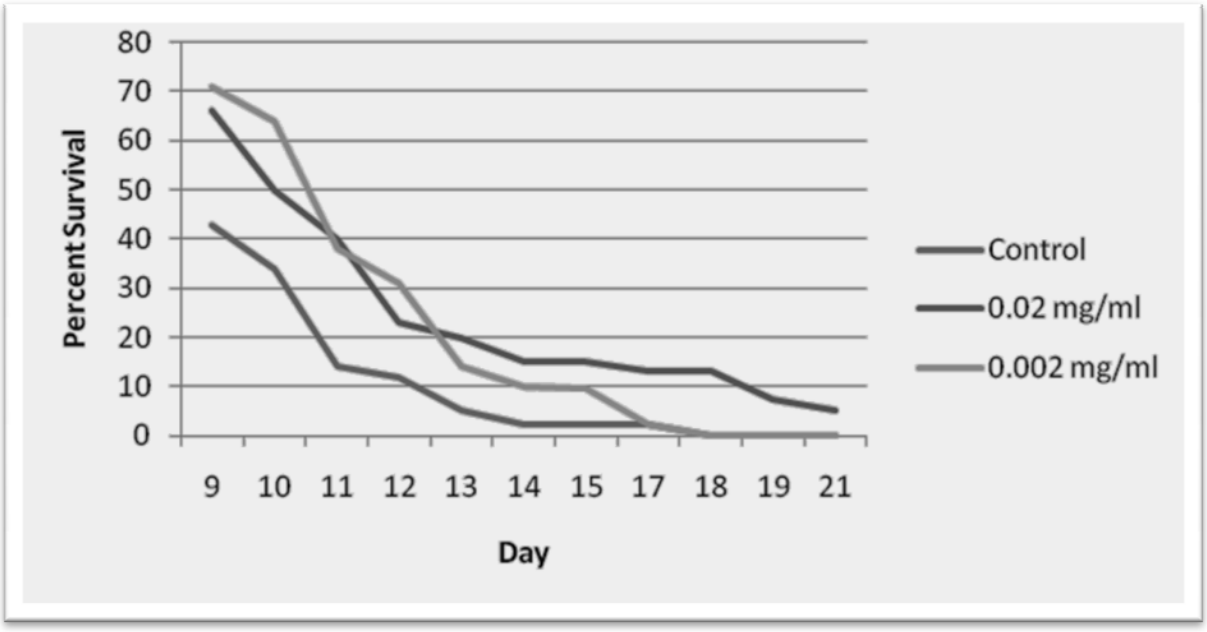

Figure 1. Effect of Oxytocin on Survival- The two groups that were exposed to oxytocin had an increased longevity compared to the control group.

Offspring

The offspring of three groups, A (0.02mg/mL), B (0.002mg/mL), C (Control), in trial 1 were collected and counted. As shown in Figure 2, the highest number of offspring was from the wasps that consumed a low oxytocin concentration, 0.002mg/mL. Also, the number of offspring from the wasps that consumed a high concentration of oxytocin was higher than the number of offspring in the control group.

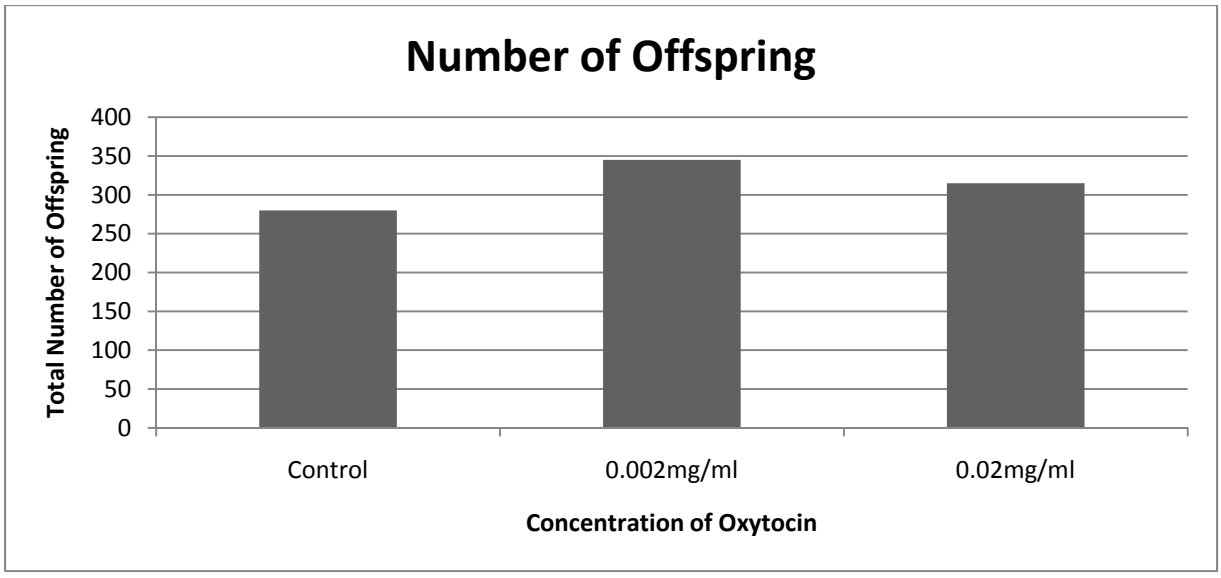

Figure 2. Effect of Oxytocin Concentration on Offspring Concentration- The number of offspring from the wasps that consumed oxytocin was higher than the number of offspring in the control group.

Diapause

There were eggs that stayed in diapause, which is the delay in development in response to regularly and recurring periods of adverse environmental conditions. After cracking all the hosts and counting the number of hosts containing diapause, the results showed that the hosts from the wasps that consumed the highest oxytocin concentration (0.02mg/mL) contained the highest number of hosts in diapause.

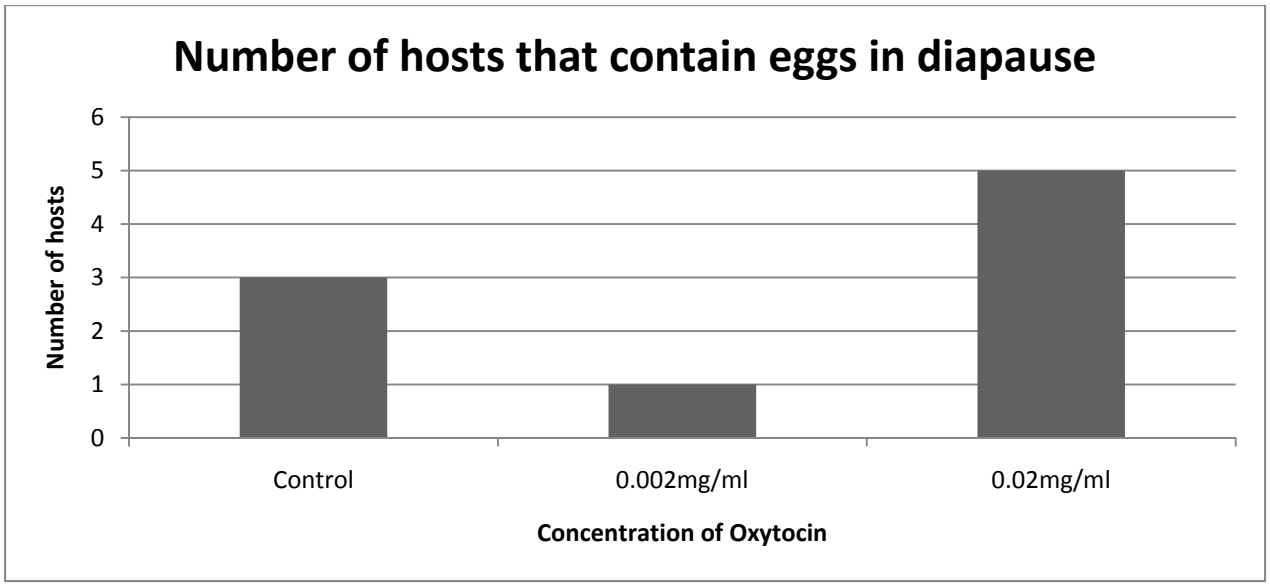

Figure 3. Number of Larvae in diapause- It shows that the hosts from the wasps that consumed the highest oxytocin concentration (0.02mg/mL) contained the highest number of hosts in diapause.

Oxytocin-like Gene Expression

The data of the relative gene expression from oxytocin like receptors showed a high gene expression in the young adult stage (Figure 4). Other developmental stages expressed low gene expressions such as Delta Delta CT values of 0.02256 in old adult-young adult, 0.0625 in old adult-black pupa, and 0.0625 in old adult-white pupa.

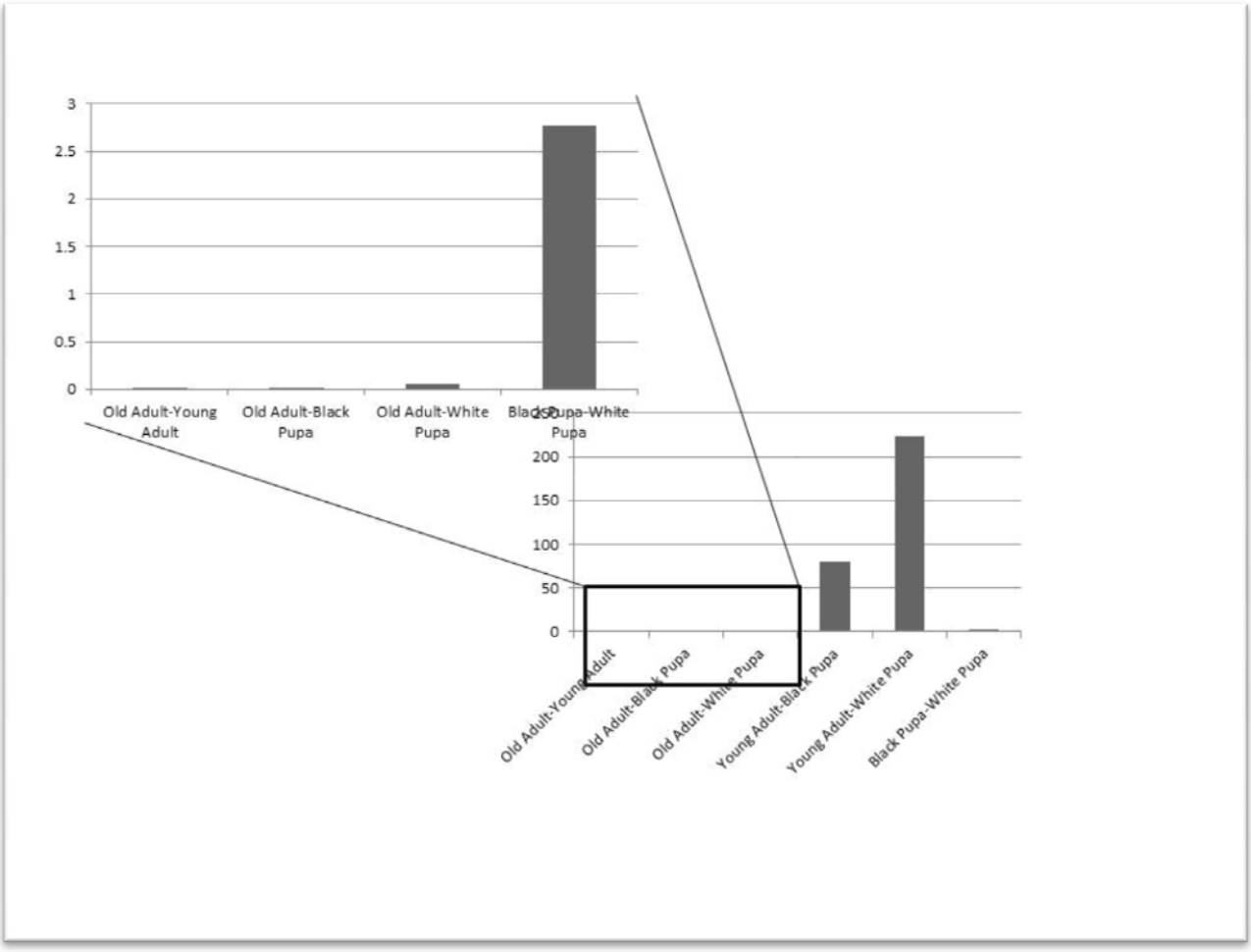

Figure 4. Relative Oxytocin Receptor Gene Expressions- It shows a high gene expression in the young adult stage, but the other developmental stages expressed low gene expressions.

Discussion

It has been found that there are oxytocin-like receptors present in some insects such as *Nasoniavitripennis*(Stafflinger et al, 2008). However, no research has been done to discover the effects that the exposure of oxytocin would bring to change the behavior of insects such as the longevity, copulation rate and patterns, quantity of total offspring, and quantity of offspring in diapause.

Nasonia vitripennis(*N. v.*)and *Nasonia giraulti*(*N.g.*) were separated in groups in this research and exposed to different concentrations of oxytocin. Intriguingly, the data showed that the group that consumed oxytocin survived longer than the control group. Also, the group that consumed a higher concentration of oxytocin produced fewer offspring and caused more eggs in diapause than the one consumed a lower concentration of oxytocin which showed a higher

number of offspring and fewer eggs in diapause than the control group. Even though it was hypothesized that there would be a more aggressive pattern in the process of copulating *N. v.* and *N.g.* with oxytocin, no significant difference was found in the data. Since there were a higher number of eggs in diapause produced from the group that consumed oxytocin, it is possible that oxytocin might have depressed the female wasps.

Discovering that the oxytocin-like receptors were functioning in *N.v.* and *N.g.*, identifying the gene expression of those receptors in different developmental stages became significant. Therefore, quantitative PCR was run on RNA samples of N.v. from four different life stages. The data were represented by comparing relative gene expressions with each stage (Figure. 4). The young adult stage had the highest oxytocin-like receptors gene expression; therefore, it is assumed that exposing oxytocin to the wasps in young adult stages would be most effective in a research. Also, these data supported our hypothesis that there is a higher oxytocin-like receptors gene expression in earlier life stages.

Given time, accurate primers, and a large quantity of samples, this finding could be used to enhance many scientific fields to start using oxytocin or other hormones to attempt to control the behavior of organisms such as longevity, copulation rates, and others.

Literature Cited

Bordenstein SR, JH Werren (1998). "Effects of A and B Wolbachia and Host Genotype on Interspecies Cytoplasmic Incompatibility in Nasonia."*Genetics Society of America*. (148): 1833-1844.

Lippert TH, AO Mueck, H Seeger, A Pfaff (2003). "Effects of Oxytocin Outside Pregnancy." *Hormone Res*. (60): 262–271.

Panksepp J. (1992). "Oxytocin Effects on Emotional Processes: Separation Distress, Social Bonding, and Relationships to Psychiatric Disorders." *Annals of the New York Academy of Sciences*. (652): 243–252.

Stafflinger E, KK Hansen, F Hauser, M Schneider, G Cazzamali, M Williamson, CJP Grimmelikhuijzen, (2008). "Cloning and identification of an oxytocin/vasopressin-like receptor and its ligand from insects." *PNAS*. (105): 3262–3267.

Zeeman GG, FS Khan-Dawood, MY Dawood, (1997). "Oxytocin And Its Receptor In Pregnancy and Parturition: Current Concepts And Clinical Implications" *The American College of Obstetricians and* Gynecologists. (89): 873-883.

EVALUATION OF CLIMATE TRENDS AND SALAMANDER POPULATION DENSITIES: A THREE-YEAR STUDY

Wade Hubbs
Camden Central High School, Camden

Abstract

Trends between salamander densities and climate data were evaluated for three years. Artificial cover boards were used for salamander monitoring. Captured salamanders (97 total) were identified by species, measured, and released. Temperature and precipitation data were collected from a weather station near the study area. Salamander density was the highest (4.45 individuals/m^2) when precipitation was the greatest (307.3 mm, 2009) and the lowest (1.15 individuals/m^2), when temperatures were the highest (16.5 °C , 2010). Salamander density and climate correlation coefficients were strong (0.95 for precipitation and -0.82 for temperature). Based on these findings, climate fluctuations can result in salamander declines.

Introduction

Scientists have estimated that one-third of the 5,743 known amphibian species are endangered or threatened with extinction (Wake, 2009). Worldwide declines have been reported for approximately 43% of the amphibian species (Pounds, A., Carnaval, & Corn, S. 2005). Since amphibians are considered the indicator species of overall environmental health, these reports of population declines have resulted in much public concern.

Tennessee has 77 amphibians thus making it the third most diverse state, following North Carolina with 90 amphibians, and Virginia with 78 (TWRA, 2009). Tennessee has 21 species of frogs and 56 species of salamanders. Six of the frogs and 24 of the salamanders are currently listed as Species of Greatest Conservation Need (GCN) in the State's Wildlife Action Plan.

More field research over longer periods is needed in order to understand the cause for amphibian declines. Scientists should focus on salamander populations that are doing well, and not just those that are declining or threatened. Scientists may be able to interpret what is happening in declining populations by understanding what makes other populations or species more stable (Science Daily, 2010).

The reasons for amphibian declines are thought to be due to factors such as ultraviolet radiation, acid rain, pesticide use, and deforestation (Lannoo, 2005). Global warming has also been found to affect amphibians. Human activities have resulted in large increases in the

concentration of carbon dioxide, methane, nitrous oxide and other heat-trapping gases in the earth's atmosphere during the past century. These gases, known as the greenhouse gases, are coming from emissions from cars, power plants, and other human activities. The average global temperature rose by more than 0.74 degrees Celsius and rose by as much as 3 degrees Celsius in some regions over the last century. Scientists have projected that if the increase in man-made greenhouse gas emissions continues, temperatures will rise by as much as three degrees Celsius by the end of the century (Pew Center on Global Climate Change).

There is growing evidence that accelerated climate change has already affected fish and wildlife populations and their habitats. The Intergovernmental Panel on Climate Change (IPCC) Fourth Assessment Report estimates that 20 to 30 percent of the world's plant and animal species are likely to be at increasing high risk of extinction as global mean temperatures exceed a warming of 1.5 to 2.5 degrees Celsius above preindustrial levels. Climate change will likely result in abrupt ecosystem changes and increased species extinctions (U. S. Fish & Wildlife Service Website).

Experimental Procedure

The purpose of this study was to investigate trends between terrestrial salamander densities and climate data. Terrestrial salamanders were monitored using artificial cover boards for three years. Precipitation and temperature data were collected from a weather station located within five miles of the study area. Monthly counts were used to calculate the terrestrial salamander density.

Terrestrial salamanders were chosen as the target species for this study because they are known to be good indicators of forest health (Droege and Welsh, 2001). In 2008, twenty survey stations were established along two transects. Two twenty-station transects were added in August, 2009. The stations, placed 20-meters apart, consisted of 1-m by 0.25-m cover boards along a 200-meter transect. Each station was marked with numbered blue flagging for easy identification during field monitoring. *Peterson's Field Guide for Reptiles and Amphibians* (third edition, 1998) was used for salamander identification. The observations were performed by a crew of two people. The cover boards were checked by lifting the board, scanning, and securing all salamanders. Once the salamanders were captured, they were placed in a moistened 3.78-l plastic bag to prevent desiccation. The salamanders were counted, measured (snout to vent length, mm), and identified by species. Salamanders were released by carefully placing them

back under the cover boards. At each station, one crewmember took measurements while the other crewmember recorded data. Data recorded included date, time, outside temperature, field observations, number, length (mm), and species of salamanders observed at each station. During this study, bimonthly (2009, 2010) and monthly (2008) counts were conducted during the fall season (September through November).

Data were analyzed after the three-year monitoring period. The monthly salamander density was calculated by dividing the total number of salamanders observed by the total cover board area. Precipitation and temperature data for the area were collected from a nearby weather station. Historical climate data were also downloaded from the National Climatic Data Center's website. Microsoft Excel's Data Analysis Tools were used to calculate correlation coefficients and perform regression analyses.

Data

The salamander data collected during the three-year study period are summarized in Table 1. Salamander density was the greatest during 2009 and the lowest in 2010.

Table 1: Salamander Count and Density Data for Three-Year Study

Sampling Period	Number of Salamanders Captured	Total Square Area of Cover Boards ($m^{2)}$	Salamander Density (individuals/m^2)
September, 2008	3	5	0.60
October, 2008	9	5	1.80
November, 2008	3	5	0.60
2008 Total:	**15**		**3.00**
September, 2009	10	5	2.00
October, 2009	27	20	1.35

November, 2009	22	20	1.10
2009 Total:	**59**		**4.45**
September, 2010	7	20	0.35
October, 2010	6	20	0.30
November, 2010	10	20	0.50
2010 Total:	**23**		**1.15**

Precipitation and temperature data were downloaded from a remote automated weather station located within five miles of the study area (National Interagency Fire Center's Weather Station, "Camden Tower ID: MCMDT1"). Historical climate data for the region were downloaded from the National Climatic Data Center. The climate data and salamander densities for the three-year study are shown in Figure 1. Salamander density was the highest (4.45 individuals/m^2) during the period, with the highest precipitation (307.3 mm in 2009). Salamander density was the lowest (1.15 individuals/m^2) during the warmest study period (16.5 °C in 2010). Salamander density declined by 74.2% from 2009 to 2010.

Figure 3: Salamander Densities and Climate Data for Three-Year Study Period

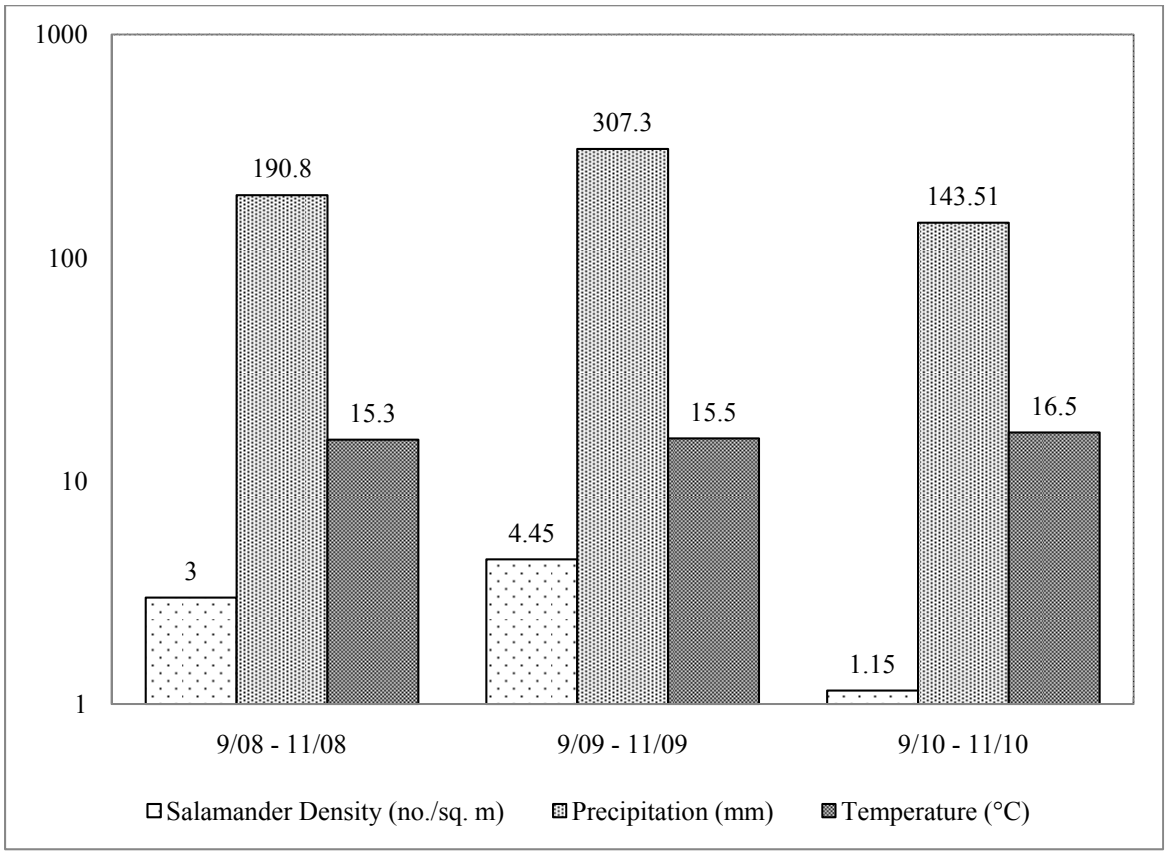

Historical data for the region are shown in Figures 2 and 3. The temperature during the fall of 2010 was 0.4°C higher than the average fall temperature for the region (16.1°C) and the precipitation was 55 mm below average (233.68 mm of precipitation in 2010).

Figure 4: Fall Precipitation for Jackson, TN 1950-2010 (Sept-Nov)

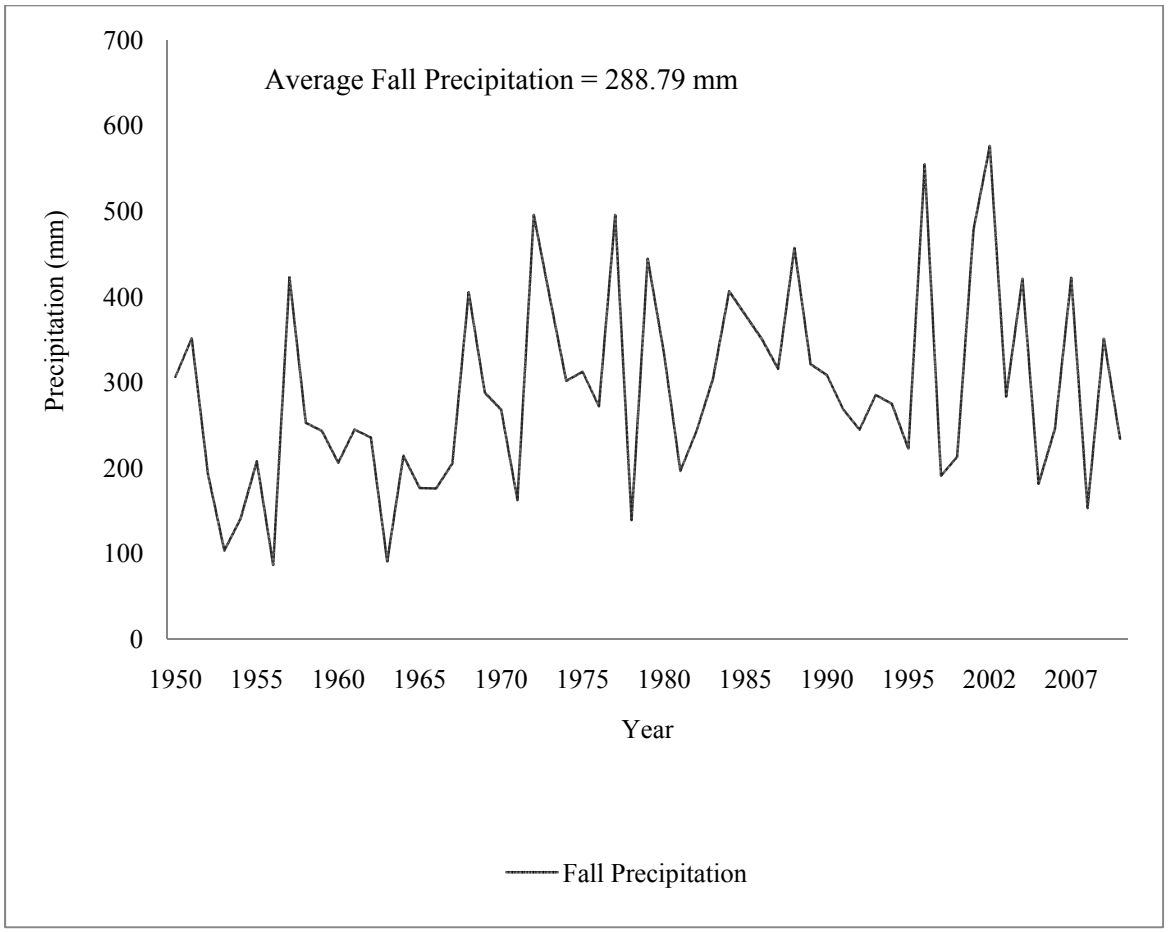

Figure 5: Average Fall Temperature for Jackson, TN 1950 - 2010 (Sept. - Nov.)

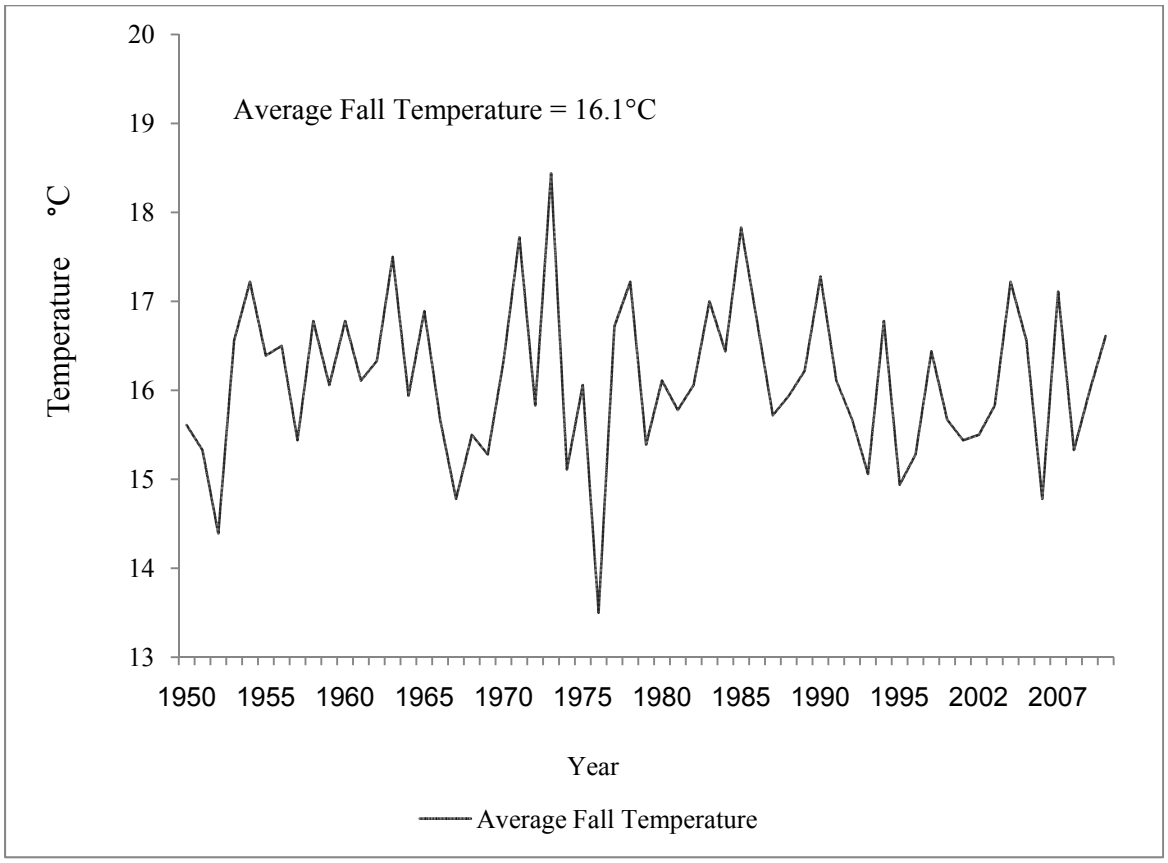

Note: Historical Climate Data downloaded from National Climatic Data Center (http://www.ncdc.noaa.gov/oa/climate/research/cag3/cag3.html)

Correlation and regression analyses were performed using Microsoft Excel's Data Analysis Tools. The correlation results are summarized in Table 2, and the scatterplots are shown in Figures 4 and 5.

Table 2: Correlation Coefficients for Monthly Salamander Densities and Climate Data	
Climate Data	**Correlation Coefficients Salamander Density (individuals/m^2)**
Monthly Precipitation (mm)	0.95
Monthly Mean Temperature (°C)	-0.82

The correlation coefficients for the climate data and salamander densities were strong. The scatterplots also indicated a strong correlation between climate data and salamander density as shown in Figures 4 and 5.

Figure 6: Linear Regression Analysis for Salamander Density and Monthly Average Temperature

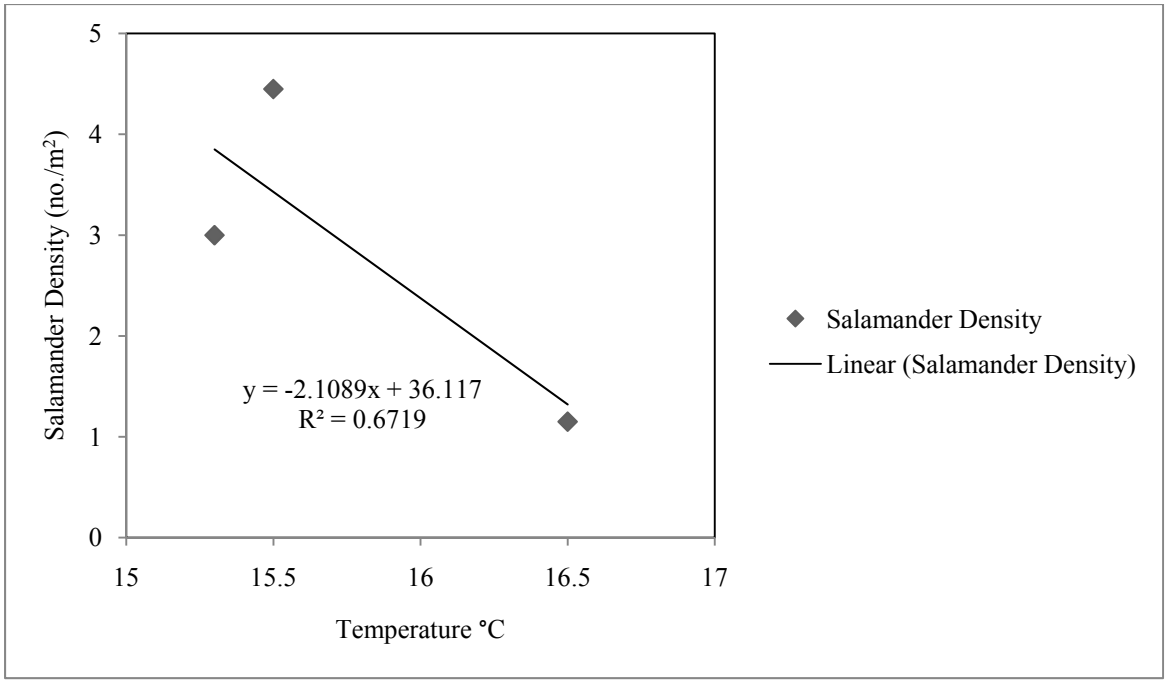

Figure 7: Linear Regression Analysis for Salamander Density and Precipitation

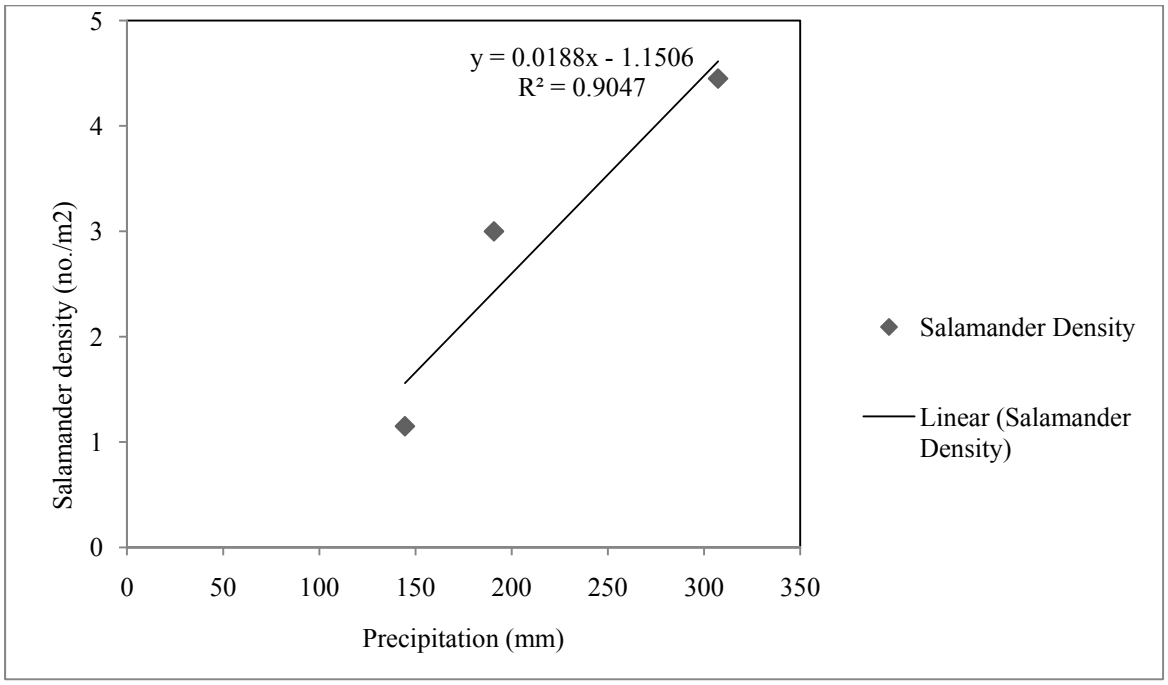

Conclusions

The monthly salamander observations and data analyses resulted in the following conclusions and recommendations:

1. Salamander density was the highest (4.45 individuals/m^2) during the study period with the most precipitation (307.3 mm in 2009).
2. Salamander density was the lowest (1.15 individuals/m^2) during the warmest study period (16.5°C in 2010).
3. The correlation coefficients for the salamander density and climate data were strong (0.95 for precipitation and -0.82 for temperature).
4. The scatterplots of the salamander densities and the average fall temperatures showed that as temperature increases, salamander density decreases.
5. The scatterplots of the salamander densities and monthly total precipitation showed that salamander density increased as precipitation increased.
6. In 2010, when the salamander density was the lowest, the average fall temperature was 0.4°C higher than the average for the region (16.1°C) and the precipitation was 50 mm below normal.
7. Salamander density declined by 74.2% from 2009 to 2010.

8. The highest salamander densities were observed during the two years when average fall temperatures were below normal (2008 and 2009).
9. During field observations, it was noted that salamanders were more prevalent in soils with higher moisture content.
10. A longer study period and more transects would provide more data for interpretation, thus yielding more definitive results.

Literature Cited

Conant, Roger and Joseph T. Collins. Peterson's Field Guide, Reptiles and Amphibians, Eastern/Central North America. Third ed. Boston: Houghton Mifflin, 1998.

Droege, S. and H. H. Welsh. "A Case for Using Plethodontid Salamanders for Monitoring Biodiversity and Ecosystem Integrity of North American Forests." Conservation Biology. 15:558-569. 2001.

Lannoo, M. (editor). 2005. Amphibian Declines, The Conservation Status of United States' Species. University of California Press, Berkeley and Los Angeles, CA.

Pew Center. *Climate Change 101.* January 2009. <www.pewclimate,org>.

Pounds, A., A.C.O.Q. Carnaval, and S. Corn. 2005. Climate Change, Biodiversity Loss, and Amphibian Declines. Pages 19-20 in Amphibian Conservation Action Plan, Proceedings: IUCN/SSC, Amphibian Conservation Summit 2005.

Tennessee Wildlife Resources Agency. 2009. Climate Change and Potential Impacts to Wildlife in Tennessee. Nashville:TWRA.

University of Maryland. Young salamanders' movement over land helps stabilize populations. Science Daily 27 April 2010. 09 November 2010 <http://www.sciencedaily.com-/releases/2010/03/100330142433.htm>.

U.S. Fish & Wildlife Service. Climate change is real. 2 Dec 2010. 09 November 2010. http://www.fws.gov/home/climatechange/climate101.html.

Wake, David. 2009. Dramatic declines in neotropical salamander populations are an important part of the global amphibian crisis. *PNAS* 106.9: 3231-3236.

Reaction-Driven Mixing During Acid/Base Neutralization

Gavin Brent Nixon
Greenbrier High School, Greenbrier

Abstract

Reaction-driven mixing was first reported in 2010 by a research group from the Netherlands, who developed a mathematical model for the process. The research project presented here was carried out in order to demonstrate the process in the laboratory, and to develop a simple relationship to describe the process. It was found using an apparatus that allowed careful layering of acid and base solutions that density difference significantly influenced the rate at which mixing occurred. A simple mathematical relationship was derived from these data. The mixing rate at all tested solution concentrations was slow. Even at the highest measured rate, mixing only occurred at 2.083 $mL \cdot hr^{-1}$.

Introduction

Reaction-driven mixing is the process by which substances capable of reacting with one another will mix during the reaction without mechanical agitation (http://www.sciencenews.org/view/generic/id/55779/title/Self-stirring_liquids , August 2010). Prior research in this area appears to be limited and very elusive, and a mathematical model for the process was only recently reported (http://pubs.acs.org/doi/abs/10.1021/ac50043a080, 2010). To date only a few different reactants have been demonstrated to undergo spontaneous mixing at the interface between them if not previously mixed. Difficulty has probably resided in the creation of an apparatus needed for this process to happen (http://www.freepatentsonline.com/5595712.html, 2010).

Density gradients (especially linear density gradients) were utilized through this research to carefully layer the reactants and to allow the reaction to proceed. A density gradient is a variation in density between two liquids that would ordinarily be miscible (http://www.science-projects.com/GradCent.htm). This process is often encountered both intentionally and unintentionally throughout the chemical manufacturing industry (http://www.science-projects.com/GradCent.htm, 2010).

Convection often drives mixing in unexpected ways between fluids. In fact this could play a previously unrecognized role in geochemical processes. Research suggests that convection can cause mixing. However, when that action is performed mechanically, the reaction certainly accelerates. In the beginning research on the subject, scientists layered hydrochloric acid containing phenolphthalein indicator (low density) on top of sodium hydroxide

(high density) in a special cell designed to prevent any mechanical agitation. Convection instability occurred when these two reacted to form sodium chloride (http://pubs.acs.orgt/cen/news/88/i06/8806notw5.html, 2010). This instability could also occur when rivers or streams flow into lakes where neutralization occurs.

Methods and Materials

Test solutions were made as follows: 0.25 M HCl, 1.0 M HCl, 0.25 M NaOH, 0.5 M NaOH, 1.0 M NaOH, 1.5 M NaOH, 1.0 NH_3, 0.5 M $HC_2H_3O_2$, and 1.0 $HC_2H_3O_2$. Phenolphthalein was added to the acids to visualize the interface where the reaction was occurring and to determine when mixing had occurred. The degree of mixing was measured as the height of the colored space within the funnel. The density of each test solution was determined by weighing 10 cm^3. An apparatus was constructed as shown in Figure I to allow one solution to be gently layered beneath the second solution to form two distinct layers. The stopcocks were used to restrict flow so that a clear pink line formed from the phenolphthalein at the interface between the two solutions.

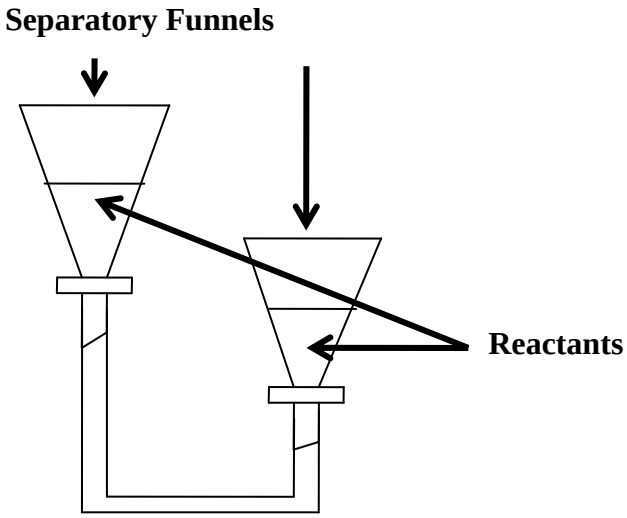

Figure I

Results

Table I shows that the concentration of the solutions increased the density increased in response. Reaction-driven mixing is a slow process, as shown in Figures II and III, where the solutions were only thoroughly mixed after 24 hours had elapsed. It also can be determined that as concentration and density (as long as the density difference is minimal) increase the rate of reaction only slightly. The mixing only occurred from bottom to top, so only the top 50 mL of solution became pink from the phenolphthalein that had been previously added to the top acid layer.

The greater the density difference between the two solutions, the less likely the mixing process was to occur within a reasonable time. For example, the layering of 1.5 M NaOH beneath 1.0 M HCl (density difference 0.0648 g/cm^3) only showed a 3.0 mm thick layer of indicator color change after 7 days of exposure. On the other hand, 1.0 M NH_3 layered beneath 1.0 M $HC_2H_3O_3$ (density difference 0.0078 g/cm^3) mixed as shown in Figure II. Even though the NH_3 solution had the lower density, it formed a layer beneath the $HC_2H_3O_2$ solution with the apparatus described above.

Table 1 Solution Densities ($g \cdot cm^{-3}$)

1.0M HCl	1.0142
1.0 M NaOH	1.0220
1.5 M NaOH	1.0790
1.0 M NH_3	0.9826
1.0 M $C_2H_3O_2$	0.9804
0.25 M HCl	0.9852
0.25 M NaOH	0.9749

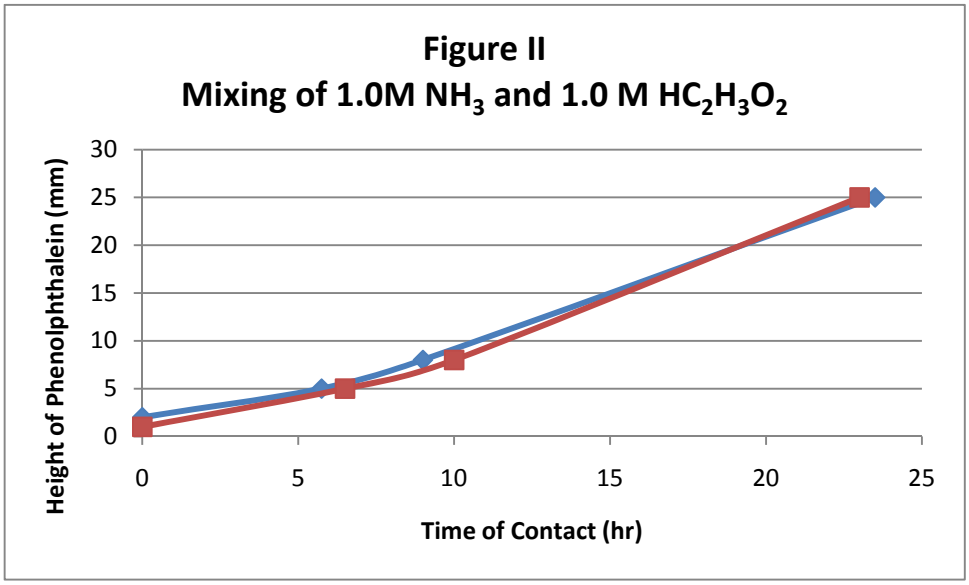

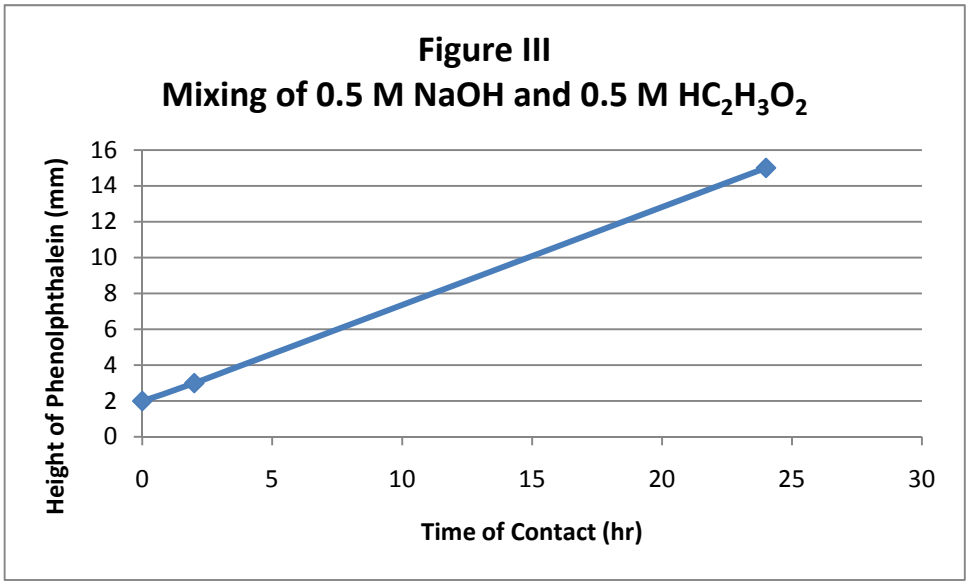

Conclusions

The rate of mixing is determined by concentration, density, and the nature of the solutions. The rate in the case of 1.0 M NH_3 layered beneath 1.0 M $HC_2H_3O_3$ with a density difference of 0.0078 $g \cdot cm^{-3}$ is calculated to be 2.083 $mL \cdot hr^{-1}$, and for 0.50 M NaOH layered beneath 0.50 M $HC_2H_3O_3$ with a density difference of 0.0400 $g \cdot cm^{-3}$ is calculated to be 1.250 $mL \cdot hr^{-1}$. Obviously, the rate of mixing in $mL.hr^{-1}$ is inversely proportional to the difference in density between the bottom and top layers ($D_b - D_t$). Therefore, a simple relationship that approximately relates density difference to rate of mixing would be, $(D_b - D_t) = kR$ where k = 0.0374 $(cm^3)^2 \cdot g^{-1} \cdot hr^{-1}$. Likely the enthalpy of reaction (ΔH) drives the mixing process, and for the acid-base neutralization:

$$H^+ + OH^- \longrightarrow H_2O \quad \Delta H = 55.8\ kJ \cdot mol^{-1}$$

The amount of solution-solution contact is limited by the area of the interface, so only a minimal amount of energy is generated. Reaction-driven mixing as shown here is a very slow process regardless of the density difference or concentration, and therefore, it is unlikely to be commercially feasible.

Future Direction

This study could be extended to a wide variety of different liquids both solutions and pure compounds. Possible organic reactions could include esterification. Additional research is now being planned that involves simultaneous collection of pH data during the course of the reaction, time-lapse photography to accurately document the reaction, and refining of the mathematics to identify the components (including enthalpy and concentration) of the coefficient of proportionality.

Acknowledgements

I would like to acknowledge Mr. Ronnie Nixon for encouragement and support throughout this research.

Literature Cited

http://pubs.acs.orgt/cen/news/88/i06/8806notw5.html. Accessed August 17, 2010.

http://www.sciencenews.org/view/generic/id/55779/title/Self-stirring_liquids. Accessed August 17, 2010.

http://www.science-projects.com/GradCent.htm. Accessed August 17, 2010.

http://www.eng.umd.edu/~nsw/ench485/lab10.htm. Accessed August 17, 2010.

http://www.freepatentsonline.com/5595712.html. Accessed August 17, 2010.

http://pubs.acs.org/doi/abs/10.1021/ac50043a080. Accessed August 17, 2010.

http://www.informaworld.com/smpp/contentudb=allncontent=a769247039~frm=abslink. Accessed August 17, 2010.

Crystallization with Vibrations II

Della Coleman
Northwest High School, Clarksville

Abstract

Sound has always been, and will continue to be, a prominent variable in the environment of the world. From Micro to macro the force of noise is at work, even on the object of this study, crystals. In this study a pattern of two different frequencies was applied to a crystallizing solution of $C_6H_{12}O_6$ (sucrose) and H_2O. Aspects of crystallization were further expanded upon in the 2010 – 2011 experiment as time became an added element. The use of a resonance frequency of the container, B_4 (493.88Hz), coupled with a harmonic frequency E_4 (329.63Hz), was the needed element in order to produce a changed crystal formation. Finding that the B_4/E_4 frequencies yielded a more concentrated area of crystal formations than the naturally crystallizing mixture, the results support the possibility of increasing the density of metals using resonance frequency. Because of the constant force of molecular frequency and sonic frequency on matter, this study gives insight into the structural formation of solid structures in the world.

Introduction

Crystals are solids having, in all three dimensions of space, a regular repeating internal unit of structure; and the study of crystals is crystallography. Pertinent information to the study of crystallization, are the factors that affect the crystallizing process, which are the steps of crystallization, analysis of a crystal structure, and the physics of sound. Factors that affect the crystallization process are nucleation sites, mechanic disturbances, and saturation. Firstly, it should be known that nucleation is the process by which the smallest solid phase of a mixture aggregate with the capability of spontaneous growth, this point is a factor that the results depend on ("Definition of Nucleation" n.d.). If there are several nucleation sites, this will result in several smaller crystals, oppositely; if there are only a few nucleation sites, the crystals formed will be larger but fewer. Any mechanic disturbances during the crystallization process can greatly affect the developing structure of a crystal. Saturation is the last physical factor in crystallization; if a solution is supersaturated or the solute is too soluble, small crystals will develop (Boyle, 2007). Along with these factors it is important to know the steps of crystallization which consists of nucleation, which breaks down further into first order nucleation and second order nucleation, and growth ("Crystal Growth" n.d.). Analysis of a crystal structure is very important for this experiment because it is the point where data are formulated and then compared to other results. Typically, a crystal is observed through x-ray diffraction, a method that is based upon the crystals' layers' ability to diffract light (Bezoari 2008). Lastly, it is most

important to know the physics of sound, so the frequency can be calculated to show the power of the vibrations affecting the crystal. The particular frequencies used in this experiment were based on an A_4 = 440.00 Hz cycle tuning system. All this information is used to understand all aspects of this experiment. One other experiment known of, compared to this experiment showed that sonic to ultrasonic frequencies yielded "plagioclase crystals that were less euhedral and had lower aspect ratios." The results proved that the crystal size distributions were steeper for the vibrated experiments, with a higher population density of smaller crystals (Bartels 2002). The results of Bartel's experiment show that vibrations do have an affect on crystallization. Compared to the experiment conducted in this situation, the results confirm the smaller size and denser area the crystals formed. It can be seen that there is more research that can prove to be valuable in this field. Research in this field can lead to the development of creating a way to eliminate sound from crystallization or even apply sound to the process for optimal crystals. It was because of these enhancements that this project was created. With this experiment the affect of sound vibrations on crystallization were studied.

Material and Methods

The evaporation technique of crystallization was used in order to accomplish this experiment. The evaporation technique called for a saturated mixture and a great amount of time. The experiment began by dissolving sucrose in water. A saturated mixture consisting of 40ml of water and 140ml of sugar was created. The measurement was based on a 3:1 ratio; therefore, the amount of milliliters of water was multiplied by three, and an additional 20mL of sugar was mixed in, to assure super saturation. The same mixture was replicated making two identical solutions. A graduated cylinder was used for measuring the amounts of water and sugar, a coil stove, and a metal pot were then used to heat the mixture, and a metal spoon was used to stir it. Both mixtures were heated for approximately 6 minutes. Immediately after being heated the mixtures were poured into their specified containers. Upon pouring the mixtures in their metal containers, a paper towel, measuring 27.9 x 27.9, cm was secured around the opening of each container using a rubber band. Once the mixture for the independent variable was poured into its container, the B_4 pitch alternated with the E_4 pitch of 440.00 Hz was applied to the independent variable, using a KORG Chromatic Tuner at a caliber of 440 Hz. The tuner was recorded for five

minutes on the B_4 pitch then the E_4 pitch, later burned to a CD-ROM. A stereo was then used to play the disc at a volume of 20 milliliters. The solutions were then placed in a room with a temperature of about 20-21 degrees Celsius. The controlled sample was placed away from the independent sample in a separate room to ensure natural crystallization. While the controlled sample was left alone, the independent variable experienced the constant disturbance of two alternating frequencies, separated by a small lapse of silence about two seconds every ten minutes. Both samples were left in their rooms for the remainder of the experiment, which lasted for a week. The entire experiment was performed in Northwest High School. Once the crystallization process was completed, the excess solution was drained from the containers, and the lower forming crystals were examined. Small crystals were chipped away from the larger mass in order to be viewed under a spectroscope.

Left, stereo system, (right) cover used to muffle excess sound
All pictures were taken by Della Coleman in Northwest High School

Data & Results 2009-2010

During the experiment performed in 2010 observations were made every day which are listed below.

Day 1 Thursday January 28

The mixtures show no signs of crystallization and have been sitting for twenty four hours.

Day 2 Friday January 29

There are still no signs of sugar crystallization. The controlled sample was moved to insure best conditions for its natural process to occur. The batteries of the sound mechanism were changed.

Day 3 Saturday January 30

The beginnings of crystals are forming in the controlled sample. Some signs of crystal formation are showing in the affected variable. The batteries were changed again.

Day 4 Sunday January 31

The batteries were changed At approximately 10:00 a.m. Further crystallization has occurred within the controlled sample. No further crystallization seems to have occurred within the independent sample. Batteries were changed once more at approximately 11:00 p.m.

Day 5 Monday February 1

The suspension process was begun on the fifth day. A sugar crystal from each variable was collected and tied to the end of fishing twine while the other end of the fishing twine was then tied to a wooden pencil. The pencil was laid at the opening of its container to anchor the fishing twine. As an end result, the crystal was suspended over the developing crystals at the bottom of each container. This is in hopes of inducing crystal growth on the suspended crystal for a larger more applicable crystal. The batteries were changed at 3:45 p.m.; batteries were again changed at 10:50 P.M. (Not because they ran out of power but to ensure a constant frequency.) At 10:53 it was observed that the controlled mixture was extremely cloudy so to crystal suspension.

(Cloudy controlled sample)

(suspension setup independent left controlled Right)

Day 6, February 2

The independent sample has clouded over just like the control sample. This is most likely dueo to the sugar mixture drying since the paper towel cover was removed during

suspension and kept that way. The covers have been reapplied. At 6:30 p.m. batteries were changed.

Day 7 February 3

The batteries changed at 6:27 a.m. and once again at 4:12 p.m. (In order to ensure a constant frequency)

Data were collected using a microscope, weights and electronic scale at the end of the experiment. Fragments of both variables were viewed under a microscope for structural differences at the school facility; once this test was performed, another sample of crystals was put under a weight test; both samples were of the same weight, but different shape, then placed under copper and aluminum weights till they cracked.

Structure Test for 2010 Experiment

Controlled: Observed under a microscope, the crystalline structure of the controlled sample appeared to be constructed of an assemblage of multiple small square crystals, with no particular organization.

Independent: The independent variable had a similar structure to the controlled sample but had more rounded due to being cut into smaller pieces for observation.

Weight test data for 2010 Experiment

Mass of the weights	Cracking point of Controlled	Cracking point of Independent
53.7g	Did not crack	Did not crack
107.4g	Did not crack	Did not crack
161.2g	Did not crack	Did not crack
200.7g	Did not crack	Did not crack
378.3g	Cracked	Cracked

Data Results for 2011 Experiment

Controlled Variable 01/14/11

Independent Variable 01/24/11

First attempt of experiment was performed December 22, 2010. Both mixtures were created and allowed to crystallize in their specified environments. The results of this first trial were invalid because the independent variable fell off of the stereo system on which it was placed, causing improper crystallization. The experiment was performed again; first, the controlled variable was performed from January 6, 2011 until January 14, 2011. After the variable having been analyzed, the independent variable was attempted again from January 17, 2011 until January 24, 2011. This trial was a success, and the results were collected January 24, 2011. Observations and results are as follows:

Structural Analysis

Controlled Variable: exhibited isolated nucleation sights comprised of several compacted crystals

Nucleation sites of Controlled Variable

Mass Controlled: 32.1 g

Independent Variable: exhibited one unified bottom layer of small compact crystals which were concentrated along the walls of the container.

Nucleation sites of Independent Variable

Mass Independent: 70.2 g

Observed through a microscope and stereoscope, the crystal size of the independent crystals was smaller when compared to the size of the Controlled crystals. Though size was slightly different, there seemed to be no deviation in crystalline shape. Correspondingly, due to the size of the Independent crystals, the Independent variable consequently, had a higher density and heavier weight than the Controlled crystals.

Calculating the amount of energy applied to the independent variable gives insight into how much energy is necessary to affect the structure of the sugar crystal. Using Planck's constant, which is h= 6.626 x 10^{-34} J*s, which assumes that energy is proportional to the frequency of a vibration, the amount to energy in joules was calculated using the equations $E = h * f$ where E is energy and f is frequency in Hertz, the result is provided below.

E = (6.626 x 10^{-34} J*s)(440Hz)

Joules were than converted to electron volts, using the conversion factor of 1J per $1.602 \cdot 10^{-19}$ eV

E= 1.8197 x 10^{-12} electron volts (this is the photon energy)

*This information is important in understanding the amount of energy that was actually transmitted to the independent solution.

An apparatus of a 24W power was used to administer the frequency, and two pitches one of B natural and one of E natural pitch. The power and set up of 2011's experiment were the two ultimate factors which yielded opposing results of 2010's experiment.

Conclusion

The extended study of how frequency affects the crystallization process, was based on the hypothesis that the power and note of the applied frequencies would affect the crystalline structure of the crystallized sugar. Rather than alter the structure, the independent variable was diminished in size by the resonant frequency and its harmonic fifth. Compared to the control crystals the independent crystals were constructed of a similar central square system only of smaller form. Consequently, the growths of the independent crystals were much more compact than the nucleation of the controlled crystals, pointing toward a more dense concentration of the independent crystals. Based on the results of this experiment, it is believed that a resonance frequency as well as strong transmittance of the frequency is necessary in altering the crystallization process, and solely responsible for an opposite outcome of the previous experiment. Using the found information, it can be better understood how a crystalline structure behaves in its environment and how to weaken or strengthen the structure by applying sound. More than prevalent, sound continues to pollute this world, altering the structure of matter and proving to be a method of chemical use. Once again, the imperfections of this experiment consist of technology inferior to the equipment necessary for examining a crystal, and the restraint of time. Improving the accuracy of the experiment, more trials will need to be done. Making adjustments to the sizes of the containers in which the crystallizations took place, note of the frequencies, and the power of the frequencies, the experimental results were much easier to collect and more valid. Furthering this study to other salts/crystals, frequencies, containers, and implementing the resonance frequency of the crystal itself would be a good direction for this experiment. Conclusively, the application of this experiment to the real world is the ability to modify crystallization for ideal properties of crystals which may lead to a new substance. Not only does the property of sound affect crystals, which this experiment gave insight into, but it affects all things on this planet.

Acknowledgements

Special thanks to Mrs. Constance Brown, Austin Peay Physics Department and Northwest High School administration for providing support and equipment for my experiment. Many thanks, as well, to TJAS and Dr. Jack Rhoton for the opportunity to compete in and learn about the world of experimentation.

2011 Bibliography

Angelov, Georgi. " SpringerLink - Metal Science and Heat Treatment, Volume 8, Number 9." *Welcome to SpringerLink*. N.p., n.d. Web. 8 Oct. 2010. <http://www.springerlink.com/content/u877294723414436/>.

B., Hazes, and Dunlop KV. "A modified vapor-diffusion crystallization protoco... [Acta Crystallogr D Biol Crystallogr. 2005] - PubMed result." *National Center for Biotechnology Information*. N.p., n.d. Web. 8 Oct. 2010. <http://www.ncbi.nlm.nih.gov/pubmed/16041068>.

Duffin, Ross W.. "Scales: Just vs Equal Temperament."*Michigan Technological University - Department of Physics*. N.p., n.d. Web. 18 Apr. 2011.

"FREQUENCY & WAVELENGTH CALCULATOR." *Calculator City: A Web Resource for Mathematics: Algebra, Geometry, Trigonometry, Calculus, Finance, Measurement Converters Science: Chemistry, Physics, Astronomy*. N.p., n.d. Web. 11 Feb. 2011. <http://www.1728.com/freqwave.htm>.

Genck, Wayne. "Process Engineering | Crystallization: Ultrasonics makes sound progress | Chemical Processing." *Chemical Processing*. N.p., n.d. Web. 8 Oct. 2010. <http://www.chemicalprocessing.com/articles/2006/036.html>.

Glass, Alexander J.. "Non Optical Applications of Photonic Crystal Structures." *University of*

New Mexico. N.p., n.d. Web. 7 Oct. 2010. <www.dtic.mil/cgi-bin/GetTRDoc?Location=U2&doc=GetTRDoc.pdf&AD=ADA438232>.

Landon, joseph. "WHAT ARE SOME PIEZO ELECTIC CRYSTALS AND HOW CAN I TEST THEIR PIEZO ELECTR?." *MadSciNet: The 24-hour exploding laboratory.*. N.p., n.d. Web. 22 Feb. 2011. <http://www.madsci.org/posts/archives/1999-07/931327791.Eg.q.html>.

Lowe, Belle. "Crystallization." *ChestofBooks.com: Read Books Online for Free*. N.p., n.d. Web. 8 Oct. 2010. <http://chestofbooks.com/food/science/Experimental-Cookery/Crystallization.html>.

"Planck's Constant and the Energy of a Photon." *University of Colorado Boulder*. N.p., n.d. Web. 11 Feb. 2011. <http://www.colorado.edu/physics/2000/quantumzone/photoelectric2.html>.

"Quick Crystallization with sound waves." *www.cartage.org*. N.p., n.d. Web. 8 Oct. 2010. <www.cartage.org.lb/en/themes/sciences/Physics/SolidStatePhysics/PropertiesSolids/DynamicProperties/QuickCrystallization/QuickCrystallization.htm>.

Strouse, Charles E.. "About J." *The Molecular Instrumentation Ce*. N.p., n.d. Web. 8 Oct. 2010. <http://mic.ucla.edu/x-ray%20diffraction/tutorials.htm#Preface>.

"Temperature as a Crystallization Variable." *Hampton Research*. N.p., n.d. Web. 8 Oct. 2010. <www.hamptonresearch.com/documents/growth_101/8.pdf>.

Whymark, R.R.. "ScienceDirect - Ultrasonics : Acoustic field positioning for containerless processing." *ScienceDirect - Home*. N.p., n.d. Web. 8 Oct. 2010. <http://www.sciencedirect.com/science?_ob=ArticleURL&_udi=B6TW2-46S64K6-9C&_user=10&_coverDate=11%2F30%2F1975&_rdoc=1&_fmt=high&_orig=search&

_origin=search&_sort=d&_docanchor=&view=c&_searchStrId=1651565429&_rerunOrigin=google&_acct=C000050221&_version=1&_>.

Zascka, Anton, and Kaspar Hegetschweiler. "Crystallization structure of 1,3,5/2,4,6-hexahydroxycyclohexane, C6H12O6, scyool-inositol." *ftp.oldenbourg.de*. N.p., n.d. Web. 30 Jan. 2011. <ftp://ftp.oldenbourg.de/pub/download/frei/ncs/223-4/1267-2318.pdf>.

2010 Bibliography

Bartels, Karen, and Tanya Furman. "Effect of sonic and ultrasonic frequencies on the crystallization of basalt -- Bartels and Furman 87 (23): 217 -- American Mineralogist." *American Mineralogist*. N.p., n.d. Web. 1 Nov. 2009. <http://ammin.geoscienceworld.org/cgi/content/abstract/87/2-3/217>.

"Basis (crystal structure) definition of Basis (crystal structure) in the Free Online Encyclopedia.." *Encyclopedia*. N.p., n.d. Web. 12 Feb. 2010.

Bezoari, Massimo. "Crystal." *Gale Encyclopedia of Science*. 4th ed. 0. *Gale Virtual Reference*. Web. 1 Nov. 2009.

Boyle, Paul. " Crystal Growing Guide ." *NCSU Chemistry X-ray Facility* . N.p., 21 Aug. 2007. Web. 1 Nov. 2009.

Cooper, Christopher. *Matter*. New York: Dorling Kindersley, 1992. Print.

"Definition of nucleation - Chemistry Dictionary." *Periodic Table of Elements and Chemistry*. N.p., n.d. Web. 12 Feb. 2010.

"Frequencies and Wavelengths of Musical Notes." *Electroherbalism Home Page*. N.p., n.d. Web. 1 Nov. 2009.

"Frequencies of Musical Notes." *Michigan Technological University - Department of Physics*. N.p., n.d. Web. 1 Nov. 2009.

"Gravity Nullified Quartz Crystals Charged by High Frequency Currents Lose Their Weight." *Web Info*. N.p., n.d. Web. 1 Nov. 2009.

Lachicotte, Rene. "Crystal Growth." *OLD Chemistry Department home page*. N.p., n.d. Web. 11 Nov. 2009.

Lee, Lerner, and Lerner Brenda. "n/a." *n/a*. n/a ed. 0. *Gale Virtual Reference Library.*. Web. 1 Nov. 2009.

Lerner, Ed, and Brenda Lerner. "Nucleation and Nucleate." *World of Earth Science*. n/a ed. 203. *Gale Virtual Refernce*. Web. 1 Nov. 2009.

McGrath, Kimberly. *World of Invention*. Detroit: Thomson Gale, 2006. Print.

McGrath, Kimberly. *World of Scientific Discovery*. Detroit: Bridget Travers, 2007. Print.

“Minerals - Minerals And Their Uses." *Science Encyclopedia*. N.p., n.d. Web. 1 Nov. 2010.

Serway, Raymond, and Jerry Faughn. "n/a." *College Physics Fifth Edition*. United States of America: Saunders College Publishing, 1985. 896. Print.

Staples, Richard. "Getting Crystals Your Crystallographer Will Treasure." *Center for Crystallographic Research Department of Chemistry Michigan State University*. N.p., 15 Jan. 2008. Web. 1 Nov. 2009.

Experiment Central. Detroit: N/A, 2004. Print.

ABSTRACTS OF PAPERS

Presented at the Annual Meeting
Belmont University
Nashville, Tennessee
April 15, 2011

The Effect of Fertilizer Pollution on Algal Profiles in Richland and Henry Creeks

Catherine Caffey, Lauren Lu & Shanna Rucker
School for Science and Math at Vanderbilt, Nashville

Abstract

Aquatic systems are a vital part of the global biosphere; however, the detrimental effects of pollution on the aquatic systems are difficult to quantify. This study proposes algae as a biological method to indicate aquatic ecosystem health. The purpose of this study was to determine the effect of varying levels of fertilizer pollution on the periphytic algal profiles of Richland and Henry Creeks in Nashville, Tennessee. Based upon previous experimental data, it was hypothesized that the algae *Navicula* would be more prevalent in higher concentrations of fertilizer pollution than *Cymbella.* Algae were sampled from both creeks; the samples were swabbed onto gridded slides and placed in an apparatus used to simulate the flow of a creek. There were five of these devices, each containing a different level of pollution both above and below the EP A standard. Of the most prevalent species observed, only *Protococcus* was found to thrive under increasing concentrations of fertilizer. *Navicula, Cymbella,* and *Gomphonema* all displayed a negative trend in prevalence with increasing fertilizer concentration. These results suggest that *Protococcus* is an opportunistic species that could be used as a bioindicator for fertilizer pollution because of its sensitivity to the varying water conditions.

The Effects of pH on Enzyme Catalysis

Imani Chatman & Caroline Daws
Siegel High School, Murfreesboro

Abstract

Catalase is affected by changes in pH, which hinder its ability to decompose hydrogen peroxide. We measured the effects of pH on enzyme catalysis by using five different buffer solutions and a neutral control. We extracted fresh catalase from calf liver to use as the enzyme in these reactions. After letting our solutions catalyze for fifteen minutes, we then assayed each solution using potassium permanganate. Although only solutions two and seven proved to be conclusive according to titration data, pH solutions ten and twelve indicated surprising results by producing white, foamy

bubbles after the catalase was added. Our results did show that catalase performs best at pH seven, which followed our hypothesis. However, the basic solutions catalyzed at a more efficient rate than was expected.

Measuring Rate of Passage of Aspirin and Bufferin® through a Semi-permeable Membrane

Ashley Elain Corson
Greenbrier High School, Greenbrier

Abstract

Aspirin and Bufferin are *aTC* non-narcotic analgesics that are absorbed post-stomach by the wall of the duodenum to provide relief from common pains. In the research, an apparatus was constructed, utilizing a semi-permeable membrane, to simulate the absorption of test materials within the duodenum. Artificial gastric juice was placed in the apparatus along with the test sample of aspirin or buffered aspirin and a stirring bar. A semi-permeable membrane was placed over the opening, and the device was inverted into a beaker containing water and a pH electrode. Time was measured in thirty second intervals while the pH level was recorded. Three tests for each sample were carried out. For aspirin, the data showed that the test material lowered the pH levels significantly as compared to the buffered aspirin. Contrasting the results of aspirin and buffered aspirin, the materials did not lower the pH level as the control did. These results proved that the materials did pass through the semi-permeable membrane at a constant rate during the 900-second time period.

The Effects of Surface Area on Electrical Production in a Microbial Fuel Cell

Gavin Dorrity
Northwest High School, Clarksville

Abstract

The need for fuel sources is always increasing. As the population grows, so does the demand for energy resources. A relatively new type of resource is now being realized as another aid in the fight to meet this rising demand, that technology is microbial fuel cells. In fuel cells, electricity is conducted and transferred through the electrodes. Theoretically, the greater the surface area of the electrodes, the more energy can be collected. The focus of this experiment is to demonstrate the factor in the variation of surface area of electrodes to the electrical output of the microbial fuel cell. After performing the experiment, there were clearly more unseen variables than previously expected. The electrical variance was hypothesized to be relatively linear as the surface area increased. However, this was not necessarily the case. This experiment provides input and enlightenment into the complex nature of electrochemistry, microbiology, and environmentally green energy production.

Effects of Airplane Deicer on O. *placidus* in Tennessee Waterways

Ryan L. Driscoll & Anne M. Holmes
School for Science and Math at Vanderbilt, Nashville

Abstract

Airplane deicer runoff from the Nashville International Airport was speculated to have contributed to a crayfish kill in a contiguous water body following an abnormally severe winter in January 2010. Concern was raised over the potential impact of this pollution on the local crayfish population's health. In this study, the effect of propylene-glycol based airplane deicer on *Orconectes placidus* was observed. Thirty-four O. *placidus,* a Tennessee-native species, were caught and transferred into individual tanks with varying concentrations of deicer. The tanks contained sterilized rocks, sand, and water, which simulated sedimentary basin creek water environment. Over 14 days, the behavior and survival rate of the O. *placidus* were monitored, along with the dissolved oxygen, pH, and temperature. Due to the propylene glycol-based airplane deicer contamination, results showed a noticeable variation in the behavior -- lying laterally and only halfway submerged in the water -- and survival of O. *placidus* with six deaths total. Also the dissolved oxygen levels dropped significantly due to the deicer (average of 3.5 mg/L decrease in all groups except control). The pH did not change significantly. In conclusion, propylene-glycol based airplane deicer has negative effects on crayfish and the water quality where they reside.

The Effects of Gender on the Operant Conditioning of Mice

Jin Kim, Josh Schultz & Clayton Elrod
Siegel High School, Murfreesboro

Abstract

Does gender play a role in the onset of operant conditioning in mice? In order to test this, we constructed a modified Skinner Box with many possible exits, but only one exit in which the mice were rewarded with food for escaping. The mice were put into the box for five minutes after they earned food the first time, with each subsequent escape being recorded. The female mice escaped both with more consistency and more frequently, indicating that females showed a higher rate of operant conditioning than their male counterparts. We believe that this is because of hormonal and evolutionary discrepancies between the two sexes. This may lead to possible similarities in humans that could further our understanding of gender differences.

The Toxicity of Different Concentrations of Roundup on *Echiniscus*

Elizabeth Glass
Pope John Paul II High School, Hendersonville

Abstract

Commercially sold herbicides can have harmful effects on not only the plants they are intended to kill, but also on microorganisms that live in the soil. Individuals of the tardigrade species *Echiniscus* were exposed to varying concentrations of Roundup, data, and mortality were gathered to determine whether or not the herbicide was toxic to them. The tardigrades were checked every 1,4, 24 hours to asses movement and possible death. 24 hours after their immersion, the tardigrades were discarded and the data concluded. The data were analyzed and the LD50 calculated. The lethal dose for 50% of the population, after 8 hours, is 52.8% of 4.6% concentration, or 2.43%, indicating that Roundup is in fact very lethal to the tardigrade species *Echiniscus.* The importance of this could extend to a worldwide market of farmers and gardeners who could be permanently damaging the soil.

Characterization of Immune Response Resulting from Acute Genetic or Pharmacological Inhibition of Notch Signaling

Joseph Griggs
Pope John Paul II High School, Hendersonville

Abstract

Notch signaling is an intercellular pathway designated for cell to cell communication. Any interference with Notch signaling through deleting the Recombination Signal-Binding Protein has the potential to determine autonomous and secondary cellular responses. By using a mouse model with liver-specific disrupted Notch signaling, we were able to augment the number of cells located in a dense population adjacent to bile ducts, cells we believed to be immune cells responding to Notch deletion. Initially an Albumin Cre;RBP-$Jk^{flox/flox}$ mouse model was utilized to delete Notch pathway signaling in all liver cells, displaying immune cells as early as postnatal day (P) 15. Using CD_{45} and Ki-67 histological stains, we decided that these cells were multiplying immune cells. We then utilized an inducible deletion system, our KI9-CreEr;RBP-$Jk^{flox/flox}$ model, deleting Notch in adult mice ductile cells. Ultimately, this application indicated a less significant immune presence in comparison to the Albumin Cre;RBP-$Jk^{flox/flox}$ model. Finally, a drug treatment of Gamma secretase inhibitor (GSI) was implemented in the diet of mice, to globally inhibit Notch signaling, but there was no cell immune infiltration. We concluded that these immune cells are not a product of genetic or chemical modification of Notch signaling, but a more general immune response to liver damage.

Potential Site for the Translocation and Propagation of the Smoky Madtom, *Noturus Baileyi*

Katie Holmes & Andrea Tipton
Cleveland High School, Cleveland

Abstract

The Noturus *baileyi*, Smoky madtom, is an endangered fish known only to exist naturally in a small section of Citico Creek in Monroe County, Tennessee. They have been successfully re-introduced into Abrams Creek in Tennessee, but an alternate habitat is needed to help preserve and increase the population in case of a toxic substance entering Citico Creek. This study evaluates the potential of an alternate site, Spring Creek in the Cherokee National Forest and part of Hiwassee watershed, for translocation of the Smoky madtom to promote its survival. The study includes evaluation of the water quality and stream bed composition of both the creeks in order to determine the similarities.

Effects of the Firing Process for Eastern Dark-Fired Tobacco on Air, Water, and Soil Quality

Daniel Thomas Lawhon
Greenbrier High School

Abstract

One method that is commonly employed to process certain types of tobacco is to expose it to smoke in barns where hardwoods are burned at or near the floor (referred to as "firing"). To test for the environmental impact of fire-curing, several analyses were performed on air, water, and soil samples. The water and soil was only marginally affected. However, as expected due to the smoke produced in the process, the air quality as defined by particulate level was affected. The average particulate count in the control two miles away was 2.7 ± 0.6, and the count at the barn location was 29.7 ± 1.5.

Tgfbr2 and *Tgfbr3 si*RNA Knockdown Reduces Endocardial Cell Transformation in Chick Embryos *in Vitro*

Anh Pham, Jamille Robinson & Joey Barnett
Hume-Fogg Academic Magnet High School, Nashville

Abstract

An important early step in heart valve formation is endocardial cell epithelial to mesechymal transformation (EMT). Transforming growth factor beta (TGF) signaling is required for EMT. We posit that *Tgfbr2* and *Tgfbr3* transcription knockdown will affect cell

transformation. Results indicated that when transcription of the *Tgfbr2* and *Tgfbr3* genome was reduced, there was significant decrease in the number of transformed cells required for heart valve formation. This demonstrates a requirement for both *Tgfbr2* and *Tgfbr* 3 during endocardial cell EMT in the chick embryo model.

Effect of Ampicillin and Temperature on *E. coli* Growth Rates

Sidhartha Sinha & Daniel Hutchison
Smyrna High School, Smyrna

Abstract

In a bacterial infection, bacteria enter the bloodstream, sparking a reaction from white blood cells that fight off the bacteria. Generally, as a negative feedback response, the body increases its temperature. This process is pyrexia, more commonly known as fever. When infected by bacteria, patients are administered antibiotics to decrease bacterial growth. Our experiment involved simulating fever in the human body, using *E. coli* as the bacteria and ampicillin as the antibiotic. We tested the *E. coli* in multiple temperatures, both with and without ampicillin, to determine the growth rate of bacteria in a range of conditions. We proposed that the growth rate of *E. coli* would decrease as the temperature increased; a decrease in growth would also occur when ampicillin was present. Furthermore, we hypothesized that higher temperatures and ampicillin would have a multiplicative effect on decreasing the growth of the *E. coli.* Based on statistical analysis of our data using ANOVA, there is no significant interaction between temperature and antibiotics that affects bacterial growth.

Yes, There Are Atoms: A Comparison of Three Independent Methods of Determining Avogadro's Number

Stephen Theyken
Webb School of Knoxville, Knoxville

Abstract

At the beginning of the 20th century atomic theory was still doubted by many scientists. The discovery of independent methods to measure Avogadro's number helped answer these doubts. Three methods of determining Avogadro's number were performed to verify the reality of molecules. The first method used electroplating over a set period of time to determine the number of atoms and moles of electrons transferred. The second method used oleic acid's slightly polar quality to determine the number of atoms in a set volume. The third method compared the luminance of horizontal airlight with reflected skylight. The electroplating method gave a value of 5.97 x 10^{23}, the luminance method produced an order of magnitude value, while the oleic acid method gave a number that was close to an order of magnitude from the accepted value. Thus the reality of molecules was once again verified.